Master thesis

Optimization of the process route of seamless steel tubes to increase the mechanical - technological properties

Christian Gruber, BSc

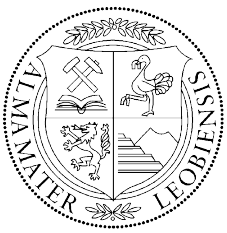

University of Leoben

Department Product Engineering

Chair of Metal Forming

August 2018

Affidavit

I declare in lieu of oath, that I wrote this thesis and performed the associated research myself, using only literature cited in this volume.

.....

Christian Gruber

Signature

Acknowledgments

My thesis would have been impossible without the great support and aid of my supervisor, industry partner, colleagues and my family. Especially I would like to express my sincere thanks to following persons:

First I would thank my supervisor **Univ.-Prof. Dipl.- Ing. Dr. mont. Bruno Buchmayr** of the **Chair of metal forming** for the helpful input and advices through the challenging assignment of tasks. The door to his office was always open whenever I had a question about my research or writing.

Further I would like to take this opportunity to thank the **voestalpine Tubulars GmbH & Co KG** for offering the topic and for supporting me with all off the test trails, materials and laboratory equipment. Particular I would gratefully mention **Dipl.- Ing. Dr. mont. Jürgen Klarner** and **Dipl.- Ing. Dr. mont. Gerald Winter** for the guidance through the whole thesis. Without their professional participation and recommendations, the results of the survey could not have been succesfully conducted.

Finally, I must express my very profound gratitude to my parents and to my girlfriend for providing me with unfailing support and continuous encouragement throughout this thesis. This accomplishment would not have been possible without them. Thank you.

Abstract

An intermediate cooling of tube blanks after the push bench in the seamless tube production process shows increased mechanical-technological properties on the final product. An analysis on grain size and microstructure development and an evaluation of the occurring phenomena of possible precipitations are tested on three different steel grades of intermediate cooled samples in comparison to traditionally processed tubes. Furthermore, spray water quenched tube blanks are reviewed by means of an increase of productivity during intermediate cooling. A complete mechanical – technological profile of the different steel grades was built with included assessment on recrystallized fractions during deforming and precipitation effects on strength, toughness and grain size development. Also the influence of the varying austenite grain sizes on the CCT diagram and following on the phase transformation kinetics has been observed in detail. The results from the trials give a recommendation on the optimal process route for thermomechanical treated seamless tubes with a perfect initial state for rapid cooled AHSS advanced high strength steel tubes.

Kurzfassung

Eine Zwischenkühlung von Rohrluppen nach der Stoßbank im nahtlosen Rohrherstellungsprozess zeigt erhöhte mechanisch-technologische Eigenschaften am Endprodukt. Eine Analyse der Korngrößen- und Mikrostrukturentwicklung und eine Bewertung der auftretenden Phänomene möglicher Ausscheidungen wird an drei verschiedenen Stahlgüten von zwischengekühlten Proben im Vergleich zu traditionell gewalzten Rohren durchgeführt. Darüber hinaus werden spritzwassergekühlte Rohrluppen für eine Steigerung der Produktivität während des Umlaufes zur Zwischenkühlung geprüft. Es wurde ein komplettes mechanisch - technologisches Profil der gewählten Stahlgüten erstellt, einschließlich der Bewertung der rekristallisierten Anteile während der Umformungsschritte, sowie und Ausscheidungseffekte auf die Festigkeit, Zähigkeit und Korngrößenentwicklung. Auch der Einfluss der variierenden Austenitkorngrößen auf das dazugehörige ZTU-Diagramm und auf die Phasenumwandlungskinetik wurde im Detail beobachtet. Die Versuchsergebnisse liefern eine Empfehlung für die optimale Prozessroute für thermomechanisch gewalzte nahtlose Stahlrohre mit einem verbesserten Ausgangszustand für spritzwasser-abgeschreckte höchstfeste AHSS-Stahlrohre.

Content

Nomenclature

TMP	thermomechanical processing
A_{c1}	austenitisation starting temperature during heating
A_{c3}	austenitisation finishing temperature during heating
A_{r1}	austenite-to-ferrite finishing temperature during cooling
A_{r3}	austenite-to-ferrite starting temperature during cooling
ε	plastic strain
M_f	finishing temperature of martensitic transformation
M_s	starting temperature of martensitic transformation
n	strain hardening exponent
CCT	continuous cooling transformation
AHSS	advanced high strength steel
HSLA	high strength low alloy
BCC	body-centred cubic
FCC	face-centred cubic
DRX	dynamic recrystallisation
UTS	ultimate tensile strength
YS	yield strength

Figures

Tables

1 Introduction

The use of tubes and pipes has a long history in different industrial applications. New methods for manufacturing tubes and pipes are developing and improvement of the existing manufacturing methods is continuing. The manufacturing methods of metal tubes and pipes can be divided as seamless and welded. Tubes and pipes manufactured through different routes have their specific advantages and disadvantages. Depending on the application requirements, tubes and pipes are manufactured in different sizes and shapes. The outside diameter of tubes and pipes could be several meters to even few nanometers. The tube and pipe industries face many challenges to produce high quality tubing in a cost effective and productive way in today's marketplace. Some of these challenges are requests for tube products in a wider variety of shapes and sizes by the end users, applications that require special materials, and demand for improved product quality from manufacturer. [1]

1.1 Seamless tube production

The production of a seamless tube can be divided into three major forming steps, in which an ingot is pierced to a hollow ingot, then stretched into a mother tube and finally rolled out into the finished tube. In vast cases the above mentioned three procedural steps are carried out with the aid of three different apparatuses. The piercing frequently takes place in a cross roller piercer because the latter delivers a hollow ingot with a low wall thickness tolerance and a relatively great length. The stretching frequently occurs in a second rolling stand, which is designed as an Assel or Diescher roll stand. The tube bloom that thus results during stretching is rolled out into finished tube after intermediate heating in a subsequent size-reducing or stretch-reduction mill. [2]

Seamless tubes are produced mainly for the applications where the ranges of wall thickness extend from small to large with the diameter range up to approximately 650 mm [3]

1.1.1 State of the art tube rolling

Seamless steel tubes are produced in the following major processes, which are shown in Figure 1-1 and chronological described in Table 1-1.

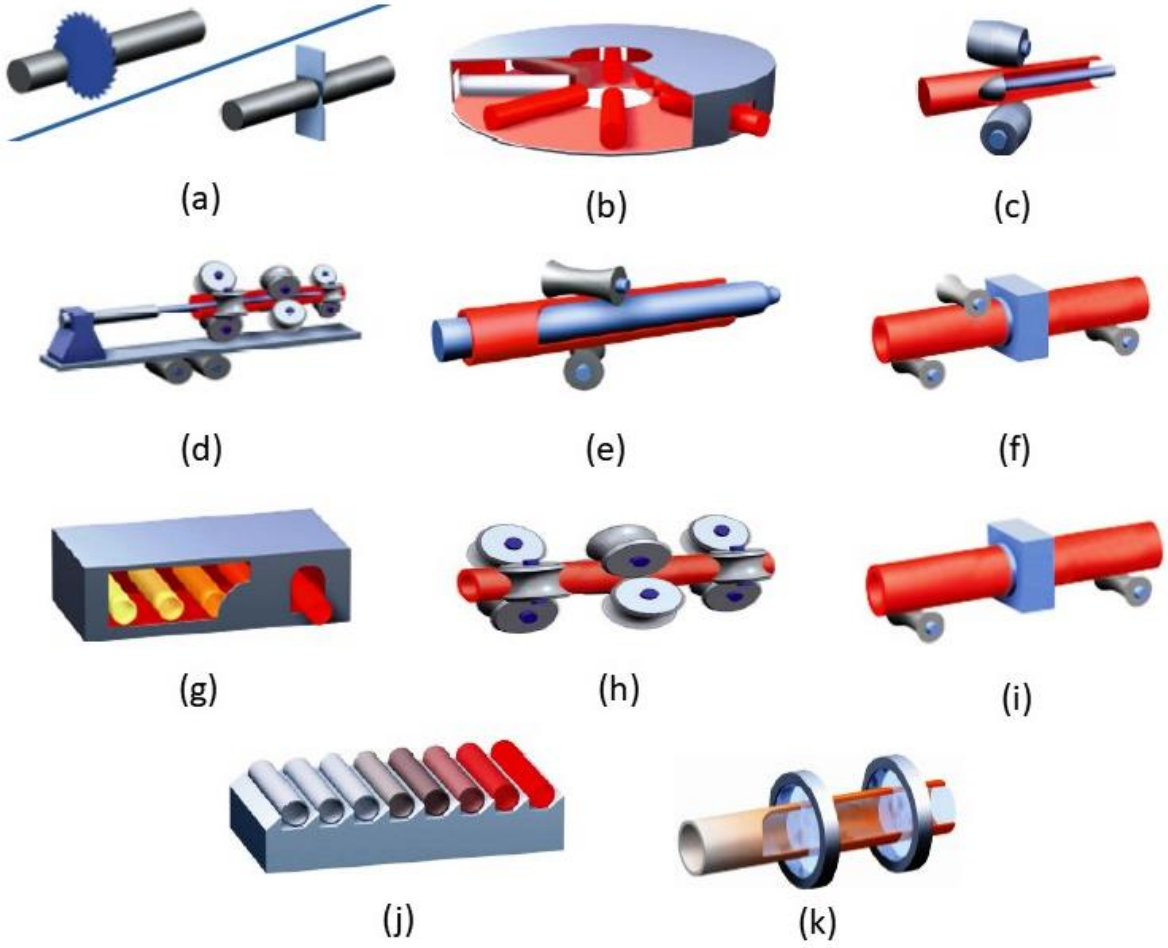

Figure 1-1: Seamless tube production route, (a) to (i) major processing steps; (j) and (k) optional [14]

Table 1-1: Seamless tube production processes in chronological order [14]

Processing Step	Description
(a) Bloom cutting	Continuous casted blooms with a diameter of about 230 mm and a length of up to 12 m are used as raw material. These blooms are sawed in case of alloyed, and sheared in case of unalloyed chemical composition to billets. Required billet-processing-weights were pre-calculated from desired final tube geometry as well as inspection requirements
(b) Rotary hearth furnace	According processing-weight-billets are heated in a rotary hearth furnace to forming temperature of about 1300 °C, depending on the alloying concept.
(c) Cross roller piercer	A piercing mill [4] is used to subject solid round billets to rolling process. Heated billets are milled against an inner plug, referred to Mannesmann principle [5], and so shaped to hollows with a specific wall thickness and diameter.
(d) Push bench	The pierced hollow is attached to the end of a mandrel bar and fixed by a crimping press. The received material tool hybrid is lifted to the push bench and pushed through non-driven stands of three-roll cages. The cross section decreases from stand to stand [6] and elongates the shell [7] on the tool to a maximum length of 22.9 m.
(e) Reeler	After elongation the mandrel bars are released by a reeler
(f) Wall thickness inspection	After tool rejection the shell geometry is inspected along the whole length and transmitted to the online control system for setting further forming operation parameters
(j) Intermediate cooling - Optional: Table 1-2	
(g) Reheating furnace	In the reheating furnace, tube shells are heated to required temperatures, depending on the amount of total alloying content from 860 °C to 1050 °C for stretch reducing.
(h) Stretch reducing mill	Reheated and descaled shells are formed in the stretch reducing mill with maximum 28 driven roller-stands to desired final diameter and wall thickness. By the transmitted input geometry [8] data the speed level of the roller stand is regulated to achieve homogeneous tube geometry.
(k) Rapid cooling system - Optional: Table 1-2	
(i) Rolling parameter inspection	Final tube inspection along the entire length reflects the quality of applied settings. The finished rolled tubes are cooled down subsequently at free air on a rake type cooling bed.

As described in Table 1-1, the processing steps (j) and (k) are optional and used to optimize the microstructure of the tubes and enhance their mechanical properties. The main role of these processes are defined in detail in Table 1-2.

Table 1-2: Optional process steps for thermomechanical treatment [14]

Optional processing step	Description
(j) Intermediate cooling	To adjust the grain refinement as a result of the phase transformation from austenite γ to ferrite α, the cooling time of the elongated shell must be controlled-temperature dissipated. [9] Grain refinement [10] is essential for the strengthening mechanism, because it simultaneously enhances both toughness and strength. Fine grained [11] tubes with special designed micro-alloying concepts are strengthened primarily by grain refinement at intermediate cooling stage. Due to this fact, tubes have a great potential to avoid additional alloying elements owing to lower required carbon contents and contribute to an increase of weldability.
(k) Rapid cooling system	In this stage, also known as accelerated cooling [12], the hot forming temperatures are dissipated from the final tubes by water spraying. The cooling interval from 1000 °C down to maximum 200 °C can be achieved. By applied water cooling, both improved mechanical properties and better surface qualities are achievable. Additionally, accelerated cooling also supports α grain refinement and improves tube strength as well as toughness. With a selective temperature loss during spray water cooling, microstructural gradients can be adjusted. This treatment, denoted as cross-section layer design, formed by accelerated cooling [13], ensures a tube wall gradient with martensite followed by bainite and ferrite/pearlite layers. Furthermore with this advanced treatment option, it is possible to design tubes with extraordinary good mechanical properties compared to single phase tubes.

1.2 Task

The aim of the thesis is to optimize the complete process route with intermediate cooling to increase the mechanical and technological properties especially of thick walled tubes. Therefore, the complete production process in terms of temperature, strain, strain rate and grain size should be followed and pictured out through the main aggregates.

Because investigations have showed that a transformation from austenite to ferrite and back in the region of the intermediate cooling section results in smaller grain sizes, this part should be highlighted. Differences in the chemical analysis by means of precipitation forming elements (Nb, V) is another factor which should be investigated.

For all this reasons a detailed analysis of the occurring phenomena in and after every deformation step must be observed to generate a standardized production route with respected efficiency. Also the possibility of a spray water cooling as intermediate cooling to decrease the cycle time of production should be considered.

2 Literature review

2.1 Thermomechanical treatment

In most commercial products in the steel industry, the external shape is the main result of the hot deformation steps, whilst the necessary mechanical properties are in the most cases obtained by the alloying and heat treatment after hot deformation. Improvements for the mechanical properties which are effects of alloying elements are frequently realized by means of heat treatments. Further the properties of materials directly quenched after deformation and then tempered sometimes show improved properties compared to traditional air-cooled and then separately quenched and tempered (Figure 2-1). [15]

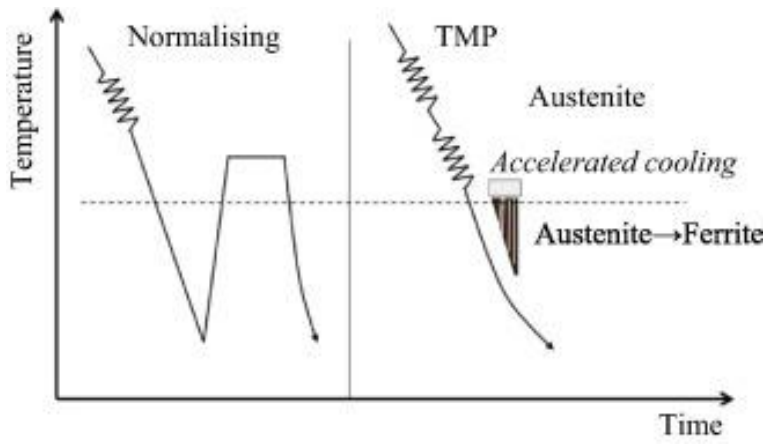

Figure 2-1: heat treatment after hot rolling vs. thermomechanical treatment [16]

Thermomechanical processing is therefore a technique designed to improve the mechanical properties of materials by controlling the temperature in the hot deformation, cooling or by direct quenching the product. This treatment eliminates a further heat treatment and also increases the productivity for advanced high strength steels AHSS. The outline of the controlled rolling is to introduce a high density of nucleation sites for α grains in a γ matrix during transformation by controlling the hot rolling conditions and so to refine the structure of the streel after transformation. Also the α nucleation sites, γ grain boundaries, interfaces of the annealing twins activated by the deformation must be considered. Therefore, the most crucial factor is the deformation temperature. In case there are no recrystallization retarding elements for the γ phase, a grain refinement is achieved by a high fraction of recrystallization at low

temperatures (800-950 °C) with a refinement in the α phase through the transformation of the fined austenite phase. Further refinement can be achieved by continuing the rolling reductions down into the non-recrystallization temperature range by elongating the γ grains and creating a high dislocation ratio for a high amount of nucleation sites for the transformation. This effect is generally used in micro alloyed steel concepts due to the effect of an increased recrystallization temperature. [15]

This microalloyed steel cocncepts were developed to provide superior new properties without the use of a large amount of expensive alloying elements. A significant improvement in ther mechanical properties is achieved by micro addition of carbonitride formers to low or medium carbon steel grades, always in conjunction with a controlled solution treatment and finish rolling temperature or by a thermomechanical processing. This leads to a precipitation strengthening in addition to a refinement of the austenite and further ferrite grains. This synergy of microalloying and thermomechanical treatment makes ferrite pearlite steels more affordable for manufacturers and costumers by replacing the conventional C-Mn-Si steels or heat treated alloy steel grades. More recently, these concepts are also employable in bainitic, martensitic and multi-phase steel grades. [17]

Microalloying elements form very fine carbides (NbC, VC or TiC), nitrudes (NbN, VN or TiN) or carbonitride (Nb(C,N), V(C,N) or Ti(C,N)) precipitates which are produced either during hot rolling, during the γ – α phase transformation or in the ferrite phase during cooling. The challenge is to define the composition of microalloying elements without resorting to the rather sophisticated rolling rolling sequence to develop a balanced set of properties. The increasing need to produce microalloyed grades with specific properties to meet customer requirements has given a rise to a new approach to alloy design known as microstructural engineering steels. This has focused attention on the prediction of mechanical properties as a function of process variables and the inherent characteristics of the steel to achieve optimum service performance at the least cost. [18]

2.1.1 Thermomechanical processing

In the conventional hot rolling process (Figure 2-2) is the breaking down of the original coarse cast grain structure performed by repeated recrystallization in the austenitic region. Cause the reheating and the finish rolling temperatures during the hot deformation need to be high (1100 - 1250 °C), it results in coarse austenite grain and finally coarse ferrite, impairing both strength and toughness. Is was originally designed to produce the required external shape of the workpiece at the shortest possible time without regarding the resultant mechanical

properties. After rolling, the steel is often air-cooled, although a water spray cooling is possible for the as rolled products. [19,20]

During hot rolling, austenite grains may recrystallize. A most influencing factor on the ferrite grain refinement if hot working is carried out within a temperature range where no recrystallization of the austenite can occur. The austenite grain will then be elongated to provide many more nucleation sites for ferrite formation. The final as rolled product will have inherited the fine grain size. The finer the grain size, the greater its beneficial effects on both strength and notch toughness. The practical application of these concepts have led to a new group of microalloyed steels which are called thermomechanical or temperature controlled rolled steels. [19,20]

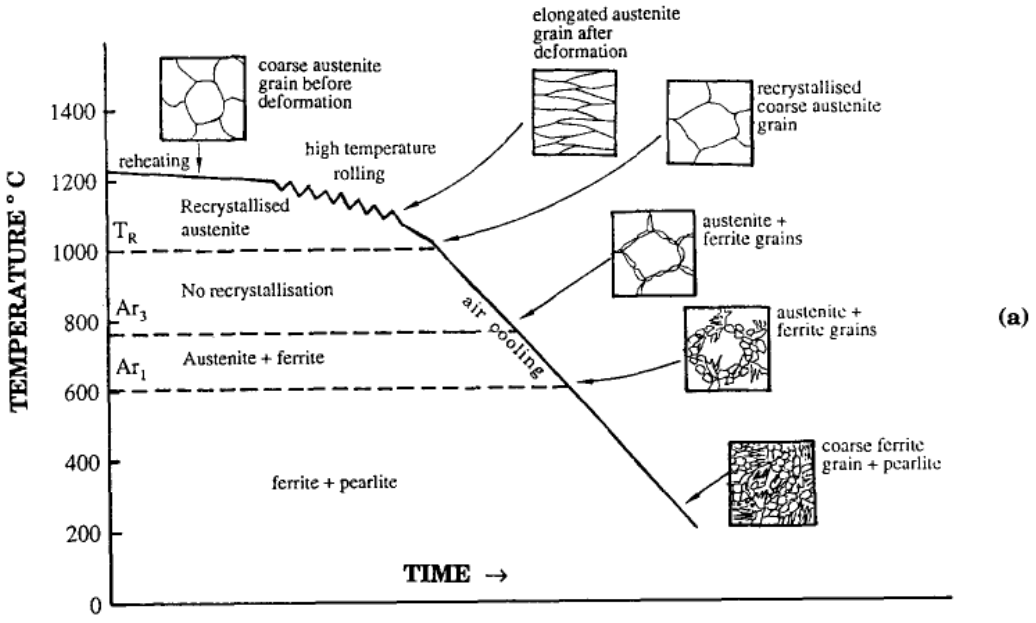

Figure 2-2: conventional hot rolling [20]

In comparison to the conventional rolling is the thermomechanical rolling shown in Figure 2-4. It is characterized by a high billet soaking temperature of about 1200 °C to ensure near complete microalloy dissolution, and then to impose a moderate to heavy deformation at a much lower finishing temperature (950-750 °C). [21] In contrast to the conventional rolling where the roughing and finishing operations are continuous, there is a delay between these two stages in the thermo-mechanical rolling, in order to reduce steel temperature. Rolling below recrystallization stop temperature refines the recrystallized austenite grains continuously during and after each deformation. Subsequent transformation into ferritic microstructure after rolling will produce a matrix with finer grain size and confers substantial improvement to the mechanical properties. At the same time, it also keeps enough

microalloyed carbonitrides dissolved in the austenite to give subsequent strengthening by precipitation. But it is difficult to easily lower the finish rolling temperature within a production route with high speed in combination with use of interstand cooling, lower rolling speed or to introduce a delay in the rolling schedule. More significantly, the cooling time delays tend to prolong processing time, and the required low deformation temperatures is may not viable to existing mills due to excessive loads. [20]

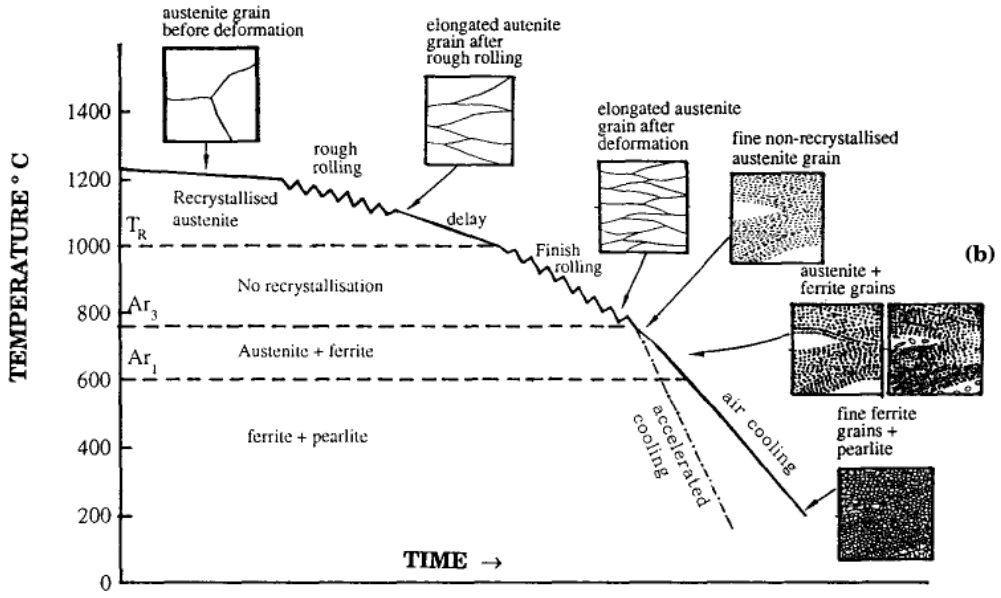

Figure 2-3: Thermo-mechanical processing [20]

Consequently, a novel thermo-mechanical processing route, known as recrystallization controlled rolling (RCR), shown in Figure 2-4, assumes predominant importance in the rolling process. Its aim is to refine the grains without the use of severe low temperature controlled rolling. Therefore, it involves the control of the austenite grain growth during reheating at 1060-1120 °C, repeated deformation above recrystallization stop and with accelerated cooling after finish rolling to maximize the ferrite nucleation rate. The success of this technique depends on the both achieving and maintaining a fine austenite grain size. This necessitates the use of fine and stable dispersion of TiN particles, which is able to suppress grain coarsening. It also enables higher austenitizing temperatures to be used to dissolve VC or NbC, thus allowing precipitation strengthening whilst preserving a fine austenite grain size prior to rolling. [22]

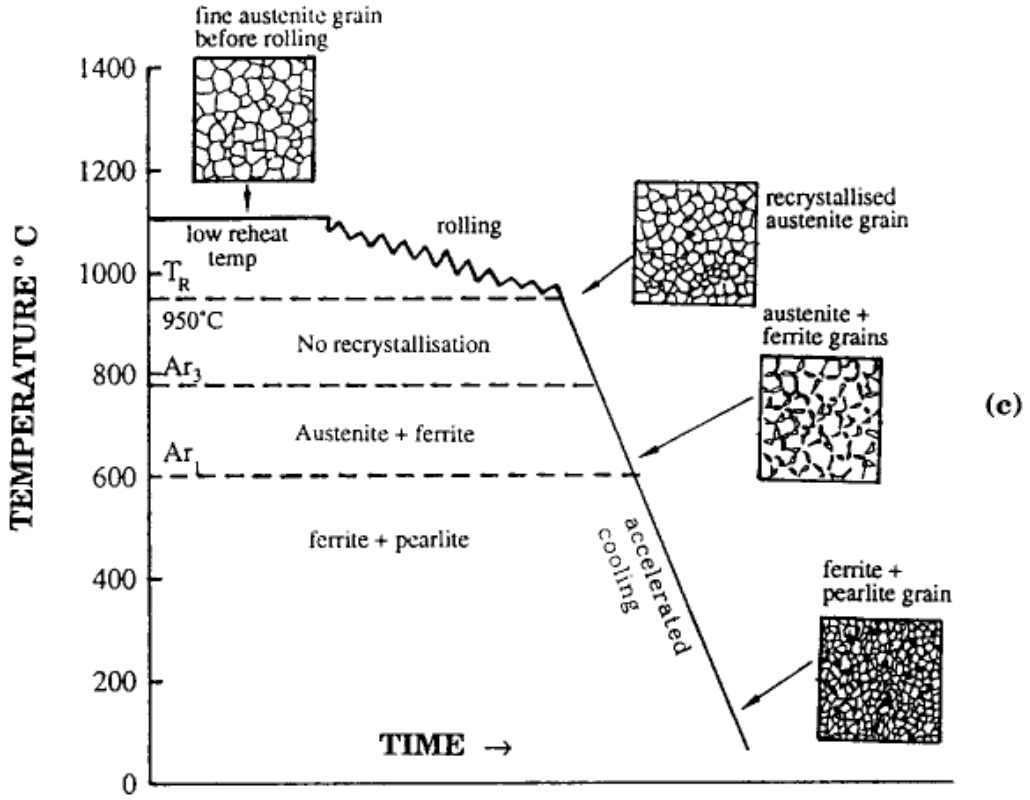

Figure 2-4: Recristallization controlled rolling [20]

Raising the cooling rate in the RCR process with a water quench after thermomechanical processing generally contributes to greater strengthening response arising from further grain refinement and enhanced precipitation dispersion. This enables to produce different microstructures like martensitic or bainitic phase by overcoming the difficulty of raising the strength without detrimental to the toughness. [23] Furthermore, an interrupted accelerated cooling can cause a double enhancement of grain refinement and an increase of precipitation strengthening in a rise of yield strength and elongation for low carbon steels microalloyed with titanium and vanadium. [24] For low manganese steels microalloyed with vanadium or titanium a direct quenching from the finish rolling temperature and tempering these steels produce higher yield strength and elongation then the conventional quenched and tempered heat treatment. [25]

2.2 γ to α transformation

The phase transformation from the austenite (γ) phase can be classified into two groups, the first group is the diffusional transformation of ferrite (α) or pearlite, which proceeds with nucleation and growth mechanism; whilst the second group is the martensitic transformation, which proceeds by a shear mechanism. This mechanism occurs, when steel is faster cooled than its critical cooling rate. [15]

When α forms from γ, nucleates mainly build at the γ grain boundaries. Then three phenomena occur simultaneously during diffusional phase transformation: (1) lattice change, (2) compositional change and (3) recrystallization. When the cooling rate is small, polygonal ferrite forms and some of the adjacent α grains with similar orientation coalesce into one grain. Nevertheless, one γ grain is usually divided into several α grains by transformation. General results a smaller γ grain into a smaller α grain. Is the cooling rate accelerated and the supercooling of the γ phase is large that many fine α grains form. However, when the supercooling is sufficiently large, acicular α with Widmanstätten structure forms.

The orientation relationship between the γ and α phases is the Kurdjumov – Sachs (K-S) orientation relationship similar to lath martensite, i.e.:

$$\langle 111\rangle_{\gamma}//\langle 011\rangle_{\alpha}, [\bar{1}01]_{\gamma}//[\bar{1}1\bar{1}]_{\alpha} \qquad (2.1)$$

There are 24 variants satisfying this orientation relationship. When the α grain is nucleated at the γ grain boundary, the α grain satisfies the K-S orientation relationship with one of the adjacent γ grains. The incoherent α – γ interface without the K-S relationship grows fasten the other boundary. When supercooling is low, the incoherent interface grows so that a grain becomes polygonal. After the completion of transformation, the orientation relationship between the phases is hardly detectable. [15]

2.2.1 Effect of alloying elements on phase transformation

The alloying elements in steels can basically divided into two groups. The first group are the elements which stabilize the γ phase by lowering the A_{r3} temperature and retard the decomposition of γ. Nickel, manganese, cobalt, copper, carbon and nitrogen are these γ formers. Alloying elements such as silicon, aluminum, phosphorous, chromium, vanadium, molybdenum, tungsten, titanium, tantalum, niobium and zirconium are on the other hand α formers and raise the A_{r3} temperature but retard decomposition of γ by slowing down the diffusivity of carbon in the austenite phase and some other reasons such as grain boundary

enrichment. Furthermore, the elements chromium, vanadium, molybdenum, tungsten, titanium, tantalum, niobium and zirconium are strong carbide formers and precipitate alloy carbides independently. Moreover, these elements except of molybdenum and tungsten can form nitrides in steels. And if carbon and nitrogen are involved, they can also form carbonitrides, which can be precipitated in the γ phase according to the solubility product of the alloying element and the carbon and nitrogen. Of course, carbonitrides precipitate more in the ferrite phase due to the lower solubility. [15]

When polygonal ferrite forms from austenite during slow cooling, α stabilizing elements enrich in the ferrite phase and γ forming elements remain in the austenite. Local equilibrium conditions are considered usually only on the interface. Orthoequilibrium is the condition in which alloying elements are partitioned into both phases to equilibrate chemical potentials of alloying elements in both phases. However, when a cooling with a usual cooling rate is applied, partition of carbon is easier to achieve due to its higher diffusivity than a partition of the other alloying elements with a bigger atomic radius. This state is then so called paraequilibrium.

When α is formed during transformation, carbon gets enriched in the austenite phase and pearlite transformation begins. If now carbide forming elements are existing, following things can occur:

1) Alloy Carbides of niobium NbC, vanadium V_4C_3 and titanium TiC etc. precipitate during the phase transformation
2) Once carbide forming elements come into the ferrite, carbon precipitates as iron carbide; this further changes to alloy carbide in the ferrite phase because of the stronger thermodynamic force.
3) Carbide forming elements come into the ferrite after transformation and then alloy carbides precipitate in α directly

In case that scenario 1 happens, it is observed that alloy carbides form as rows of very fine particles at the α-γ interface during the growth of the ferrite. This phenomenon can occur both during isothermal holding and continuous cooling. As shown in Figure 2-5, at the γ side α-γ coherent interface $\{111\}_\gamma//\{110\}_\alpha$ carbon enriches the local equilibrium condition and alloy carbide precipitates. The carbon concentration is decreased by the precipitation and the incoherent interface of ledge close to $\langle 112\rangle_\alpha$ grows rapidly. By a large number of ledges, the macroscopic α interface appears to growth in the direction of $\langle 111\rangle_\gamma//\langle 110\rangle_\alpha$. [15]

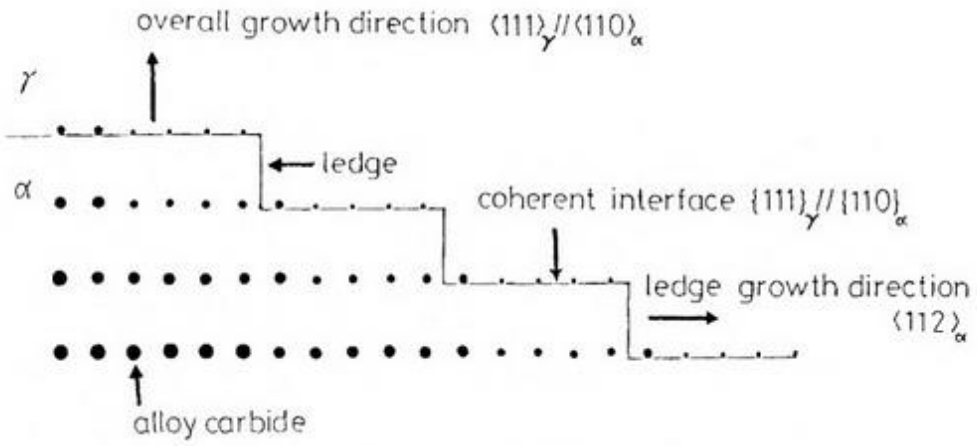

Figure 2-5: Ledge mechanism of growth during γ -> α transformation [15]

2.3 Transformation kinetics

2.3.1 Transformation kinetics of γ (isothermal)

When ferrite or pearlite forms from austenite by isothermal holding below the transformation temperature, nuclei form preferentially at the prior γ grain boundaries. Thus, their transformation kinetics can usually be expressed by including the effect of γ grain size as:

$$X = 1 - e^{[-k(T)\left(\frac{t^n}{d^m}\right)]} \quad (2.2)$$

Whereas X is the transformed fraction, t is the isothermal holding time, d is the diameter of the austenite grain and k(T) is the rate constant which depends on the transformation temperature and corresponds directly to the curve of the isothermal transformation diagram (TTT). The values for n and m depend on both, the transformation mechanism and type of nucleation site. The transformation where all the nuclei are nucleated at an early stage in the reaction and where the progress of transformation is controlled mostly by their growth is called site saturation. Any γ grain is assumed to be a tetrakaidecahedra, and the nucleation sites at the γ grain boundary can be classified into surface, edges and corners as shown in Figure 2-6. The actual nucleation sites are not limited to any one of such types, and the value of m would be the weighted average of the various nucleation sites and would not always be an integer. Sometimes, the nucleation site is varied by supercooling (accelerated cooling). Then the nucleation site of α is moved gradually from edge to surface by the decrease in transformation temperature with cooling rate. [15]

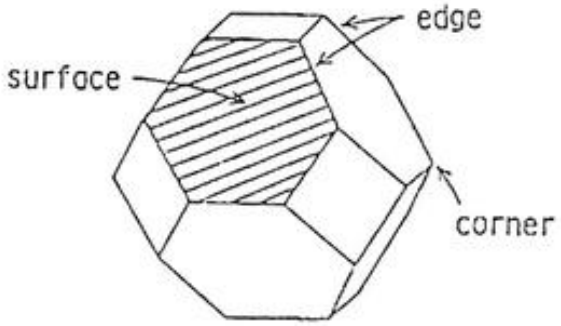

Figure 2-6: schematic diagram of an austenite grain [15]

2.3.2 Continuous cooling transformation kinetics of γ

In case of continuous cooling, Scheil considered the austenite to ferrite transformation. He assumed in his model that γ consumes its fractional nucleation time and when the sum of a number of such fraction equals unity the transformation starts:

$$\int_{t=0}^{t=t_n} \frac{dt}{\tau(T)} = \int_{T_e}^{T} \frac{dt}{dT} * \frac{dT}{\tau_{(T)}} = 1 \quad (2.3)$$

Now extend this Scheil's additivity rule to the entire range of transformation. In this case the incubation time $\tau_{(T)}$ is extended to the time required for the reaction to reach a certain fractional completion X by isothermal holding at temperature T. If equation 2.2 and 2.3 are combined, following equation comes to wear:

$$X_{(t)} = 1 - e^{\left(-\frac{1}{d^m}\left(\int_T^{T_e} \frac{K_{(T)}^{\frac{1}{n}}}{Q_{(T)}} dT\right)^n\right)} \quad (2.4)$$

Where in $Q_{(T)}$ = -dT/dt and is a cooling rate. This equation expresses the transformed fraction at temperature T during cooling from the γ condition with a cooling rate $Q_{(T)}$. Furthermore, from equation 2.2 and 2.4 can be obtained following:

$$t_{(T)} = \frac{1}{K_{(T)}^{\frac{t}{n}}} \int_T^{T_e} \frac{K_{(T)}^{\frac{1}{n}}}{Q_{(T)}} dT' = t_{eq} \quad (2.5)$$

This equation tells us that the fraction transformed by cooling from T_e to T with cooling rate $Q_{(T)}$ is equal to that obtained by the isothermal holding at temperature T for time $t_{(T)}$. Thus, t(T) is the equivalent cooling time, t_{eq} is the isothermal holding time which gives the equivalent transformed fraction with continuous cooling. The curve produced by t_e successive plot of such t_{eq} at each temperature during cooling with cooling rate $Q_{(T)}$ the equivalent cooling curve. The transformation behaviour for a given cooling curve can be predicted from the TTT diagram. [15]

2.3.3 Transformation from recrystallized γ

The grain size just after transformation is generally finer than that if the phase before transformation. Especially in cooling transformations. Figure 2-7 shows the relationship between austenite and ferrite grain sizes before and after transformation in three air-cooled silicon-manganese steels. There is no difference in the relationship for the transformation from isotropic strain-free γ grains between the normalized and the as-rolled steels, when the composition and the cooling rates are the same. [15]

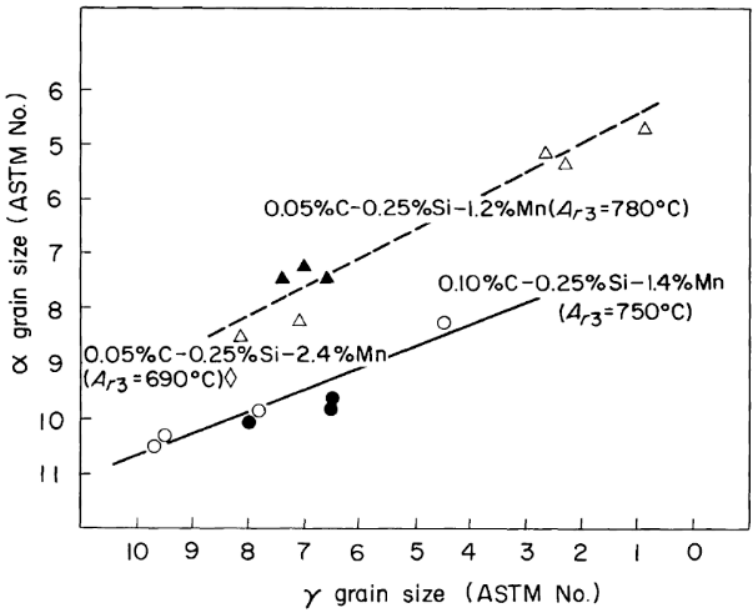

Figure 2-7: γ and α grain size before and after transformation [15]

Transformed α grains are generally finer than γ grains and finer γ grains transform to the finer α-pearlite structure, for α grains nucleate at γ grain boundaries, α grains of normalized steels are generally finer than those of as-rolled steel, because the γ grains at normalizing temperatures are finer than those recrystallized and grown down to the transformation after conventional hot-reductions. The grain refinement in controlled rolled products are mainly forced by the refinement of recrystallized γ grains by low temperature finishing rolling.

Refining the γ grains before transformation raises the A_{r3} temperature and increases the amount of proeutectoid α, as shown in Figure 2-8. [15]

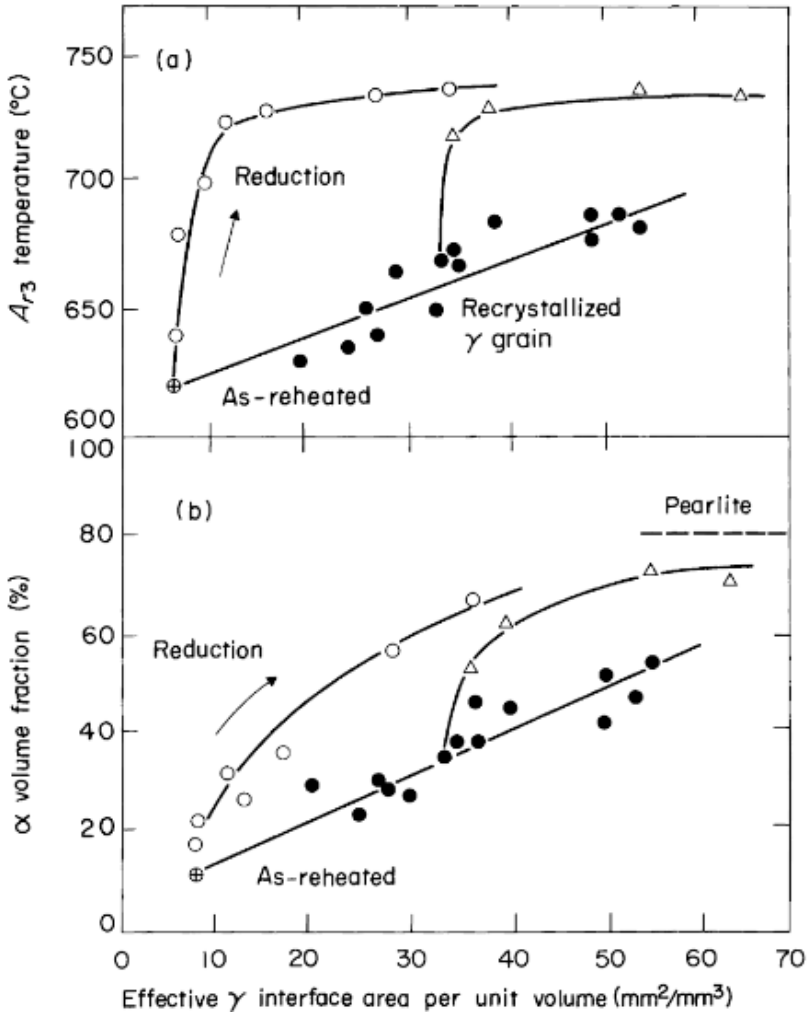

Figure 2-8: Change of transformation behaviour with effective γ interfacial area [15]

2.3.4 Expression for α grain size (isothermal)

In general, ferrites nucleate at γ grain boundaries and grow into the austenite grains. The grain size of α formed from γ is directly related to the process of transformation. When ferrites nucleate at the γ grain boundary surfaces, they grow as ellipsoid with the an aspect ratio of 3:1 and is shown in Figure 2-9. [15]

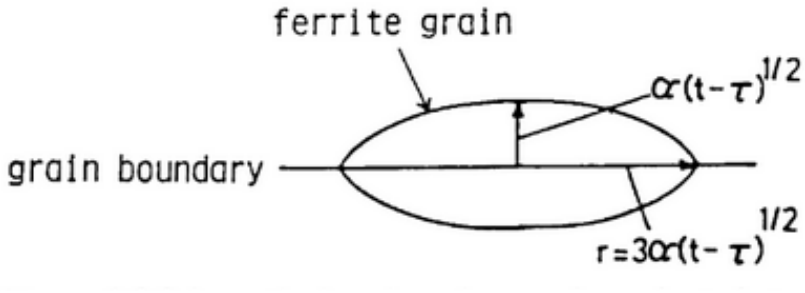

Figure 2-9: α grain nucleation at γ grain boundary [15]

Nevertheless, for grain boundary nucleation, a small γ grain leads to a small α grain. The effect of γ grain size on α grain size depends on the type of nucleation site and becomes large in the following ascending order: 1) homogeneous; 2) grain surfaces and 3) grain edges. The γ grain is refined by the repeated static recrystallization during multipass rolling in the first stage of controlled rolling. The relation of recrystallized γ grain size and the rolling parameters such as temperature, pass reduction and rolling speed are the most influencing factors. For carbon-manganese steels following equation describes the evolution of the grain size during recrystallization:

$$D_R = 25(\frac{1}{\beta} ln \frac{Z}{A})^{-\frac{2}{3}} \varepsilon^{-1} {D_0}^{\frac{1}{2}} \qquad (2.6)$$

In this equation the recrystallized grain size is expressed in terms of the initial grain size D_0, strain ε, and the Zener Hollomon parameter Z:

$$Z = \dot{\varepsilon} e^{\frac{Q}{RT}} \qquad (2.7)$$

In general, the γ grain size is refined by increasing the Zener Parameter or by increasing the flow stress. It should be added that the grain refinement in γ turns out to be less effective in α grain refinement in the case of grain surface nucleation D_α is proportional to $D_\gamma^{1/3}$. This means that when D_γ is reduced to one eight of the initial, D_α would be reduced to one half.

The type of predominant nucleation site of α depends on the site density and the nucleation frequency at each given site. In more fundamental terms it is determined by the α-γ interfacial energy, degree of supercooling and the γ grain size. In a typical controlled rolling where the ferrites transform with fairly high supercooling, γ grain surfaces are considered to be the dominant nucleation site of α. [15]

2.3.5 α grain size by continuous cooling transformation

As assumed that ferrite nucleates prefentially at γ grain surfaces, at continuous cooling transformation can be considered as the sum of short time isothermal holding at a temperature level. Figure 2-10 explains the relation between isothermal and continuous cooling transformation and a schematic drawing showing the formation process of α during the transformation. [15]

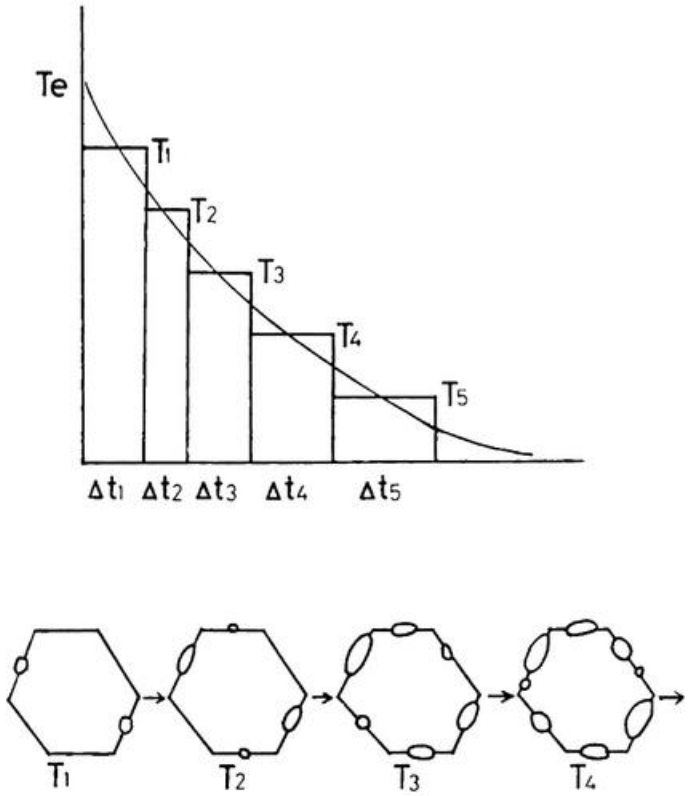

Figure 2-10: connection between isothermal and continuous cooling transformation [15]

During the transformation, carbon enriches and retain in the γ phase and influences the nucleation and growth rate of α. However, ferrite nucleation mostly occurs in the early stages of transformation and can be assumed that both nucleation and growth rates of α are a function of an instantaneous temperature for a short time and not an exact function of thermal history. Once a α grain is nucleated, thereafter a growth with a corresponding growth rate at each temperature level during cooling occurs. [15]

2.4 Recrystallization

Usually steels are deformed by slip at room temperature and work hardened by the increase in dislocation density. At elevated temperatures both slip deformation and grain boundary sliding occur when steels are deformed at low strain rate and is called creep. General grain boundary sliding depends significantly on the temperature and on the strain rate. Slip in the creep deformation arises from the movement of dislocations accompanying the drag of solute atoms, which also is strongly connected with the temperature and strain rate. If the strain rate gets increased by deformation, such as in hot rolling of austenite, the grain boundary sliding hardly occurs even at high temperatures and only the slip takes place by the movement of dislocations without the dragging effect of solute atoms. However, the recovery occurs to some extent during work-hardening. When the dislocation density is increased to a certain value, the recrystallization can take place during deformation. Recovery and recrystallization occurring during deformation are called dynamic recovery or dynamic recrystallization.

For example, when aluminium is tensile deformed at about 300 °C at a strain rate of 10^{-4} 1/s the steady state deformation occurs after the initial work hardening and the stress-strain curve, like shown in Figure 2-11 a, is obtained. In the steady state stage, the work hardening and the softening due to dynamic recovery are balanced. This leads to a maintaining constant stress level over a long strain rate. This restoration process is called dynamic recovery and in case of the face centered cubic (fcc) lattice of aluminium with a high stacking fault energy is therefore representative.

On the other hand, materials with a low stacking fault energy, the rate of softening due to recovery is slower in comparison to type a and shown in the first phase of Figure 2-11 b. The work hardening in this case cannot be balanced only by dynamic recovery, even at higher temperatures. The dislocation density is gradually increased and finally, the recrystallization starts to occur during deformation. The stress is lowered beyond a peak stress by dynamic recrystallization and reaches a certain steady state stress level at which the work-hardening and softening are balanced.

The austenite phase in steels initially belongs to type b, whereas in the ferrite phase, the restoration is mainly performed by dynamic recovery, since the recovery occurs very quickly. However, the dynamic recrystallization occurs under certain deformation conditions even in ferritic steels.

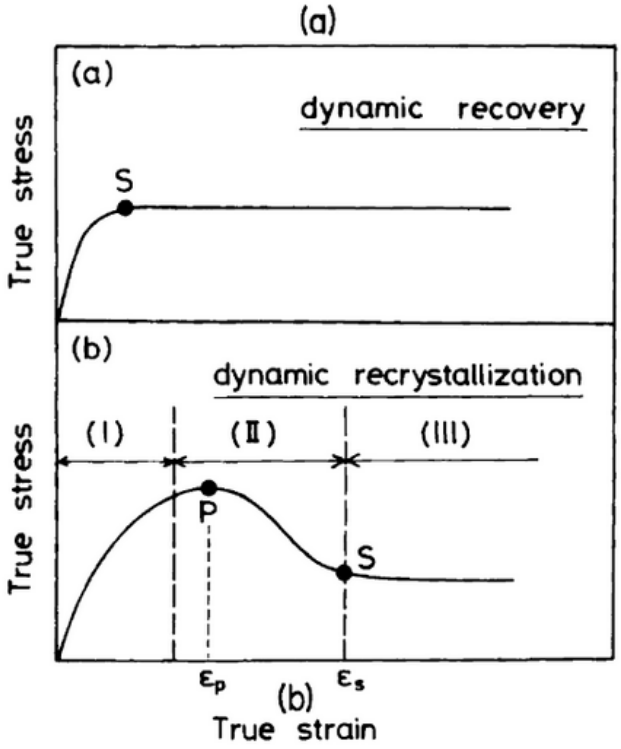

Figure 2-11: Stress-strain curves for (a) high stacking fault energy and (b) low stacking fault energy [15]

The microstructure of γ at the beginning before deformation is basically equiaxed and the boundaries are smooth and plan due to the transformation from heating up to rolling temperature. Many annealing twins exist in γ grains. By slight deformation, the grain boundaries become finely serrated and bulged. At a strain rate above the peak, many small grains are newly formed along the γ boundaries. It is characteristic that these newly formed grains contain annealing twins. Furthermore, some of the initial grains become larger by the strain-enhanced coarsening. In the stage of steady state deformation, the recrystallization occurs repeatedly during deformation. Dynamic recrystallized grains contain a few annealing twins at low Z but scarcely contain them when Z gets high. [15]

2.4.1 Dynamic recrystallization

There are two main mechanisms for dynamic recrystallization: 1) the bulging mechanism and 2) the nucleation-growth mechanism. Generally, the former operates predominantly at small strain and the latter occurs at high strain. The bulging mechanism seems to occur at a very early stage of deformation. The nucleation-growth mechanism becomes dominant at a strain rate of more than about 0.2. However, even in the range of steady-state deformation at which the strain is usually more than 0.2, the actual stain in each grain is estimated to be fairly small

since the recrystallization occurs repeatedly. Therefore, even in the steady-state deformation might be the case in which the bulging mechanism is predominant. In case of hot rolling, where the strain is fixed to a certain value, the work hardening structure is obtained under higher Z conditions and the dynamically recrystallized structure is obtained under lower Z conditions. Therefore, in order to know the γ structure immediately after hot rolling, both factors of strain and Z must be considered. Furthermore, it must be borne in mind that both strain and strain rate are increased with an increase in the amount of reduction of one pass in hot rolling.

Dynamic recrystallization becomes easier when the initial grain size of the austenite is smaller. Therefore, in the case of fine initial grain size, the ε_P and ε_S become small even at deformation under the same Z condition. [15]

2.4.2 Static recrystallization

When the hot deformation is finished at the work-hardening stage, the work-hardened γ is then softened by the usual static recrystallization during isothermal holding after deformation. However, if the strain is too small, the recrystallization cannot occur and only recovery takes place. On the other hand, when specimens are isothermally held after hot deformation to the range of the steady-state deformation, in which the dynamic recrystallization has occurred, the recrystallization ant the grain growth can occur continuously during holding after hot deformation. Such a recrystallization is called metadynamic recrystallization, i.e. the dynamically recrystallization structure is further softened by the metadynamic recrystallization. When specimens are deformed in the work hardened γ zone and dynamical recrystallized γ is coexisted, the static recrystallization occurs in work-hardened γ and the metadynamic recrystallization occurs simultaneously in dynamically recrystallized γ.

In the case of rolling in which slabs or blooms are rolled through several passes, the static recrystallization process occurring during interval between each rolling pass has a great influence on the deformation behaviour of each subsequent pass. If the softening due to the static recrystallization is not completed in the interval between each rolling pass, the work-hardening is successively accumulated by subsequent passes. With increasing holding time, the microstructure changes from partly static recrystallized γ, to a fine full recrystallized austenite matrix. By further increasing of time annealing twins in the static recrystallized austenite are gradually developed. Further the grains are coarsened. When the γ was much more heavily deformed under higher Z conditions, the static recrystallized grains become much finer. Also by increasing the holding time, γ grain boundaries become fairly straight and the γ structure becomes almost of equiaxed grains. Furthermore, the density of annealing twins is

increased. This is the typical microstructural change occurring during the metadynamic recrystallization process. Metadynamic recrystallization is completed by holding for a longer time, and the usual grain coarsening appears by further holding. The grain size right after the completion of metadynamic recrystallizationis smaller, as the grain size of dynamically recrystallized γ is smaller. However, γ grains are not refined and only increased by the metadynamic recrystallization, unlike the static recrystallization in which γ grains are once refined. [15]

2.4.3 Model to predict recrystallization and γ grain size during hot rolling

In multipass hot rolling processes, grain refinement takes place mostly through static recrystallization. The prediction of microstructural change occurring during hot deformation based principally on the model shown in Figure 2-12. [15]

The procedure of calculating γ grain size during hot rolling consists of six steps as described:

1) In order to determine recrystallized γ grain size, it is first necessary to know whether dynamic recrystallization occurs in each rolling pass. The occurrence of dynamic recrystallization is judged from strain, strain rate and the Zener-Hollomon parameter. If the rolling condition satisfies the occurrence of dynamic recrystallization, dynamically recrystallized grain size is calculated.
2) Under the condition where dynamic recrystallization does not occur, statically recrystallized grain size is calculated.
3) If recrystallization is not completed during the interpass period, the calculations for recrystallized grains and unrecrystallized grains, strain retained is calculated and added to the strain imposed in the next pass.
4) If recrystallization is complete before the next pass, subsequent change resulting from grain growth in the remainder of the interpass period is calculated.
5) In the mixed structure consisting of recrystallized grains and unrecrystallized grains, the mean grain size is calculated by taking into consideration the recrystallized fraction, where the grain size of unrecrystallized structure is assumed to be the same as that of the recrystallized structure before the previous pass.
6) A parameter representing the effective grain boundary area, consisting of grain boundaries and deformation bands, is calculated, which is to express the nucleation sites for α grains.

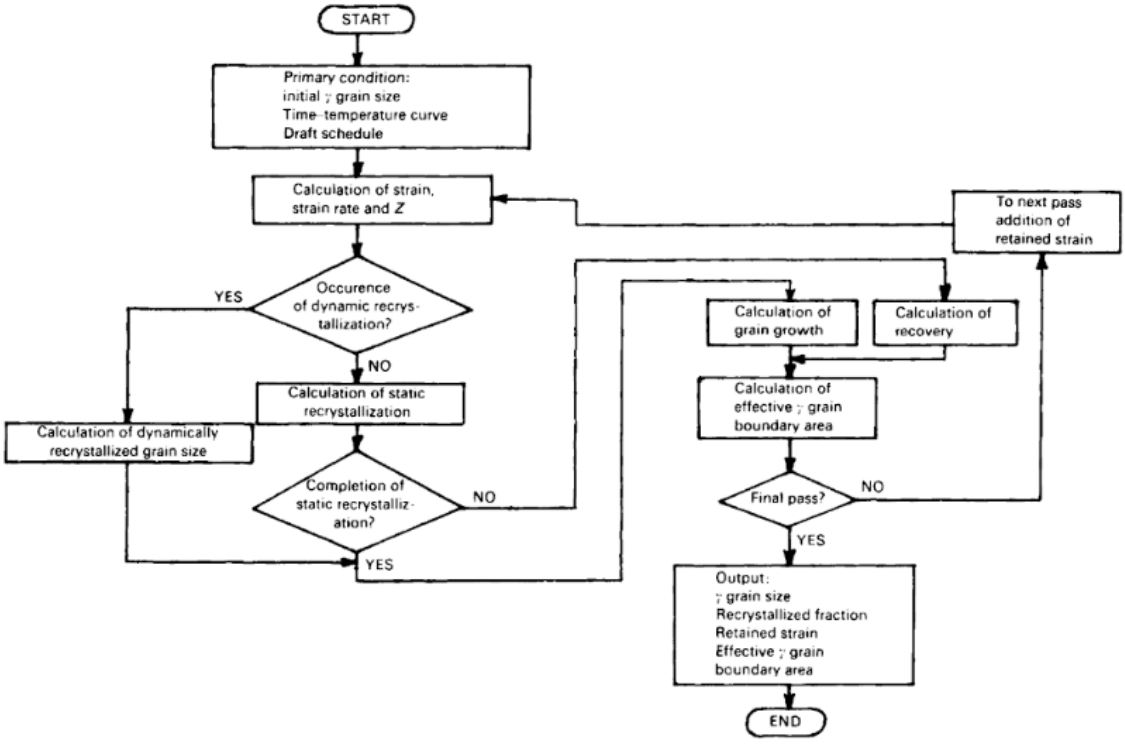

Figure 2-12: Flow chart for the grain size simulation in multipass hot rolling [15]

2.5 Precipitations

Precipitation of carbonitrides is an important phenomenon influencing the microstructure of high strength low alloy (HSLA) steels and, therefore, the mechanical properties. Considerable efforts are expended the world over to understand the precipitation phenomenon in these steels. This is crucial for a successful design of the alloys and of the thermomechanical treatment to be adopted in order to achieve the desired mechanical strength. Ti, Nb, and V are most commonly used as the alloying elements to precipitate as carbonitrides and induce grain refinement in these steels. Apart from these other elements such as Mo, Cu, Ni are added to these steels making the chemistry complex. In addition to these, Al is present in these steels resulting from the steel making process. The presence of these alloying elements makes the precipitation behaviour very complex. A comprehensive understanding of the precipitation behaviour is essential to achieve the desired properties. [26]

2.5.1 Alloy Carbides

The addition to iron-carbon alloys of elements such as Ni, Si, Mn, which do not form carbides in competition with cementite, does not basically alter the microstructures formed after transformation. However, in the case of strong carbide-forming elements such as Mo, Cr and W, cementite will be replaced by the appropriate alloy carbides, often at relatively low alloying element concentrations. Still stronger carbide- forming elements such as Nb, Ti and V are capable of forming alloy carbides preferentially at alloying concentrations less than 0.1wt%.

Carbides are formed in steels only by iron and metals that stand to the left of iron in the periodic table. In steel six kinds of carbides can be formed as shown in Table 2-1, where M denotes a sum of carbide-forming (metal) elements. The carbides placed in group I posses a complicated crystal structure; an examples is cementite (Fe_3C), or $Cr_{23}C_6$. A specific structural feature of the carbides of group II as interstitial phases is a simple crystal lattice (e.g., TiC, WC, NbC and Mo_2C).

Table 2-1: Variants of carbides in steel [27]

Group I carbides	Group II carbides
M_3C	MC
$M_{23}C_6$	M_2C
M_7C_3	
M_6C	

It should be noted that the effectiveness of the carbides as strengtheners depends on the fineness of the dispersion and the volume fraction precipitated. The fineness of the dispersion depends on the activation energy barrier for nucleation which in turn is influenced by the free energy of formation of the carbide, the interfacial energy and the misfit. The finest precipitate dispersions are generally obtained from VC, NbC, TiC, TaC and HfC. These are all close-packed intermetallic compounds. On the other hand, the carbides with complex crystal structures and low heats of formation, e.g. M_7C_3, M_6C and $M_{23}C_6$, generally form relatively coarse dispersions. [27]

2.5.2 Precipitation of alloy carbide from α

Carbide forming elements are also ferrite stabilizing. Thus, when steel is accelerated cooled and diffusion of these elements is prevented, they stay in solution in the ferrite phase. In this case, carbon exists either as iron carbide Fe_3C or in solution similar to the case of the martensitic phase. If such materials are heated, carbon precipitates firstly as Fe_3C. Above a temperature of about 450 °C, carbides of vanadium V_4C_3, Molybdenum Mo_2C, titanium TiC, niobium NbC gradually precipitate and decrease the Fe3C content. The equilibrium partition coefficient is following: chromium: 23; manganese: 10.5; vanadium: 9; molybdenum: 7.5; tantalum: 2 and less for titanium, niobium and zirconium. For instance, chromium sufficiently solves in Fe3C and enriches in Fe_3C. Thus nuclei of Cr_7C_3 form in Fe_3C or in contact with Fe_3C. This is called in situ nucleation. On the other hand, some elements like niobium are hardly solved in Fe_3C. Thus, nuclei of niobium carbide form on mainly dislocations in the ferrite matrix. Coherent precipitation of such carbides contributes markedly to the strengthening. This is then called separate nucleation, while vanadium and molybdenum solve in Fe_3C in some degree and the precipitation of $V_4C_3$and Mo_2C occurs partly by in situ nucleation although mostly by separate nucleation. [15]

2.5.3 Thermodynamic bases for precipitations

The strengthening effect of microalloying additions may be produced by the dispersion strengthening effect of fine carbo-nitride particles or by grain refinement, i.e. inhibition of grain growth by carbo-nitride particles, or by a combination of these two effects. In order to maintain a fine austenite grain size prior to transformation, particles that remain undissolved in the austenite, or particles that will precipitate during hot rolling are required. To produce the very fine particles that are responsible for dispersion strengthening (i.e. particles that are 2-5 nm in diameter), it is necessary that these should be freshly precipitated during or after transformation to ferrite. [28]

To achieve the desired metallurgical states, a detailed knowledge of the solubilities of the microalloy carbides and nitrides is required, together with a knowledge of their precipitation behaviour. An understanding of the role of different microalloying elements can be gained from the solubility product data summarised in Figure 2-13 from recent thermodynamical evaluation. Despite a simplification the individual solubilities of the microalloyed carbides and nitrides offer clear directions for the selection of microalloying additions for specific purposes. It is seen that TiN is extremely stable and can withstand dissolution at high temperatures during reheating prior to rolling or during welding. Niobium nitride and carbide have relatively low solubilities

and may precipitate out in the later stages of rolling. Vanadium on the other hand, has a rather high solubility in austenite even at temperatures as low as 1050 °C. It is also seen that the nitrides are substantially less soluble than the corresponding carbides. This is especially true for titanium and vanadium where the differences are particularly pronounced.

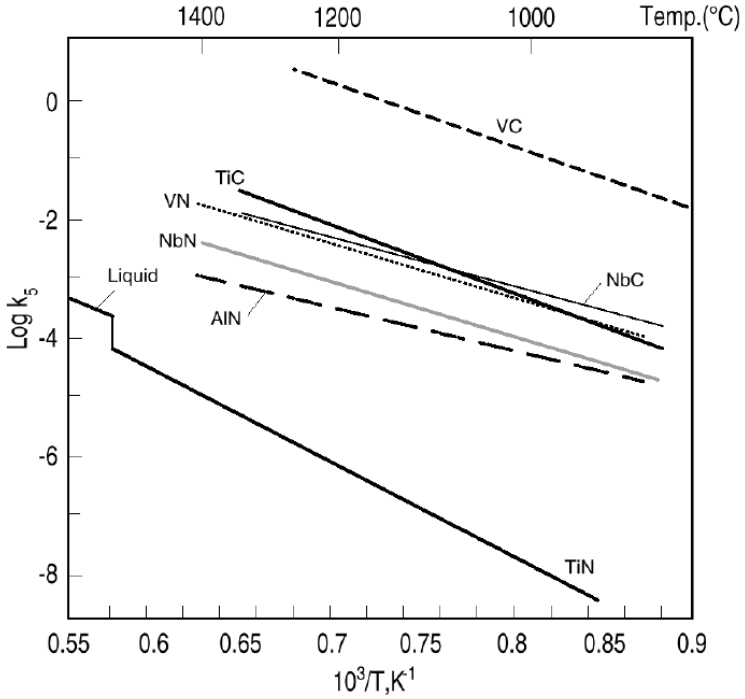

Figure 2-13: Solubility of microally carbides and nitrides [28]

As was stated above the solubility of carbides and nitrides in austenite and ferrite is usually expressed as a solubility product in terms of weight percent of microalloy element and carbon and/or nitrogen. The temperature dependence of the solubility product is expressed by the Arrhenius relationship in the form:

$$\log(k_s) = \log([M][X]) = A - \frac{B}{T} \qquad (2.8)$$

k_s is the equilibrium constant, [M] is the dissolved microalloy (wt%), [X] is the content (wt%) of nitrogen or carbon, A and B are constants and T is absolute temperature. An analysis of published data concerning the solubility of VC, VN, NbC, NbN, TiN and AlN has shown that there exist more than ten different solubility equations for each carbide/nitride, and the spread between them is significant, in most cases greater than 150 °C. It should be pointed out that the situation is even more complicated when more than one microalloy element is present and when the ratio of carbon to nitrogen is changed. The analysis of the solubility data in terms of solubility products implicitly assumes that the activity coefficients of microalloying elements as well as carbon and nitrogen are equal to unity and the microadditons are treated as a dilute

solute and any interactions between solutes in the system are neglected. Therefore, the individual solubility equations apply only to a particular composition investigated and are not capable of predicting the solubility at different compositions, where the effects of solute interactions become significant. The carbides and nitrides are also non-stoichiometric and, hence, their composition can vary when precipitated in steels. [28]

The similarity of crystal structure of carbides and nitrides enables them to show mutual solubility. Except for (V,Zr)N, all other carbides and nitrides formed by Ti, Nb, Zr and V show continuous or extended mutual solubility. For V and Zr the large difference in atomic size enables their compounds only to show limited mutual solubility. It is necessary to emphasise that aluminium differs from the microalloying elements V, Nb and Ti because it does not form a carbide in steel, but only the nitride, AlN, having a different crystal structure (hexagonal close packed). Therefore, there is no mutual solubility with the carbides/nitrides of V, Nb and Ti. [28]

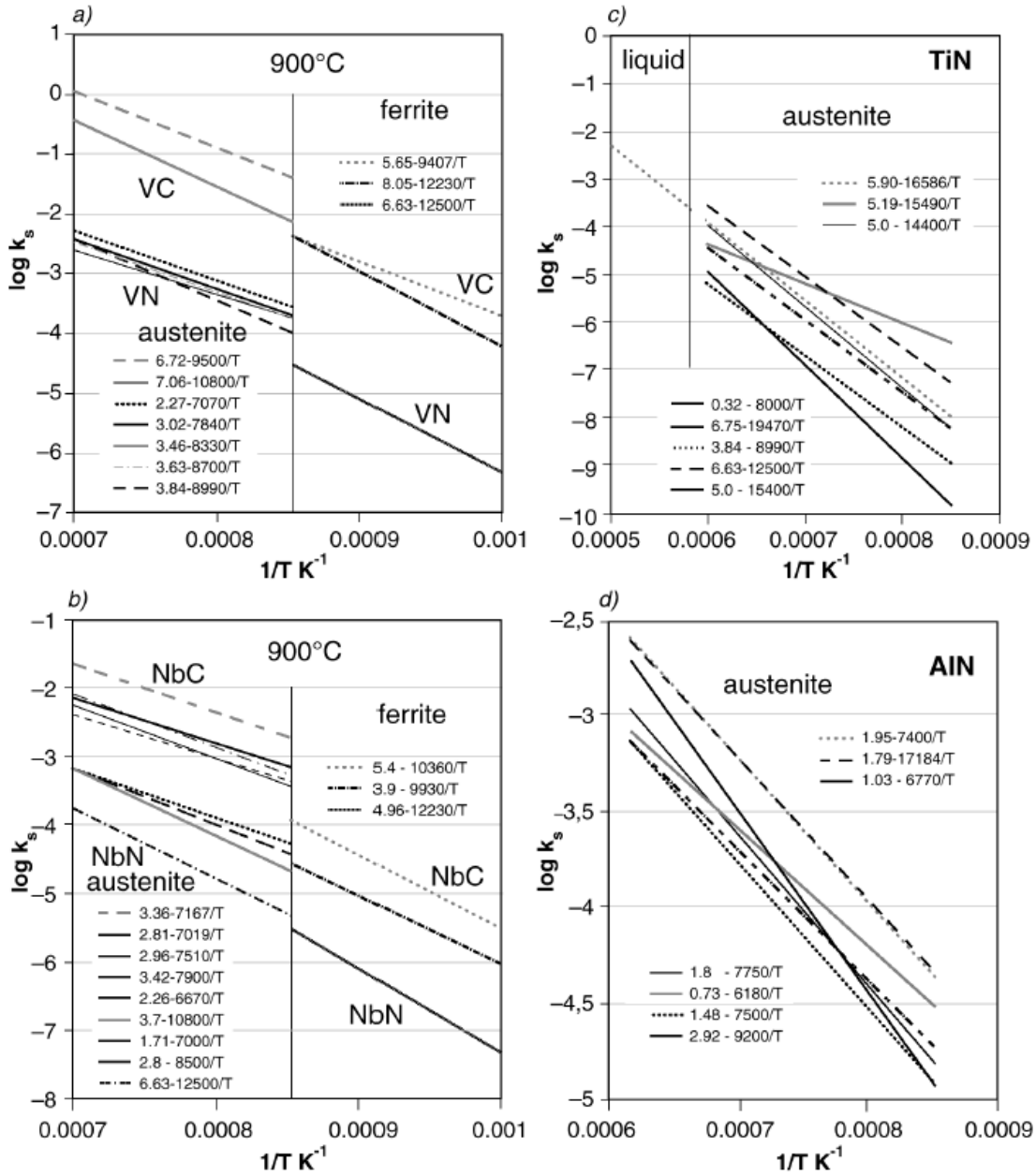

Figure 2-14: Solubility data for (a) VC and VN, (b) NbC and NbN, (c) TiN and (d) AlN [28]

2.5.3.1 Fe-V-C-N system

Thermo-Calc calculations of precipitation of V(C,N) in steels microalloyed with vanadium are shown in Figure 2-15. For V-microalloyed steels the effect of manganese on the activity of V is especially important. Mn is known to increase the activity coefficient of V and at the same time decrease the activity coefficient of C. Also shown in this figure is the mole fraction of nitrogen in carbonitrides at various temperatures and for various nitrogen contents from hyperstoichiometric levels to zero. This shows that vanadium starts to precipitate in austenite as almost pure nitride, until practically all the nitrogen is consumed. When the nitrogen is about

to be exhausted there is a gradual transition to form mixed carbonitrides. Nitrogen rich vanadium carbonitrides may precipitate during or subsequent to the γ-α transformation. Precipitation during the transformation is a result of the solubility drop of the vanadium carbo-nitrides associated with the transformation from austenite to ferrite at a given temperature.

A significant feature of the solubility of vanadium carbide in austenite is that it is considerably higher than those of the other microalloy carbides and nitrides, suggesting that vanadium carbide will be completely dissolved even at low austenitising temperatures. [28]

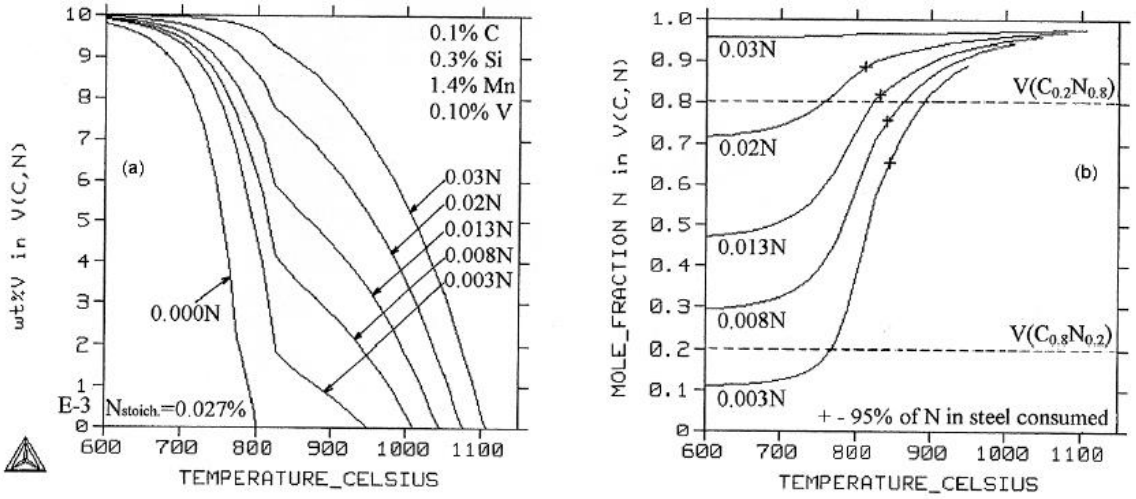

Figure 2-15: Precipitation of nitrides, nitrogen rich carbides and carbonitrides for 0.1% V [28]

2.5.3.2 Fe-Nb-C-N system

For Nb-alloyed steels, Figure 2-16 shows the difference in solubility between the nitride and the carbide, which is relatively small, mixed carbo-nitrides form at all nitrogen contents, even at the hyperstoichiometric levels. [29] Hence, for realistic contents of carbon and nitrogen in steel, relatively pure nitrides cannot form at all. Nb(C,N) is stable at low temperatures in austenite but dissolves at higher temperatures, for example, during re-heating prior to rolling. Nb(C,N) can precipitate quite readily in austenite under deformation (strain induced precipitation) and the particles so formed resist grain growth and even recrystallization of the austenite during the intermittent deformation at lower temperatures. The deformed austenite structure transforms to fine grained ferrite on cooling, which imparts both high strength and toughness to controlled rolled steels. A further precipitation of the remaining niobium as smaller particles during cooling gives rise to additional strengthening. [28]

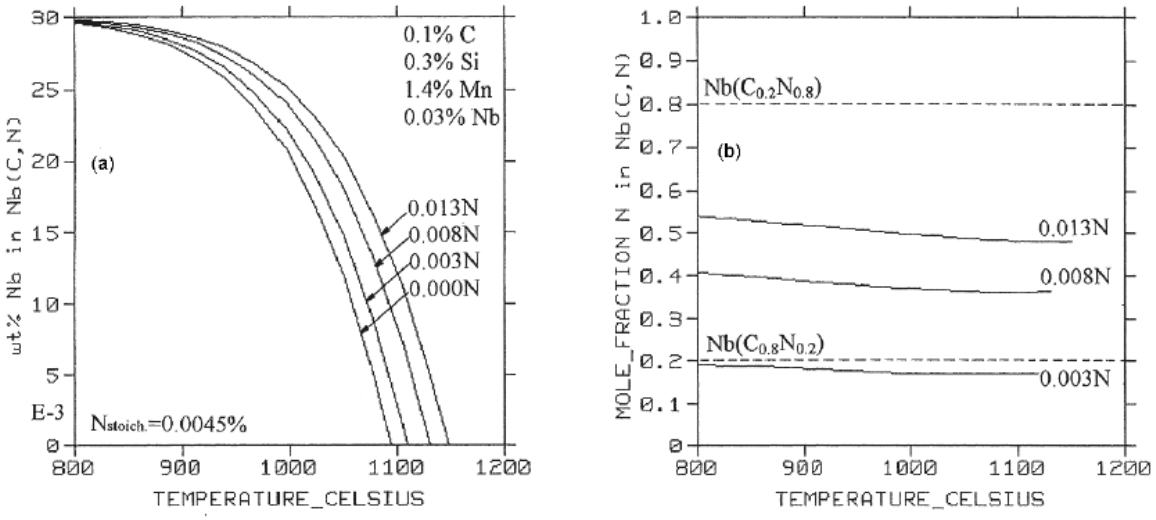

Figure 2-16: Precipitation of carbonitrides for 0.03% Nb [28]

2.5.3.3 Fe-Ti-C-N system

The calculated precipitation of TiN and TiC in steels microalloyed with titanium, is shown in Figure 2-17. Also shown in this figure is the mole fraction of nitrogen in carbo-nitrides at various temperatures for various nitrogen contents from hyperstoichiometric levels to zero. Titanium forms an extremely stable nitride TiN that is virtually insoluble in austenite and may be effective in restricting its grain growth during processing. Only a small titanium addition (about 0.01% Ti) is required for this purpose. If larger contents are present, the excess titanium can precipitate at lower temperatures as carbide TiC which contributes a precipitation hardening effect. This shows that the solubilities of titanium nitride and titanium carbide are significantly different and the precipitates formed in the austenite are almost pure nitrides, until practically all the nitrogen is consumed. It is worth noting that in the Ti-steel containing 0.01% Ti or less for controlling austenite grain size there is usually sufficient nitrogen to combine all Ti as TiN. When the nitrogen is about to be exhausted there is a gradual transition to form mixed carbo-nitrides. [28]

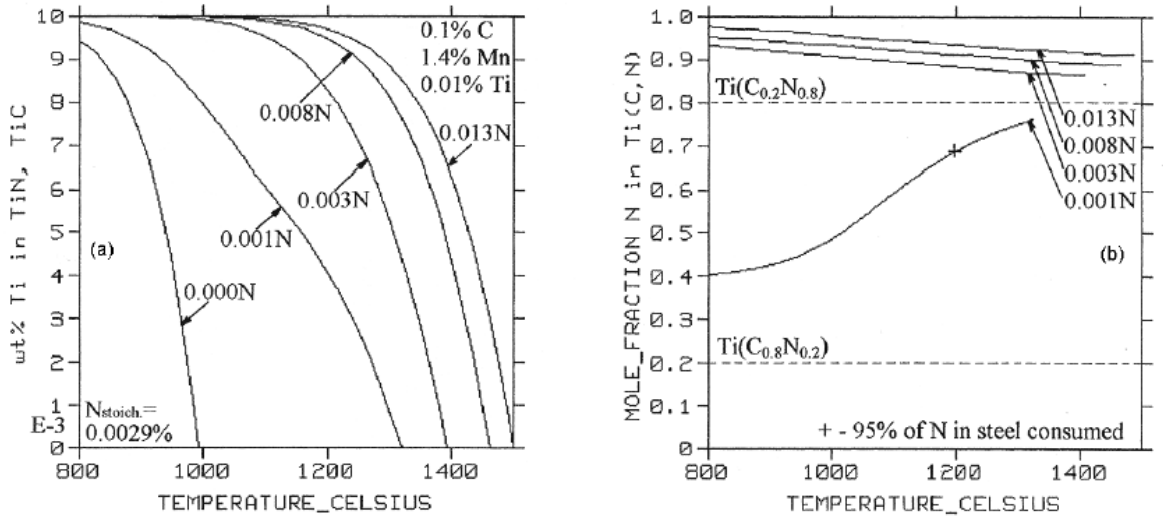

Figure 2-17: Precipitation of nitrides, nitrogen rich carbides and carbonitrides for 0.01% Ti [28]

Titanium exerts a strong affinity not only for carbon and nitrogen but also to other elements such as oxygen and sulphur. In Ti-microalloyed low-carbon steels the carbosulphide $Ti_4C_2S_2$ or sulphide TiS may form which remain undeformed during hot rolling. [30] $Ti_4C_2S_2$ is more stable than MnS and the formation of MnS is restrained by the addition of Ti to the steels. It is also clear that the formation of Ti-sulphides or carbosulphides will decrease the amount of Ti available for TiN and TiC. Therefore, for proper calculation of the precipitation of microalloyed carbides and nitrides the effect of all elements present in the steel must be considered. [28]

2.5.3.4 Fe-Al-N system

Aluminium is not usually classified as a microalloying element. The precipitation of AlN can, however, have strong effects on the properties of microalloyed steel, which are at least as significant as those produced by Nb, V or Ti additions. Al-killed steels have long been known to show improved strain ageing resistance and enhanced deep drawability, and for many years the term aluminium grain refined has been synonymous with grain size control. [31] Aluminium is normally dissolved in austenite at high temperature prior to rolling but the nitride phase is thermodynamically stable at lower temperatures. However, AlN nucleates with some difficulty in steel and has a widely different morphology from other nitrides. [32] AlN precipitation in ferrite has been extensively studied in connection with the development of favourable crystallographic textures. Considerably less investigation has been made into the precipitation of AlN in austenite. It is well known that the kinetics of AlN precipitation in austenite are generally slow and dependent upon thermal history.

2.5.3.5 Chemical composition of precipitation of multi microalloyed steels

The carbides and nitrides of V, Ti and Nb show extensive mutual solubilities which arises from the fact that they have the same cubic crystal structure and have very similar lattice parameters. The precipitation of carbo-nitrides in multiple microalloyed steels with V, Nb, Ti and Al is shown in Figure 2-18 (a), where the soluble components are expressed as a function of temperature. In Figure 2-18 (b) the mole fraction of Ti, Nb and V in M(C,N) is also included. As expected, the major part of the precipitate at the highest temperatures is TiN whilst further precipitation at lower temperatures is predominantly Nb(C,N). Thus, the primary precipitates to be formed in austenite are composite (Ti,Nb)-nitrides. The Ti and Nb contents of those depend on steel composition and precipitation temperature. Thermodynamic calculations imply that at the high temperature of 1200°C, primary (Ti,Nb,V)N particles contain ~20% of Nb and ~5% of V for multiple microalloyed steels. It is clear from this figure that the volume fraction of microalloy nitrides at high temperatures will be considerably larger in the Ti-Nb-V steel than in the single microalloyed steels. It may also be seen that AlN (with close packed hexagonal structure) has little or no solubility for other microalloying elements and starts to precipitate above 1200°C in the presence of 0.035% Al. [28]

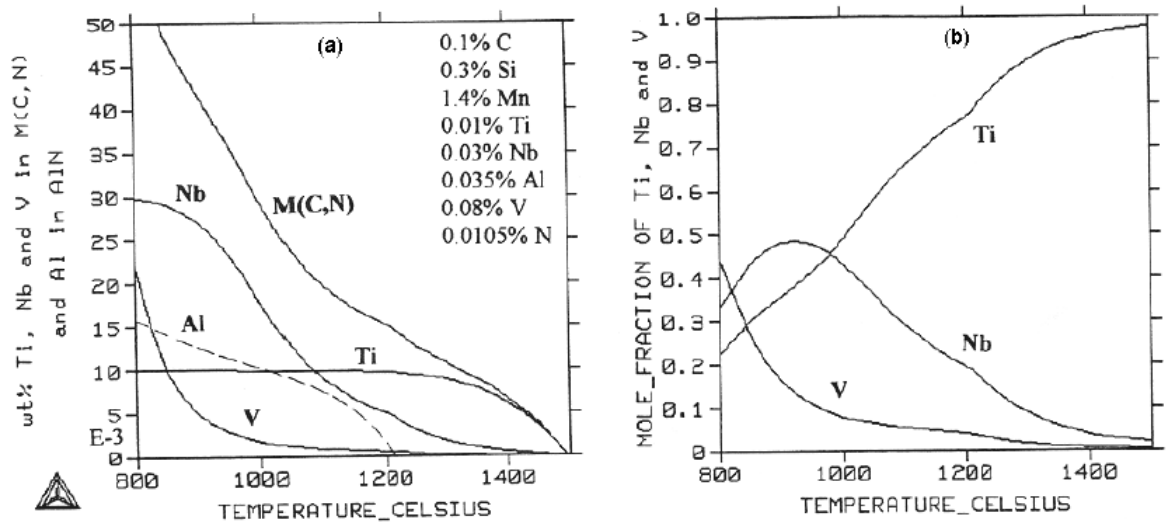

Figure 2-18: Precipitation in multi microalloyed steels [28]

It should be mentioned, however, that the uniform composition of second phase particles suggested from the thermodynamic calculations is often not the true situation in practice. The particles are frequently cored, reflecting the high temperature stability of a titanium-rich and nitrogen-rich compound in the interior of the particle with relative enrichment of Nb and V towards the surface of the particle. This suggests that these primary composite nitrides can act as nucleation centres for subsequently precipitation at relatively low temperatures, for

example forming a NbN-deposit around a core of TiN. Similar results have been obtained for Nb-V steels where niobium-vanadium nitrides have shown Nb and N enrichment in the precipitates, in accord with the higher thermodynamic stability of NbN. These coring effects may be a result of very slow diffusion of Ti in carbo-nitrides or the existence of a miscibility gap. [28]

Another important aspect of multiple microalloying is that the niobium or vanadium tied up as (Ti,Nb,V)N particles is not available for subsequent thermo-mechanical treatment. Figure 2-18 (b) shows that a significant fraction of added niobium may remain undissolved even at high reheating temperatures and cannot contribute to retardation of recrystallization and precipitation strengthening. Vanadium, on the other hand, exhibits higher solubility and is therefore normally fully available for precipitation strengthening in ferrite. [28]

2.5.4 Thermodynamic driving force

The precipitation process proceeds at a perceptible rate only if there is a driving force, that is, a free energy difference between the product and parent phases. This driving force enters the steady state nucleation rate in a central way and must be known with some accuracy if nucleation rates are to be calculated, or even estimated. The chemical driving force for nucleation of VN and VC in V-microalloyed steels, determined from the HSLA database are illustrated in Figure 2-19. It can be seen that, as the temperature is decreased the driving force increases monotonically and changes slope after the austenite to ferrite transformation. The dominating effect of N on the driving force is clearly seen in this figure. [28]

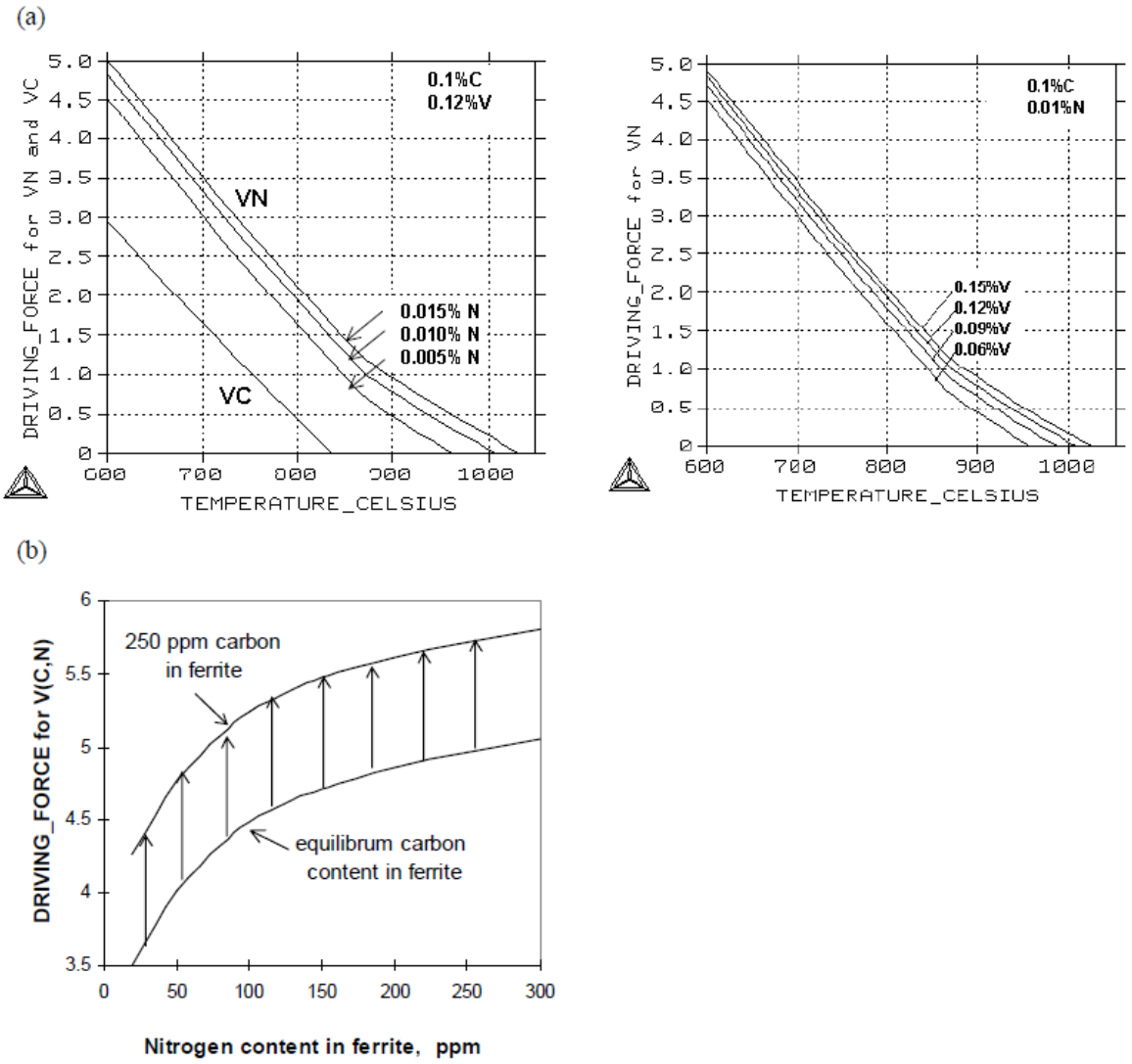

Figure 2-19: Chemical driving force for VC and VN [28]

2.5.5 Effects in austenite

In commercial V-microalloyed steels small amounts of Ti (~ 0.01%) are commonly added to prevent excessive grain coarsening at high temperatures. The technical background to this is that Ti reacts with the nitrogen in the steel to form a fine dispersion of very stable TiN. For this to occur in typical HSLA steels the normal levels of N in basic oxygen furnace (BOF) and electric arc furnace (EAF) steel making, i.e. 0.004 – 0.015%, are sufficient. However, to attain the fine TiN size necessary for effective grain growth control fast cooling is needed during the solidification of the steel, as in continuous casting of slabs or blooms. [28]

However, the TiN precipitation may be affected by a second microalloy addition, such as V, in various ways. This alone, but especially together with the formation of a second precipitate, may affect the grain coarsening behaviour significantly. [28]

It is also well established that TiN forms as a fine precipitate dispersion early after solidification in Ti-V and Ti-Nb HSLA-steels having less than about 0.02%Ti. At lower temperatures when the solubility of Nb(C,N) and V(C,N) has been exceeded many experimental studies have shown that these phases co-precipitate on already existing TiN-particles to a large extent. Of course, as the driving force for carbonitride formation increases at lower temperatures in the austenite regime the probability for nucleation of new carbonitride, rich in V or Nb and eventually pure V- or Nb-carbonitrides, increases. [28]

An interesting feature of (Ti,V)(C,N) precipitation found in austenite of Ti-V steels is that the particles exhibit compositional gradients such that the external parts are richer in V and the interior is richer in Ti. [33] Electron microscopy and microanalysis of the (Ti,V)- carbonitrides formed in austenite show furthermore that the compositional gradients of the particles are not always smooth. The outer V-rich part occurs commonly as dendrites. [34] At first this may appear natural in view of the sequential precipitation of Ti and V during cooling. However, a prerequisite is then that the interdiffusion of Ti and V in the (Ti,V)- carbonitride is substantially lower than in austenite. Otherwise there will be ample time for homogenisation of the elements to occur. [35]

2.5.5.1 Austenite grain growth behaviour

Grains in HSLA steels may coarsen either by normal primary grain coarsening or abnormal grain coarsening. The characteristic features of normal grain growth can be seen in steels without grain refining particles which show a gradual increase in grain size with increasing temperature. [36,37] In the presence of pinning particles however, the grain growth process frequently occurs by the growth of a few selected grains to abnormally large dimensions and other grains will not be able to grow until further particle coarsening has occurred. This type of grain growth is known as abnormal grain growth or secondary recrystallization. [38,39] Abnormal grain growth can only occur when normal grain growth is inhibited and is particularly likely to occur as the temperature is raised and as the particle dispersion becomes unstable. [40] The abnormal grain growth might occur due to the presence of additional heterogeneities, e.g. in the particle distribution. Where locally, the ratio of the particle size to the volume fraction is larger than the mean value, some grains might start to grow preferentially. [41]

Although there have been some studies of the effect of carbides and nitrides on the austenite grain coarsening temperature, however, there are still a number of questions pertaining to both the function of Al and Ti in vanadium microalloyed steels and their influence on austenite grain growth, which should be investigated further in order to understand the relative importance of the interaction of V with Al and Ti in microalloyed steels. The steels which are analysed are four commercial high strength Al-V-N steels and one Al-V-Ti-N steel whose compositions are given in Table 2-2. The specimens were austenitised for 0.5 hours in an argon atmosphere at temperatures between 900 °C and 1200 °C. [42]

The results of austenite grain coarsening behaviour as a function of temperature is shown in Figure 2-20. Except for the Al-V-Ti-N steel, all other Al-V-N steels clearly show two-stage grain growth. Below a critical temperature range, defined as the grain coarsening temperatures, the change in grain size is very small, while above this critical temperature range the grain size increases with temperature very rapidly. In the grain coarsening temperature ranges there is a duplex structure represented by the cross-hatching, there a kind of abnormal grain growth in the grain coarsening temperature range is occurring. When the temperatures were higher than the grain coarsening temperatures, the dissolution of precipitates in the steels allows more grains to grow, which is considered to be a normal process. It should be noted that this kind of two-stage grain growth and mixed grain growth behaviour will not be reflected if only the average of the grain size measurement is given. As expected for the Ti free steels, Steel 2 with high Al and N contents possesses the highest grain coarsening temperature, which is about 1100-1150 °C. The grain coarsening temperatures for the three low Al and N steels are about 950-1000 °C. Steel 1 with lowest volume fraction of AlN among these steels has the largest grain size at 950 °C. [42]

Table 2-2: Steel composition of experimental steels in weight percent [42]

No.	C [%]	Si [%]	Mn [%]	P [%]	S [%]	Al [%]	N [%]	V [%]	Ti [%]
1	0.13	0.30	1.43	0.010	0.003	0.032	0.002	0.10	-
2	0.12	0.31	1.43	0.011	0.002	0.037	0.015	0.10	-
3	0.12	0.31	1.45	0.011	0.003	0.026	0.0049	0.10	-
4	0.13	0.30	1.45	0.012	0.003	0.029	0.0043	0.049	-
Ti Steel	0.074	0.37	1.53	0.013	0.007	0.027	0.018	0.13	0.012

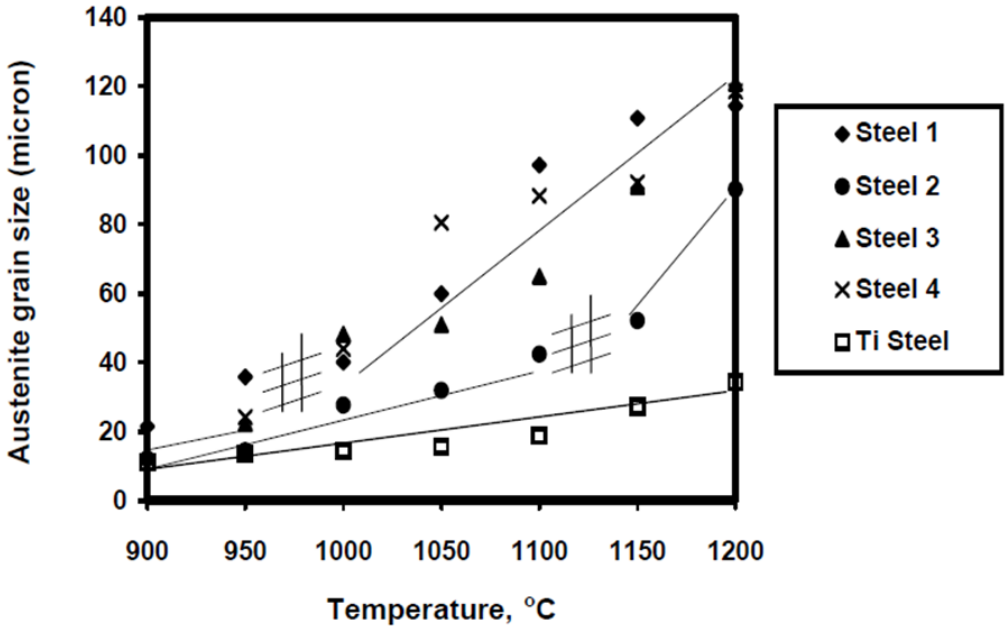

Figure 2-20: Austenite grain size over temperature for different steel grades [42]

From the bottom graph in Figure 2-20, it can be seen that compared with the austenite grain size of the other four Al-V-N steels, the Al-V-Ti-N steel has the smallest austenite grain size. Another obvious feature is that in contrast with other Al-V-N steels which followed an abnormal grain growth behaviour, the austenite grain growth of the Al-V-Ti-N steel retains a steady slow growth up to 1200 °C, i.e. it has the characteristics of normal grain growth. [42]

2.5.6 Effects on recrystallization

One of the most essential features of microalloying additions is their influence on recrystallization during controlled rolling, either to prevent recrystallization and thereby producing stretched austenite grains during hot deformation and conditioning the austenite to form fine ferrite grains during transformation, or to minimise their effect on recrystallization thereby allowing repeated recrystallization to occur during multiple deformation and a gradual refinement of austenite and the subsequent ferrite. The effect of the microalloying elements on recrystallization differs widely, especially so for V and Nb, as demonstrated in the classical graph due to Cuddy. [43] Figure 2-21 shows the recrystallization stop temperature as a function of the microalloy content (atom %), as dissolved when the hot deformation starts.

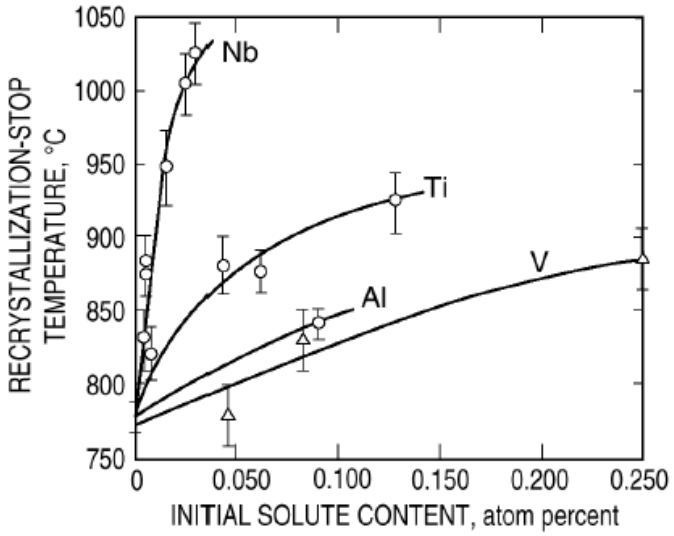

Figure 2-21: increase of recrystallization stop temperature [28]

The mechanism by which the microalloying elements act to raise the recrystallization stop temperature based either on solute drag [44,45,46] or particle pinning have been proposed. [47,48,49] The view most commonly upheld today seems to be that strain-induced microalloy carbonitrides formed during the hot deformation suppress recrystallization during the interpass time. For Nb-steels convincing evidence has been presented that the pinning force created by the observed Nb carbonitride dispersion at the recrystallization stop temperature exceeds that of the driving force for recrystallization. [50,51]

2.5.6.1 Effects of Nb, Mo and V on recrystallization kinetics of austenite

The interaction of microadditions in steel in a solid state depends on their state under conditions of performed plastic working. Microadditions dissolved in a solid solution raise the temperature of recrystallization of plastically deformed austenite as a result of segregation on dislocations and grain boundaries, causing decrease of recovery rate and mobility of grain boundaries. Instead, microadditions precipitating on dislocations in the form of dispersive particles of MX interstitial phases, slow down the course of dynamic recovery and possibly also dynamic recrystallization during the plastic deformation and additionally decrease the rate of thermal recovery and static or metadynamic recrystallization and limit grain growth of recrystallized austenite in the intervals between successive stages of deformation and after its finish. [52,53,54,55] The impact of concentration of several elements, dissolved in a solid solution or bounded in dispersive carbide particles, on the course of thermal recovery and static recrystallization of austenite at the temperature of 1000 °C and 900 °C of steel consisting of 0.05% C, 1.2% Mn and 0.3% Si, after hot deformation with a rate of 2 s^{-1}, is presented in

Figure 2-22. Segments of lines with small slope to the time axis, running from the beginning of the system, correspond with the course of static recovery. The remaining parts of kinetic curves describe the course of static recrystallization. Comparison of these curves indicates that the decrease of plastic strain temperature and decrease of isothermal holding temperature from 1000 to 900 °C causes considerable extension of recovery time and decrease of austenite recrystallization rate. In case of presented steel, at the temperature of 1000 °C, Mo and partially V can be found in austenite in a dissolved state. In comparison with Mo and V, stronger influence on decreasing the rate of the course of these two thermally activated processes, is exerted by Nb, which prevailing part at this temperature is bounded in dispersive NbC carbide particles formed on dislocations in plastically deformed austenite. The strongest impact on increasing the time of recovery and recrystallization is caused by contribution of segregation of dissolved atoms and dispersive carbides, which applies to steels containing Nb and V, and in particular, containing Mo, Nb and V (Figure 2-22 a). The $t_{0.5}$ time necessary to form 50% fraction of austenite recrystallized at such temperature of steel with basic composition is equal approximately 1.5 s and increases up to 80 s when adding Mo, Nb and V in a given concentration, and the time of complete recrystallization of austenite increases even more, from about 20 to 2000 s. Broken lines marked in the figure define the probable course of the kinetic curves without the influence of dispersive carbide particles. Inhibiting impact of alloying constituents introduced into steel on the course of recovery and static recrystallization of austenite is particularly effectively noted after decreasing the temperature of plastic deformation and the temperature of isothermal holding to 900 °C (Figure 2-22 b). [56]

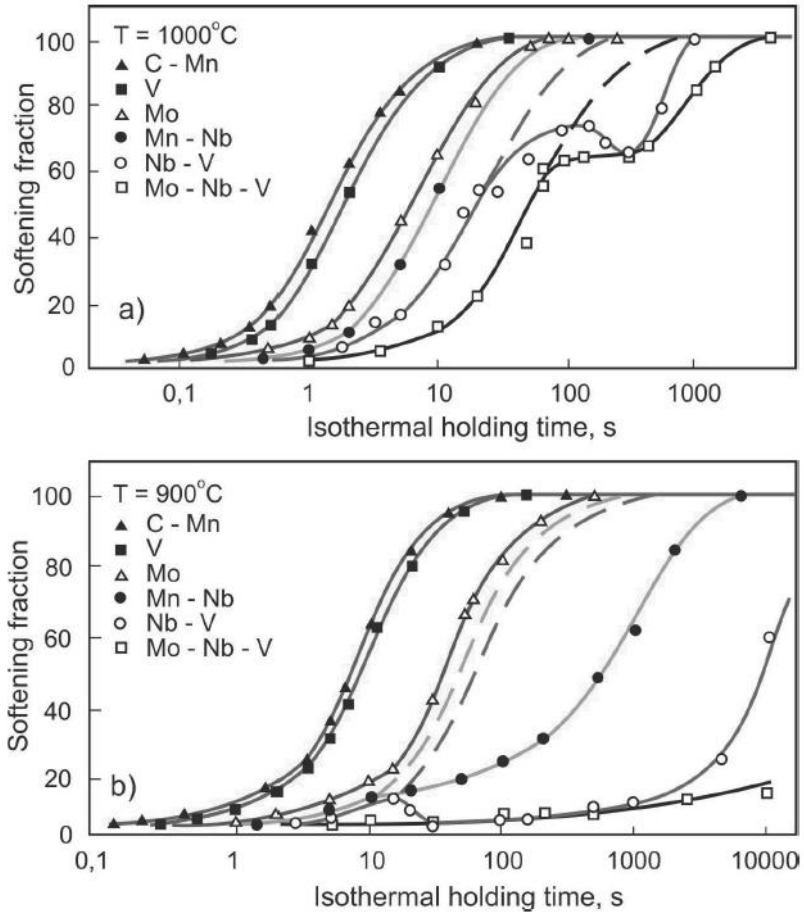

Figure 2-22: Influence of microalloying additions on recovery and recrystallization; a) 1000 °C b) 900 °C [56]

At such temperature, Mo and a slight portion of introduced V can be found in a solid solution in dissolved state. Nb and the remaining part of V are bounded into NbC and VC or V_4C_3 carbides, respectively. In this case, the $t_{0.5}$ time of austenite of steel with base composition is equal approximately 9 s and increases up to about 10^4 s when microadditions of Nb and V are introduced into steel. The grade of decay of strain hardening of austenite of steel with addition of Mo, Nb and V, caused by the recovery and static recrystallization at the temperature of 900°C after mentioned time of soaking, is equal only 20%. [57].

In addition, performed analysis indicates that apart from the temperature, considerable influence on recovery and static recrystallization kinetics is exerted by chemical and phase composition of steel. The t_R time of total recrystallization of alloy and unalloyed steels containing microadditions of elements with high chemical affinity for carbon and nitrogen, bounded in dispersive particles of carbides, carbonitrides or nitrides at recrystallization temperature, may be long. For that reason, the $t_{0.5}$ has a greater significance for technical purpose than t_R time. [58,59]

2.5.7 Effects on transformation

The primary parameters controlling the ferrite grain size produced in the austenite-ferrite transformation are the effective austenite grain boundary area, i.e. austenite grain boundary area/unit volume S_V, and the cooling rate. [28]

However, for Nb-microalloyed steels it has been shown that for a given S_V the ferrite grain size is smaller when transformed from unrecrystallized, deformed and flattened austenite grains than from recrystallized, equiaxed grains. [60] Traditionally this difference has been accounted for by the additional ferrite nucleation that takes place in the deformation bands of heavily deformed austenite. Interestingly though when the same type of experiments were conducted for V- and Ti-V-microalloyed steels no difference is found. [61,62] Deformed, unrecrystallized austenite grains transform to ferrite with virtually the same grain size as that produced from equiaxed, recrystallized austenite, Figure 2-23. Thus, for the V-steels the ferrite grain size is found to be independent of austenite grain shape and processing method. [28]

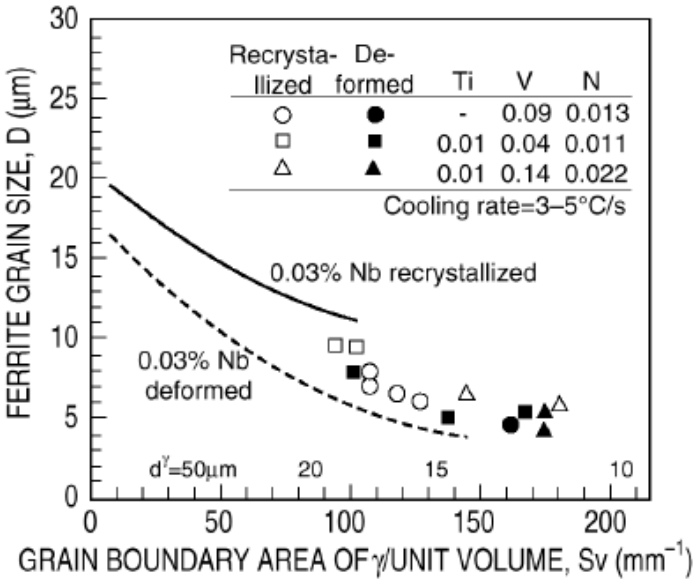

Figure 2-23: Ferrite grain size in dependence on grain boundary area [28]

As can be seen from the figure the V-steels occupy an intermediate position between the lines for recrystallized and unrecrystallized Nb-steels. An essential result is that the same degree of ferrite grain refinement can be achieved for the V-steels as for the Nb-steels, viz. about 4 μm, provided the effective austenite grain boundary area is large enough. An important and interesting feature of Ti-V and V-steels is that additional N above a level of ~ 0.003% further refines the ferrite during the austenite-ferrite transformation. [34,63,64]

2.5.8 Effects in ferrite

As regards strengthening, the effective V-carbonitrides are those formed in ferrite during the latest passage through the austenite-ferrite transformation. At equilibrium the circumstances are such that a certain, small portion of the vanadium in microalloyed steel should precipitate in austenite, especially if the contents of vanadium and nitrogen are high. However, the kinetics of V(C,N) formation in austenite are sluggish and for processing at finishing temperatures higher than 1000 °C and for normal steel compositions virtually all vanadium will be available for precipitation in ferrite. [28]

Compared to the other microalloying elements, vanadium has a higher solubility and therefore remains in solution to a much larger extent during processing in the austenite range.

Precipitation of V-carbonitrides can occur randomly in ferrite in the wake of the migrating austenite-ferrite (γ-α) boundary as general precipitation or by interphase precipitation characterised by the development of sheets of particles parallel to the γ/α-interface formed repeatedly with regular spacing. Many investigations have shown that for compositions typical of structural steels the general precipitation takes place at lower temperatures, typically below 700 °C, and the interphase precipitation at higher temperatures. [28]

It is now a well-established fact, demonstrated in several electron microscopy studies, that V(C,N)-particles are also formed in the pearlitic ferrite. Because of the lower transformation temperatures of pearlite this type of precipitation is usually finer. [65]

V-carbonitrides are sometimes observed in a fibrous morphology when cooling is slow or on holding at high temperature in the γ/α range. The typical feature of this mode of precipitation is that the fibres are perpendicular to the γ/α interface. This mode of precipitation is a distorted form of eutectoid $\gamma \rightarrow \alpha + V(C,N)$ transformation. By realising that this type of decomposition is driven by a V-gradient ahead of the α/V(C,N) interface and parallel to it given by the γ/V(C,N)- and γ/α-equilibria and producing the necessary lateral redistribution of V from γ into α+V(C,N), it may be shown by analysing isothermal sections of the Fe-V-C system that this kind of eutectoid can only form from certain austenite compositions corresponding to relatively low supersaturation. It places furthermore, restrictions on the appearance of the phase diagram. In particular, the (γ+α)/γ equilibrium surface must slope with increasing V-content to give room for this type of eutectoid transformation. [28]

2.5.8.1 Interphase precipitation

Interphase precipitations are formed in sheets parallel to the γ/α-interface by repeated nucleation of particles as the transformation front moves through the austenite. For this type

of steel composition, it is normally observed in the temperature range 800-700 °C. Despite its clear relation to the migrating γ/α-interface there has been discussions in the literature whether the interphase precipitation nucleates in the boundary, ahead of it in the austenite or behind it in the ferrite. However, firm experimental evidence now exists showing that it actually nucleates in the interface. [65] By electron microscopy of steels with high alloy contents that stabilise the austenite to room temperature it has been possible to directly observe V(C,N)-particles in the γ/α-boundary. At lower temperatures where the driving force is large we should expect general nucleation in the ferrite matrix to occur.

Also a narrow region of high carbon austenite together with the rapidly moving γ/α-boundary will not make austenite the preferred site of nucleation. Instead, heterogeneous nucleation at the interface will be the energetically favoured site. [66]

At high transformation temperatures, about 800 °C, for typical compositions of V-microalloyed structural steels the interphase precipitation consists of irregularly spaced, and often curved sheets of V(C,N)-particles. From about 700 °C the interphase precipitation is commonly found to be incomplete, and random precipitation from supersaturated ferrite after the γ/α-transformation takes over progressively with decreasing temperature.

A characteristic feature of interphase precipitation is that it becomes more refined at lower temperatures. [67,68]

2.5.8.2 Mechanism of interphase precipitation

Following models that have been proposed to explain the phenomenon fall broadly into two categories: ledge mechanisms and models based on solute diffusion control. [69,70] It was suggested that interphase particles form heterogeneously on γ/α-boundaries thereby pinning their migration normal to the boundary. Local breakaway leads to formation of mobile ledges. The ledges move sideways while the remaining part of the released boundary is stationary and enables repeated particle nucleation to occur, forming a new sheet. Hence, in this mechanism the intersheet spacing will be determined by the ledge height.

Among the models based on diffusion control the solute-depletion model due to Roberts is the most prominent and promising one. [71] The quantitative description of the solute-depletion model due to Lagneborg and Zajac considers a ferrite grain growing into austenite where the growth is controlled by carbon diffusion in austenite while maintaining local equilibrium at the interface. At a given point of this growth the interplay is analysed between the nucleation of V(C,N)-particles in the γ/α-interface, the accompanying growth of V-depleted zones around the precipitates, and the continued migration of the γ/α-boundary away from the precipitate sheet. The growth rate of a V-depleted zone is infinitely large directly after nucleation but

declines gradually with time according to a parabolic growth law. The growth of the ferrite obeys a similar parabolic time-law, but its rate can be considered constant for the short distance corresponding to the intersheet spacing relative to the size of the ferrite grain. The implication of this is that the moving γ/α-interface will after nucleation initially be in a V depleted zone, but will eventually catch up the growing depleted zone. The boundary has now returned into material with the original V-content, and nucleation of a sheet of particles will repeat itself. [28]

2.5.8.3 General precipitation

For compositions typical of V-microalloyed steels, 0.10%C-0.10%V, general precipitation of V(C,N) occurs in a temperature range from about 700 °C and below. As already discussed in the previous section this transition from interphase to general precipitation can be predicted by the solute-depletion model. [28]

Experimentally it is established that VN has a considerably lower solubility than VC, both in ferrite and austenite. The thermodynamic background to this is the much larger chemical driving force for formation of VN. This larger chemical driving force makes N-rich V(C,N) the preferred precipitation as long as there is sufficient nitrogen in the matrix. Only when the nitrogen content falls below about 0.005% that the initial V(C,N) starts to increase its C-content.

A technically very important finding is that the precipitate size diminishes considerably with increasing nitrogen content in the steel. [68] This is accompanied by a concurrent increase of precipitate density. These effects must be accounted for by an increased nucleation frequency as a result of the larger chemical driving force for precipitation of nitrogen-rich V(C,N). The difference in precipitate growth between high and low-N steels cannot be explained by differences in coalescence. Instead, it must be interpreted as resulting from the denser particle nucleation in the high-N material, thereby producing an earlier soft impingement of V-denuded zones and so slowing down the precipitate growth. [28]

In V-microalloyed steels it has been shown that the observed precipitation strengthening originates seemingly only from N-rich V(C,N), despite the fact that there is abundant V to combine with the carbon dissolved in ferrite. The normal explanation of this behaviour has been that when the first formed N-rich precipitates have consumed practically all nitrogen the chemical driving force for formation of C-rich V(C,N) is too small for profuse precipitation to occur and hence no added strength is observed. However, this issue is complex, and recently it has been shown that under certain conditions the C-content in the steel can add significantly to precipitation strengthening. [28]

2.5.8.4 Strengthening mechanism

Vanadium in structural steels dissolve in austenite at relatively low temperatures, unlike the other microalloying elements, and therefore can contribute fully to precipitation strengthening when the steel is cooled into the α phase, V is usually the preferred element when precipitation strengthening is wanted. A modest addition of 0.10%V can bring about a strength increase of about 250 MPa to 300 MPa. Another essential feature of V-steels is that nitrogen in small contents lead significantly to precipitation strengthening. Similarly, enhanced cooling through the γ/α-transformation and afterwards augments the particle hardening. [28]

Yield stresses for different V alloyed steels and under different conditions are summarized in Figure 2-24, where continuous cooling results are shown in (a) to (c) and isothermal treatments in (d) to (f). A similarity can be seen between all the figures where strength is plotted as a function of the nitrogen content. If the steel grades are separated into four classes according to carbon, vanadium and titanium content, there is in each case a nearly uniform gradient of about 5 MPa per 0.001% nitrogen. This is a clear confirmation of the preference for vanadium to form nitrides or nitrogen-rich carbonitrides. By an increasing nitrogen content, the chemical driving force for precipitation is also increased and the particles become finer and more numerous, thereby increasing the yield strength. [72]

For the isothermal transformed samples from Figure 2-24 (f) there can be seen a maximum of yield strength at about 600 °C. The loss of strength above 600 °C may be a combination of the coarser ferrite and smaller fraction of pearlite as well as a larger particle size for the vanadium containing precipitates. Below the 600 °C, the fall must be attributed to incomplete precipitation as more of the vanadium is retained in solid solution due to its low diffusivity at these temperatures. [72]

The effect of the cooling rate on strength is also of special interest as improved properties may be achieved without the addition of extra alloying elements in an economical way by accelerated cooling. Yield stresses plotted against the cooling rate (Figure 2-24 (c)) show an almost linear relationship with an slope of 25 MPa/°C/s. The more powerful effect of the cooling rate comes from the finer scaled precipitations of V(C,N) and in part as result of increased hardenability of the matrix. For example, the strong influence of carbon content at the highest cooling rate is probably mainly due to the occurrence of the hard phases such as bainite or martensite. [72]

A usual practice when considering the strength of structural steels is to express the yield strength by a series of terms representing the iron matrix, solid solution effects, grain size, precipitation hardening and in some cases the pearlite content. [73]

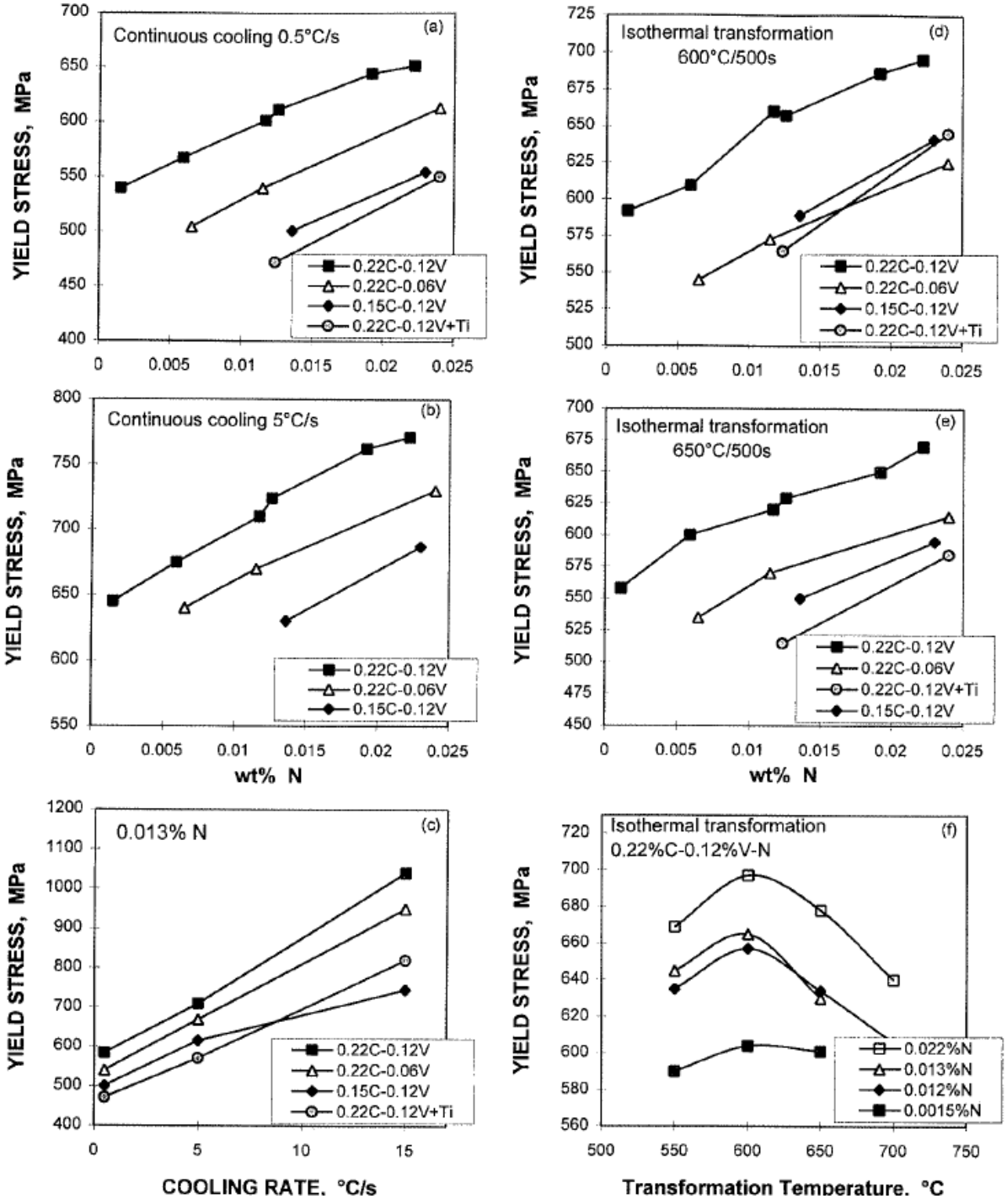

Figure 2-24: Yield stress as function of different parameters [72]

3 Experimental procedure

To optimize the process route for an improvement of the mechanical – technological properties a complete analysis of thick walled tubes (146 mm diameter and 12 mm wall thickness), especially in terms of intermediate cooling have been obtained in the experimental procedure. Therefore, three different steel grades with similar C level but differing micro-alloying element concepts were investigated under the same deformation history. The aim is to determine the effect of intermediate cooling for the different steel grades, to describe the phenomena occurring during all processing steps and finally describe the most economical operation mode. Furthermore, to increase the efficiency also a water quenching as intermediate cooling has been reviewed on tubes with 104 mm diameter and 15.84 mm wall thickness in this chapter.

3.1 Material selection

For the analysis three HSLA steel grades with the same Carbon level, but differing micro-alloying elements were chosen. A summary of the chemical composition of the grades are given in Table 3-1. Steel Grade A is the reference material without any addition of micro-alloying, whereas Steel Grade B is Vanadium microalloyed and Steel Grade C contains Niobium. These different alloying concepts should explain the effect of micro-alloying elements at different stages at the process route due to its variation of precipitation driving force. The main focus is on the intermediate cooling and the enclosed phase transformation and grain size development, resulting in optimized mechanical properties.

Table 3-1: Chemical composition

Steel grade	C [%]	Si [%]	Mn [%]	Nb [%]	V [%]
Steel Grade A	0.1541	0.2385	0.8775	0.0014	0.0036
Steel Grade B	0.1708	0.2870	1.3633	0.0017	0.0893
Steel Grade C	0.1667	0.2363	0.9220	0.0363	0.0040

3.2 Time - temperature development

The first investigated variable in the process of tube production is the temperature. Therefore, three different operational modes have been obtained to describe the limiting values for the effect of the intermediate cooling of tube blanks. These three operational modes are:

1) Conventional production route without intermediate cooling
2) Intermediate cooling of blank tubes before reheating
3) Rapid cooling in terms of spray water quenching of the blank tubes

Measured temperatures values direct from the process where used to describe the complete temperature progress from the rotary hearth furnace to the finish product in a finite difference method FDM model in MathCAD. [74,75]

The operation mode 1 and 2 were compared with all three steel grades in the tube dimension 146 x 12 mm, whereas mode 3 was analyzed with different cooling rates in the dimension 104 x 15.84 mm only on Steel Grade B, because Steel Grade A and C cannot build precipitation in that temperature range which were obtained in this area.

3.2.1 MathCAD simulation

The measured or specified temperatures for the experimental procedure were used to simulate the whole process with the FDM model. The outlet temperature from the rotary hearth furnace was measured with 1296 °C and builds the starting point of the process simulation. Furthermore, the inlet temperature into the push bench (1150 °C), the mandrel bar temperature (420 °C) and the reheating furnace temperatures (zone 1: 780 °C, zone 2: 850 °C, zone 3: 910 °C and zone 4: 930 °C) were specified in the simulation and during the rolling trial. The results for the different operational modes are shown in Figure 3-1. The red line in the chart describes the conventional production without intermediate cooling, the blue line the intermediate cooling of the tube blanks and the green one the water quenching in case of maximum cool rate as intermediate cooling.

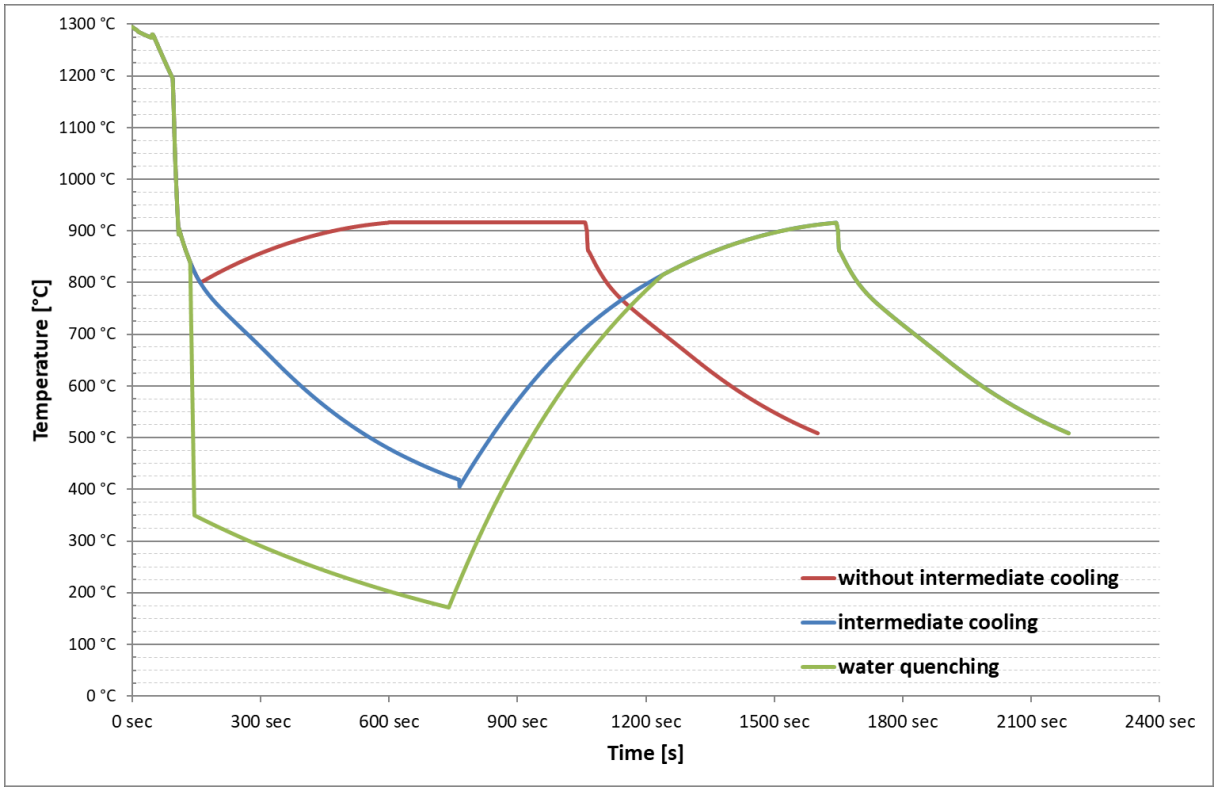

Figure 3-1: Time – temperature progress

3.3 Grain size and microstructure

The grain size is one of the most influencing parameter for the mechanical properties. A small grain size provides both higher strength and better toughness. Although the grain size influences the phase transformation and the recrystallization behavior. General a small and homogeneous grain size is requested, but due to the fact of the predetermined rolling plan and temperature, the microstructure is depending on these variables. A complete evaluation of the grain size and microstructure development through the production processes are therefore given in the next subchapters. All three steel grades were investigated from the bloom to the final tube with the different operational modes.

3.3.1 Bloom

As input material into the rotary hearth furnace casted round blooms with a diameter of about 230 mm are used. Figure 3-2 shows the casted microstructure of Steel Grade B (a) and Steel Grade C (b). Especially in Figure 3-2 (a) the casting structure with dendrites and secondary

arms can be seen. Microstructures like that are undesired for the final product due to the big grain size and inhomogeneous structure.

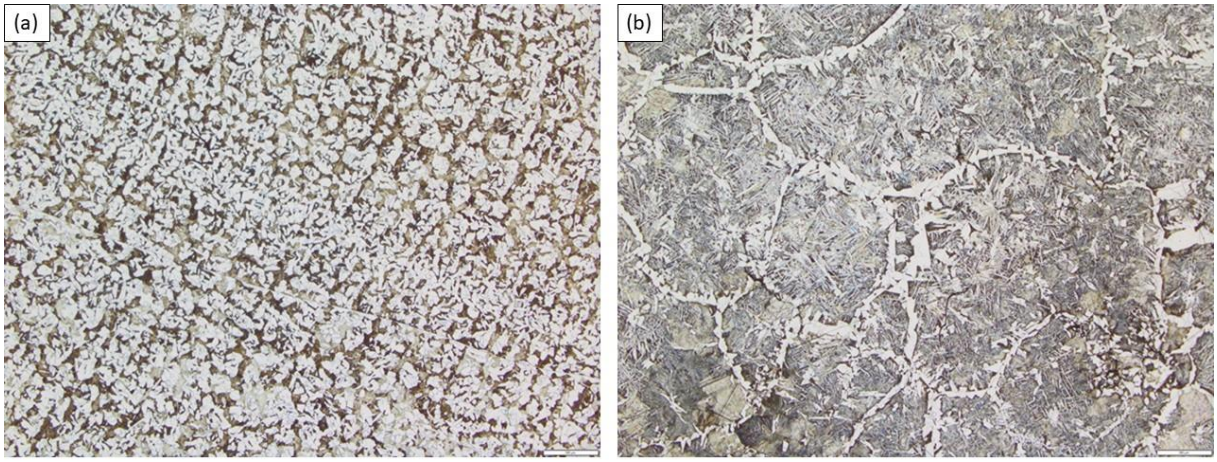

Figure 3-2: Cast microstructure of the blooms, 25x, scale: 500µm;
(a) Steel Grade B, (b) Steel Grade C

3.3.2 Bloom after rotary hearth furnace

The starting point in the time-temperature development is the bloom after the rotary hearth furnace. The microstructure has changed from the casted one to an austenitized structure in the furnace by a temperature of 1300 °C for about 3 hours. The austenite grain size of the furnace outlet is the input parameter for the whole tube rolling sequence. Therefore, samples of each steel grade has been heat-treated like in the rotary hearth furnace and water quenched. After a Bechet Beaujard etching of the prepared samples, the austenite grain size is analyzed under a light microscope. The results are shown in Figure 3-3, in which the biggest grain size is as expected obtained in Steel Grade A with no micro alloying additions and for this reason no inhibition against grain growth. The austenite grain size is at this stage of the process about 200 – 300 µm.

Figure 3-3: Microstructure after rotary hearth furnace, 50x, scale: 200µm;
(a) Steel Grade A, (b) Steel Grade B and (c) Steel Grade C

3.3.3 Hollows

After the cross rolling piercer, the bloom changed into a hollow. Due to the high strain, strain rate and temperature, complete static recrystallization is expected. Also the microscopic overview in Figure 3-4 confirms the assumption and demonstrates a totally new and recrystallized microstructure compared to the bloom. The microstructure after transformation of an air-cooled hollow is ferrite/pearlite with a grain size of about 25 – 40 µm. This big ferrite grains results from the big austenite grains after recrystallization and grain growth at a temperature after the cross roller piercer at about 1200 °C.

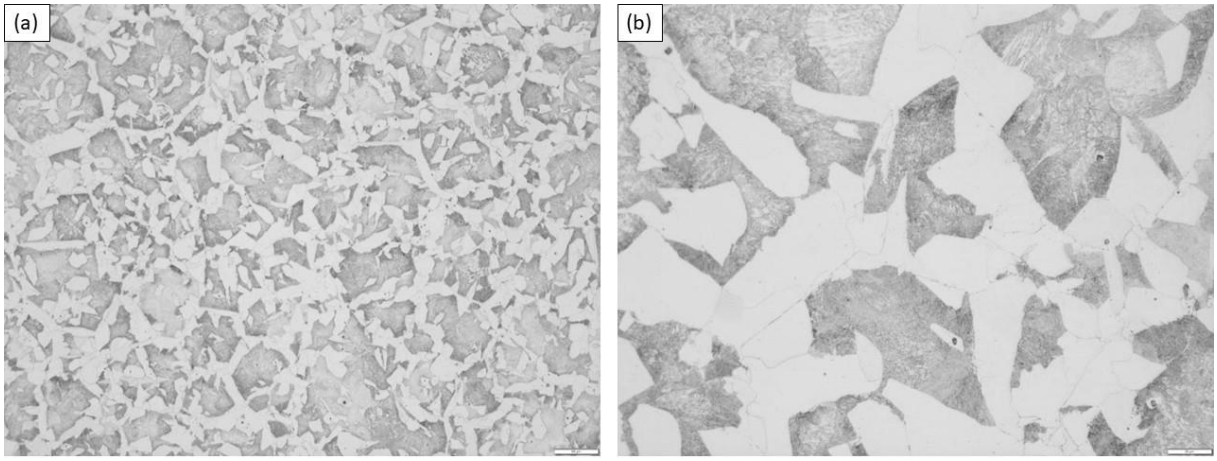

Figure 3-4: Recrystallized ferrite/pearlite microstructure after cross rolling
0.22% C-Mn-Si steel microalloyed with V and Nb (a) 100x, scale: 100µm and (b) 500x, scale: 20µm

3.3.4 Tube blanks

The second step in the tube production is the elongation with a mandrel bar in the push bench process. In this process the dimension of the resulting tube blanks in combination with the used rolling plan determines the strain, whereas the impact speed defines the strain rate. Records have shown that impact speed of 6.6 m/s provides best results in terms of tube blank geometry and was therefore used. Nevertheless, the input temperature was defined as standard rolling with a value of about 1150 °C. Due to the fact that only thick-walled tubes are analyzed, the strain and strain rates are relatively low, whereas the temperatures remains high. Furthermore, the last forming step in the push bench is only for a round and smooth surface and has in this case the smallest strain. After removing of the mandrel bar, the tube blank has a temperature of about 850 to 900 °C. The microstructure of the tube blanks are shown in Figure 3-5, (a) shows Steel Grade B with a Bechet Beaujard etched sample from a laboratory furnace trial and (b) an online sample direct quenched after the reeler.

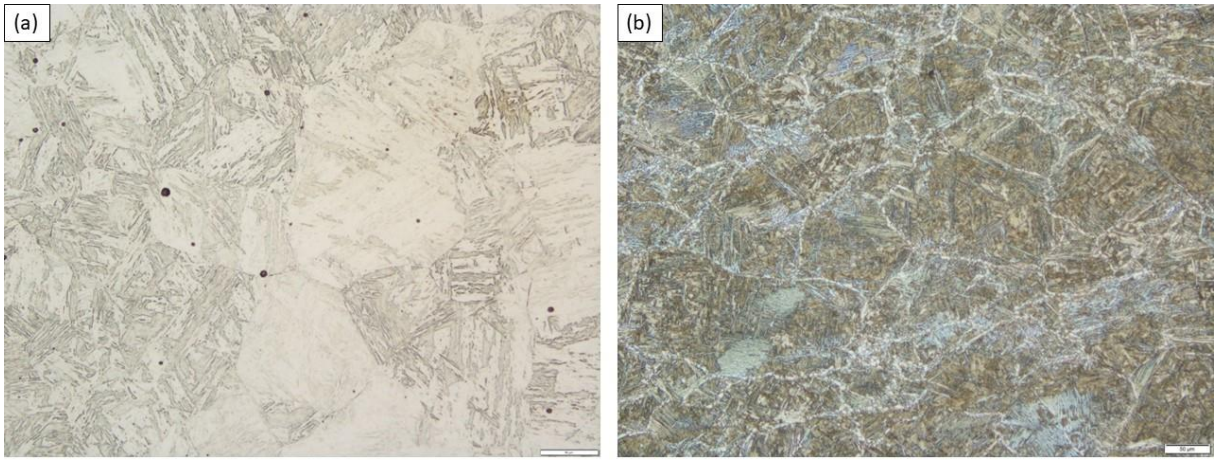

Figure 3-5: Austenite grain size after push bench and mandrel reeler, 200x, scale 50 µm
(a) Steel Grade B and (b) 0.22% C-Mn-Si steel

Both evaluations supply an unexpected big austenite grain size at this production step of 120µm for a strong deformed and recrystallized steel sample. This value for the grain size is now the new input parameter for the different operational modes. Till this step the process was the same for all trials and modes.

3.3.5 Intermediate cooling

For the operational mode 2 with intermediate cooling, the first main difference shall be analyzed in terms of optimization of the microstructure and mechanical properties. Also the effect of the intermediate cooling on precipitation shall be focused on.

First the microstructure and grain size of Steel Grade B of an air-cooled and phase transformed tube blank from the process as reference got compared to same pre-deformed and in the laboratory heat treated samples at varying temperatures. These laboratory samples got austenitized at different temperatures for an hour before they were air-cooled to room temperature and also investigated under the light microscope. The resulting microstructure with differing grain sizes are represented in Figure 3-6. In this figure it can be seen that the 1200 °C sample has nearly the same structure and grain size as the reference tube blanks. Furthermore, from this analysis, the before transformation austenite grain size of about 120µm is confirmed with Figure 2-20, which also shows this austenite grain size for a heat treatment at 1200 °C. Additional the phase transformed microstructures from the laboratory furnace heat treatment can in this way directly linked to an austenite grain size with the heat treatment temperature in Figure 2-20. For example, the 950 °C austenitized sample (which is approximately the temperature of the following reheating furnace) had an austenite grain size

of 40 µm and finally phase transformed a ferrite grain size of about 15µm. Compared to the existing grain size of the tube blank from the process, which is about 25 to 30 µm, nearly half the size. This affirms on the one side the effect of the intermediate cooling with a nearly halved ferrite grain size and a third austenite grain size due to the double phase transformation and on the other hand generates the time and driving force for precipitations at lower temperatures, especially for the V-alloyed Steel Grade B.

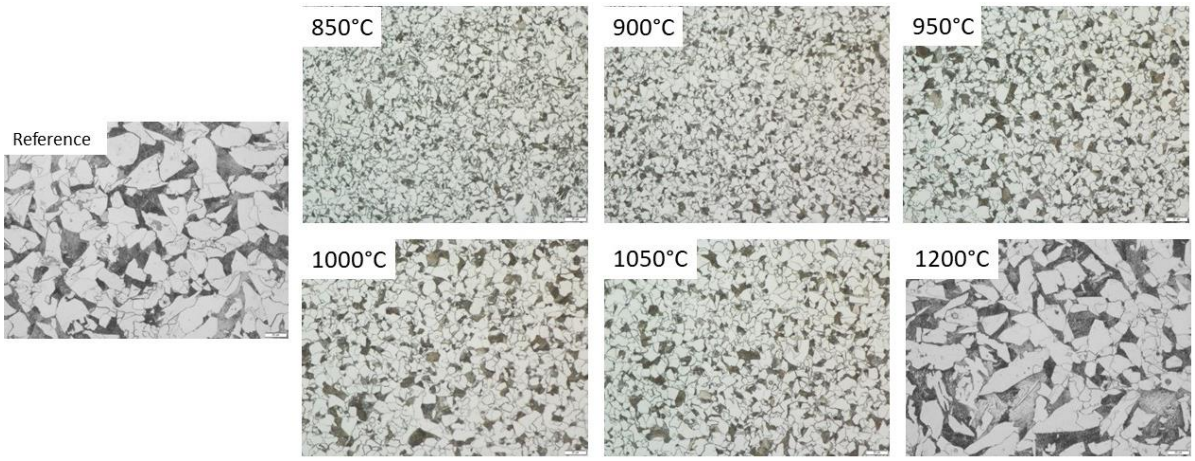

Figure 3-6: Grain size comparison between reference tube blank (Steel Grade B) after transformation on intermediate cooling with 1 hour austenitized samples at different temperatures

3.3.6 Grain size development

The grain size analysis in the last chapters served as indication points for the also carried out simulations in terms for the grain size development not only between each production steps, but for every single forming step from the used rolling plan. Here was the focus also from the output from the rotary hearth furnace till the releasing of the mandrel bar after the push bench.

As mentioned above, the starting value for the austenite grain size are the 300 µm after the rotary hearth furnace. All single deformation steps are structured in there predominate temperature, time, strain and strain rate and are listed in Table 3-2. This rolling plan is also calculated from the MathCAD model for the used dimension of 146 x 12 mm. In this table can be seen that the strain and strain rate of the cross rolling piercer is relatively high. The push bench set otherwise is continuously decreasing with each step.

The complete grain size development was calculated with the given parameters with JMatPro 10 and plotted in Figure 3-7. Also this simulation represents the output grain size of about 120 µm after the push bench, but it also can be seen that the grain size at push bench

set 8 is about 40µm and then increasing due to the low strain and the high temperature at the last deformation steps.

Table 3-2: Temperature, strain and strain rate for cross rolling and push bench set

	Temperature [K]	Time between each step[s]	Strain [-]	Strain rate [s^{-1}]
Cross rolling piecer	1513	38.100	1.40	3.3
Push bench set 1	1468	50.000	0.10	27.4
Push bench set 2	1435	0.260	0.10	33.1
Push bench set 3	1388	0.335	0.15	37.3
Push bench set 4	1330	0.450	0.20	40.7
Push bench set 5	1291	0.485	0.20	39.7
Push bench set 6	1256	0.450	0.20	35.2
Push bench set 7	1224	0.405	0.20	35.8
Push bench set 8	1195	0.370	0.06	29.9
Push bench set 9	1173	0.340	0.04	27.1
Push bench set 10	1158	0.190	0.02	22.9

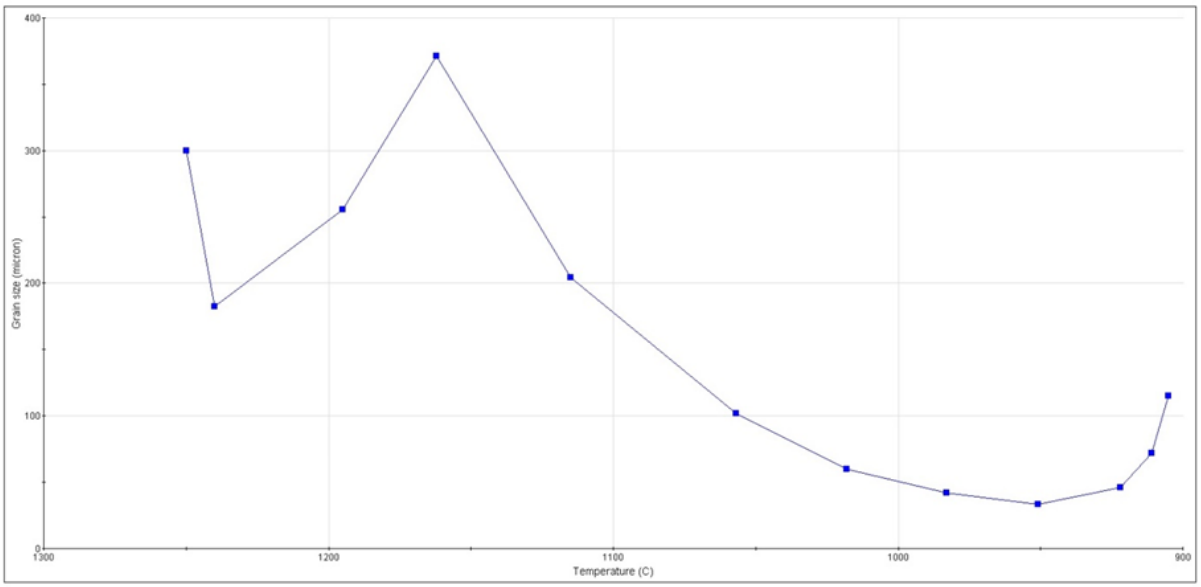

Figure 3-7: Grain size development during cross rolling and mandrel mill

3.4 Recrystallized fraction

With the same input parameters as in the last chapter the recrystallized fraction during the rolling process was calculated with JMatPro 10. Figure 3-8 shows this fraction over the temperature development. As seen from the chapter of the hollows, a full static recrystallization occurs in the step of the cross rolling. But in the push bench a maximum of 15% is statically recrystallized due to the fact of low strain and high speed of the hollow through the push bench and to less time for recrystallization.

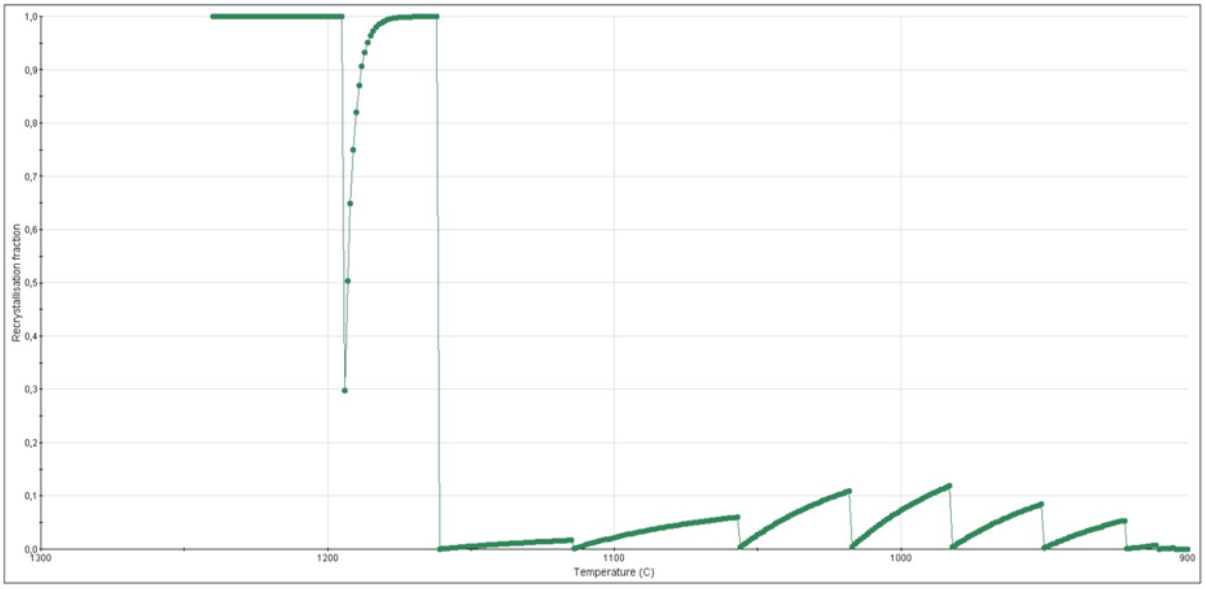

Figure 3-8: Static recrystallized fraction during cross rolling and mandrel mill

3.5 Phase transformation

At the operational mode 2 with intermediate cooling the tube blank underwent a phase transformation from austenite to ferrite/pearlite or ferrite/bainite, in operational mode 3 with accelerated cooling also martensite can be formed from austenite, depending on the cooling rate applied. To determine the resulting phase after transformation a continuous cooling transformation diagram CCT for all three steel grades have been recorded and got analyzed and compared to simulated ones in the following chapter.

3.5.1 CCT diagram

A continuous cooling transformation diagram CCT represents which types of phase change occurs at a different cooling rate. Therefore, the CCT diagram is calculated and exported with JMatPro 10 in Figure 3-9 for Steel Grade B, (a) for a grain size of 40µm and in (b) with a grain size of 120µm. These two grain sizes are chosen due to the fact that the grain size depending on the operational mode has either 40µm after the reheating furnace with intermediate cooling or 120µm for the austenite grain size of the tube blank from the rolling trail for thick wallet tubes.

Furthermore, a dilatometer recorded CCT diagram for Steel Grade B is given in Figure 3-10. In this diagram also the phase fractions are included in percent above each transformation curve reaches a new phase.

In addition to see the difference and influence of the grain size on transformation kinetics, Figure 3-11 shows an overlay of the JMatPro CCT diagrams of 40 µm and 120µm grain size. The bigger austenite grain size shifts all transformation curves to later times and this leads to more time required or lower temperature to reach the same phase transformation fraction. Also the completion of the whole transformation shifts to more time and much deeper temperatures, combined with the negative influence of bigger transformed ferrite grains in case of bigger austenite grains.

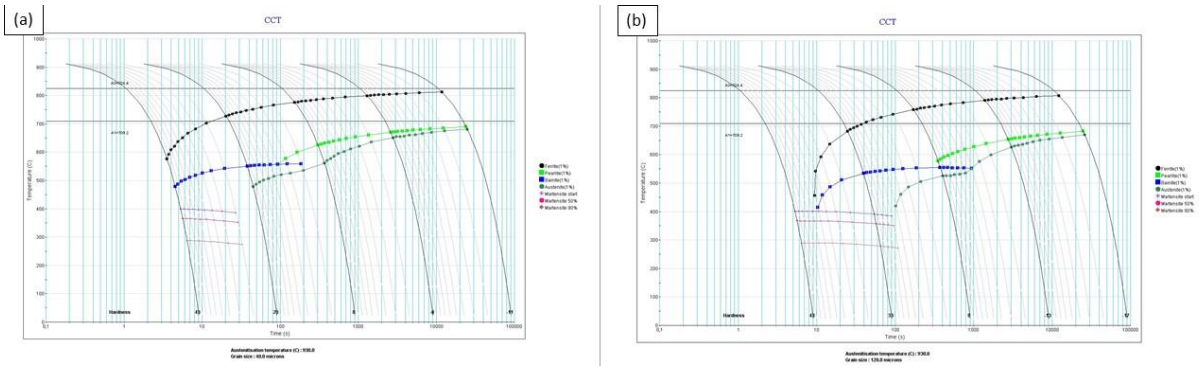

Figure 3-9: JMatPro CCT Diagram Steel Grade B for: (a) 40 µm (b) 120 µm grain size

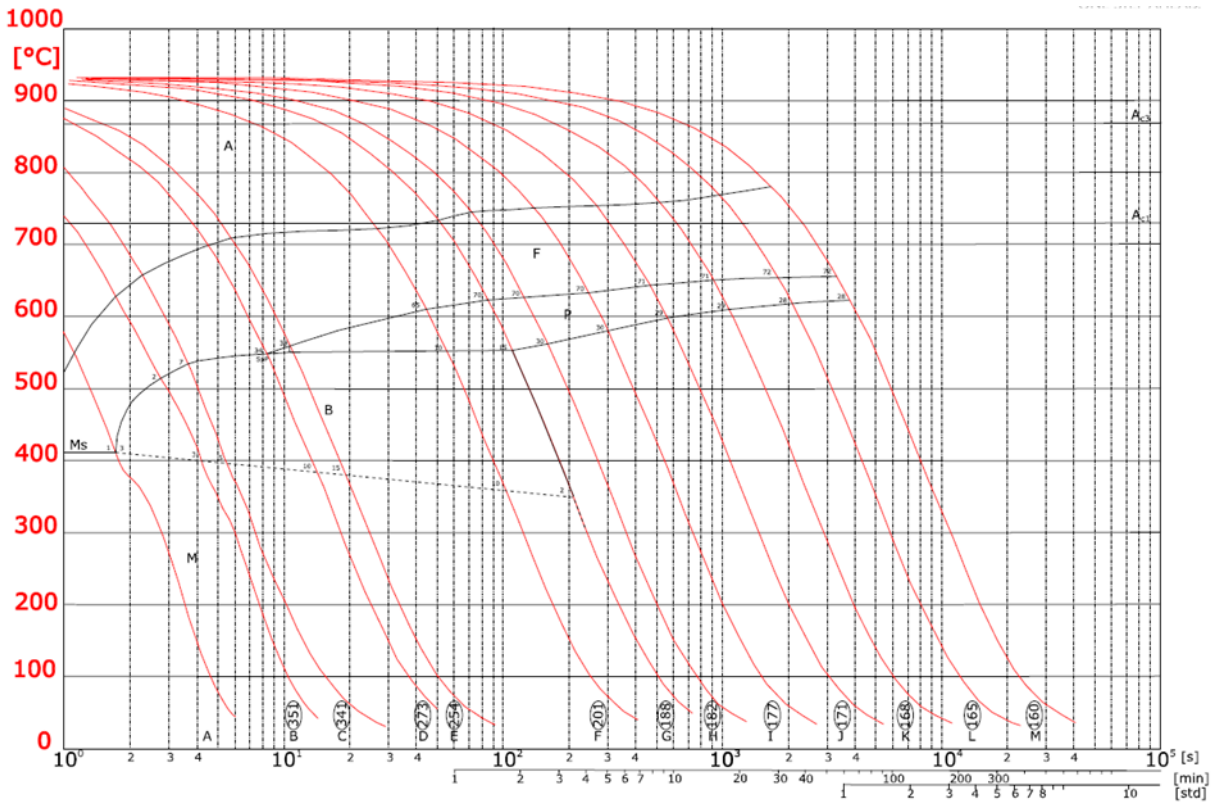

Figure 3-10: CCT Diagram: Dilatometer laboratory measurement of Steel Grade B: 40 µm austenite grain size (austenitized at 930 °C)

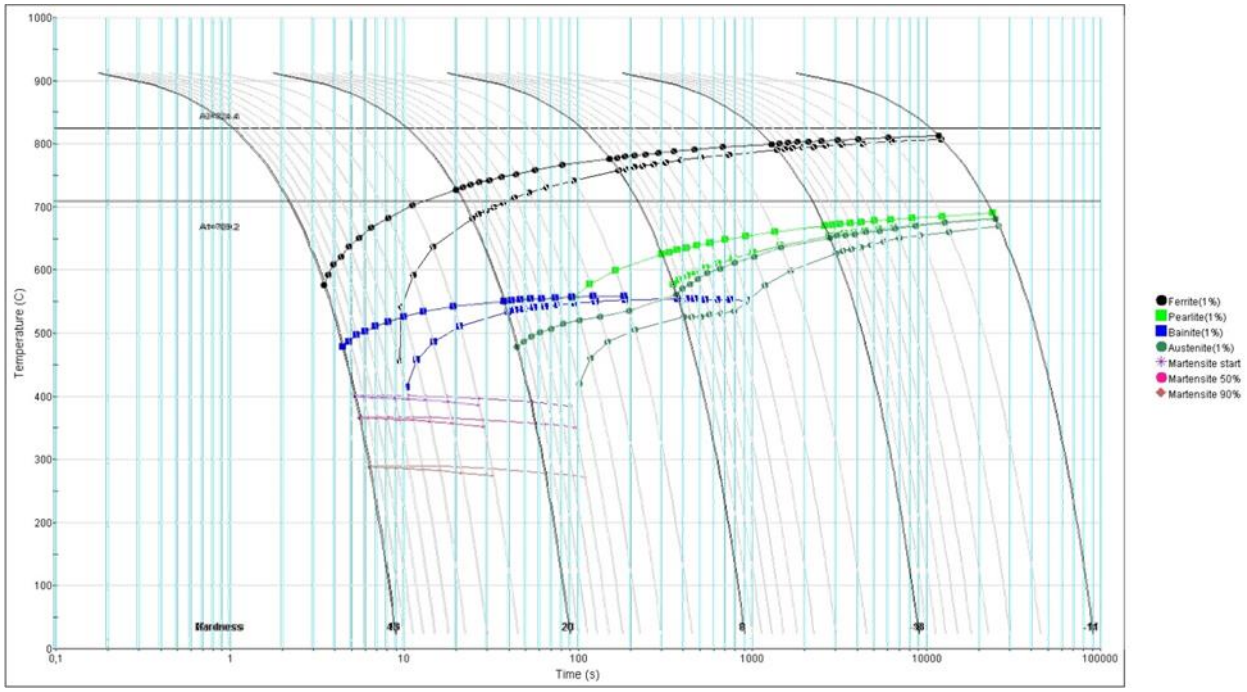

Figure 3-11: Overlain JMatPro CCT Diagrams for Steel Grade B with 40 µm and 120µm

A comparison of all three different CCT diagrams is shown in Figure 3-12, which also includes the cooling curve of the intermediate cooling for operational mode 2. In this figure can be seen, that the phase transformation end has a big dependence on the austenite grain size. The phase transformation end is about 50 °C lower and 100 s later with a grain size of 120 µm compared to 40 µm. This again reduces the efficiency of the process route and needs more time to fulfil a complete phase transformation before reheating.

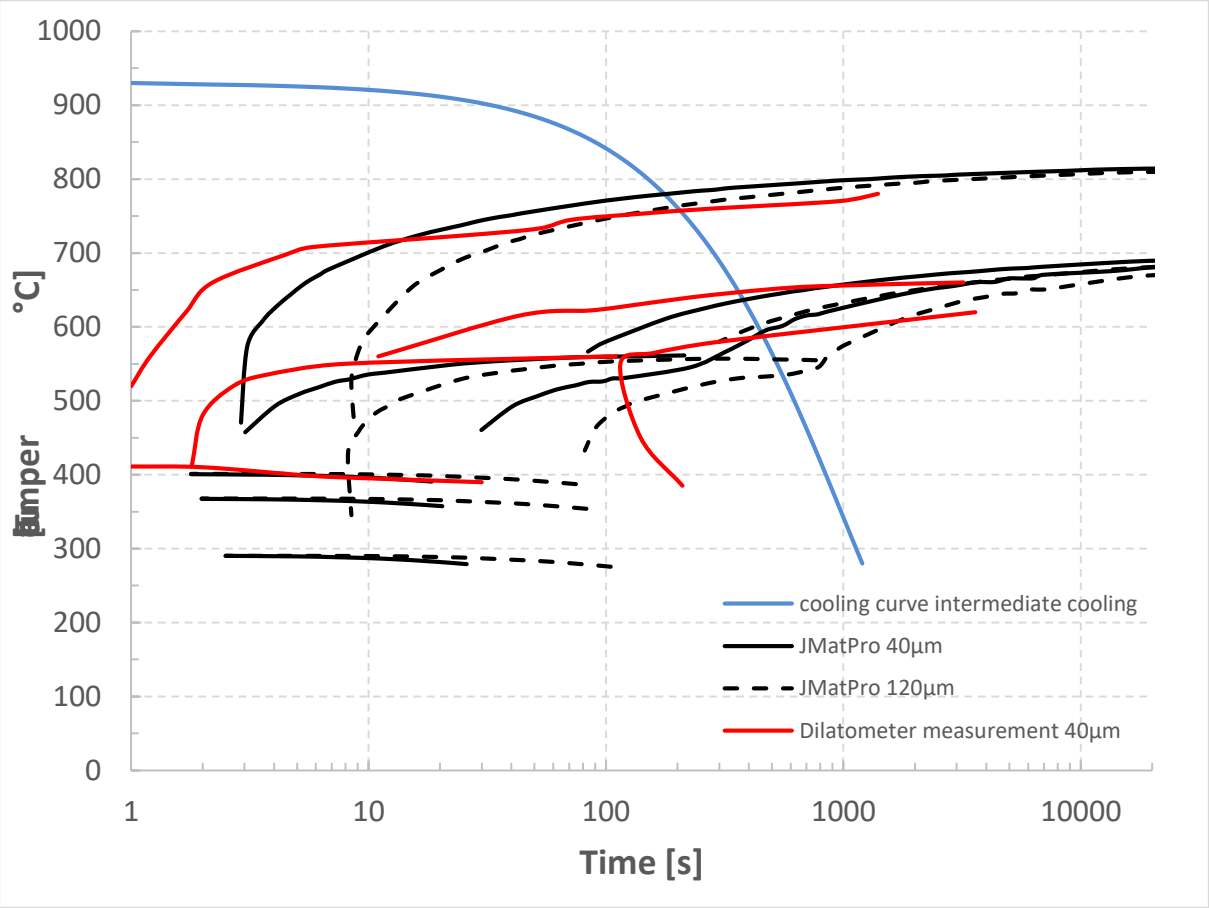

Figure 3-12: Comparison of CCT Diagrams (Steel Grade B) and the influence of grain size on transformation time and temperature, including cooling curve of intermediate cooling

General can be said that the phase transformation needs more time to be completed with a bigger austenite grain size and leads to a reduced maximum reheating furnace inlet temperature to guarantee grain refinement due to phase transformation and reverse transformation. In terms of precipitations, a CCT diagram provides no prediction of the effect.

3.6 Accelerated intermediate cooling

For operational mode 3, the accelerated cooling, another trial with Steel Grade B has been observed. This Steel Grade was chosen due to the micro-alloying effect of V in the temperature range of 950°C and below to the cooling stop temperature of the trial. For this trial tube blanks with a final tube dimension of 104 x 15.84 mm where directly water spray quenched in the rapid cooling system after the reduction process by transferring the tube blanks through the reheating furnace and stretch reducing mill without any further deformation. To explain the effect or describe an optimized process route, ten tube blanks where cooled with five different cooling stop temperatures which are shown in Table 3-3. Always two samples with each cooling stop temperature have been observed, because they were further reheated at different temperatures in the reheating furnace to may get another conclusion of the effect of the process parameters.

Table 3-3: Cooling stop temperature accelerated cooling

Tube blank number	Cooling stop temperature
Blank 1	350 °C
Blank 2	350 °C
Blank 3	470 °C
Blank 4	470 °C
Blank 5	610 °C
Blank 6	610 °C
Blank 7	670 °C
Blank 8	670 °C
Blank 9 (air-cooled, reference)	820 °C
Blank 10 (air-cooled, reference)	820 °C

The cooling stop temperatures are always measured at the surface after the rapid cooling device. Because of the thick walled tube blanks, this temperature is not representing the whole wall of the tube and indicates a temperature gradient from the outside to the inside.

3.6.1 Discontinuous precipitation

As before mentioned, the temperature gradient of the accelerated cooling leads to a gradient of the microstructure. From the CCT diagram can each phase with each temperature gradient or cooling curve be determined. Figure 3-13 faces the transition from the outside to the inside of the tube blank wall. A martensitic microstructure at the outside of the wall is demonstrated in (a), a coarse ferrite/pearlite phase in (b) and a finer segregated ferrite/perlite structure in (c).

These transition in microstructure also refers as in the literature mentioned to a transition in precipitation distribution and size. This distribution will further effect the process in terms of the reheating furnace and stretch reducing mill.

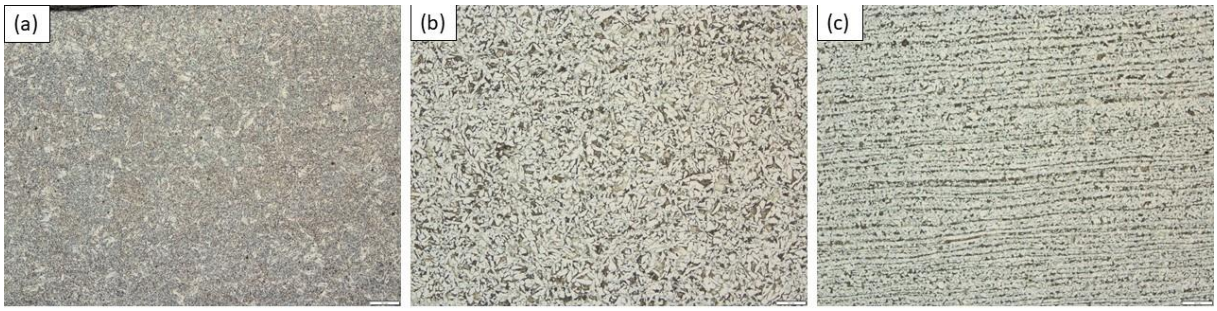

Figure 3-13: Microstructure gradient of Steel Grade B for water quenched tube blank,
500x, scale: 20µm
(a) outside, (b) middle and (c) inside of the blank tube wall

3.6.2 Abnormal grain growth by reheating

The ten water quenched samples were after water quenching to the defined cooling stop temperature air-cooled to room temperature, before they got back into the process into the reheating furnace. For the reheating furnace two groups with each cooling stop temperature were built, one group with the lowest possible reheating temperature and another group with standardized process temperatures in the reheating furnace.

Nearly all samples showed abnormal grain growth due to the discontinuous precipitations over the tube wall. Only the last two samples from Table 3-3, which are air-cooled haven't shown this effect. The consequences of an accelerated intermediate cooling system is shown in Figure 3-14. Because of the reason of abnormal grain growth, which cannot be completely removed in the stretch reducing mill, an accelerated intermediate cooling can be excluded as option for an improvement for the optimization of the mechanical properties.

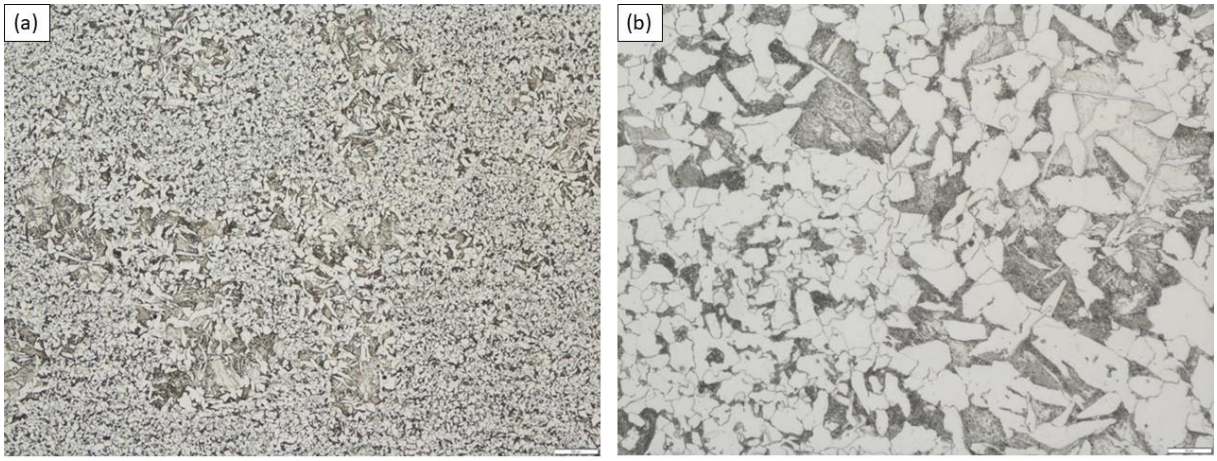

Figure 3-14: Abnormal grain growth by reverse transformation in reheating furnace
Steel Grade B: (a) 100x, scale: 100µm and (b) 500x, scale:20µm

3.7 Reheating furnace

Before the tube blanks are stretched to the final dimension, a reheating furnace is necessary to achieve the defined temperature for the last forming process in the stretch reducing mill. Further a reheating is necessary to reduce the rolling forces to not exceed a maximum of load.

Now depending on the before passed operational mode, the input parameter in the reheating furnace vary. In case of operational mode 1 without intermediate cooling, the austenite grain size is still 120 °C and the temperature is between 820 °C and 900°C. The conditions remain the same from the output of the push bench.

In contrast to that are the conditions of the operational mode 2 with intermediate cooling and a phase transformation into the ferrite/pearlite phase. Furthermore, enough time and temperature is removed to use all precipitation to inhabit grain growth till a temperature the precipitation gets dissolved. Therefore, the input parameters into the reheating furnace is a temperature of about 500 °C (complete phase transformation in CCT diagram for 120 µm grain size). The new formed austenite during reverse transformation is fined and has a grain size according the reheating furnace temperature with Figure 2-20. For standard process conditions means this a grain size of about 40 µm in a totally rebuild and homogenized austenite structure.

The following chapters show the results of the microstructure and grain sizes for all three steel grades, whereas always picture (a) is operational mode 1 without intermediate cooling and Picture (b) is operational mode 2 with the result of intermediate cooling and phase transformation. Operational mode 3 with accelerated cooling wasn't further pursued, because of the abnormal grain growth. Only the two air-cooled samples were mechanical tested and

listed in the results. These microstructures are without the last deformation in the stretch reducing mill.

3.7.1 Steel Grade A

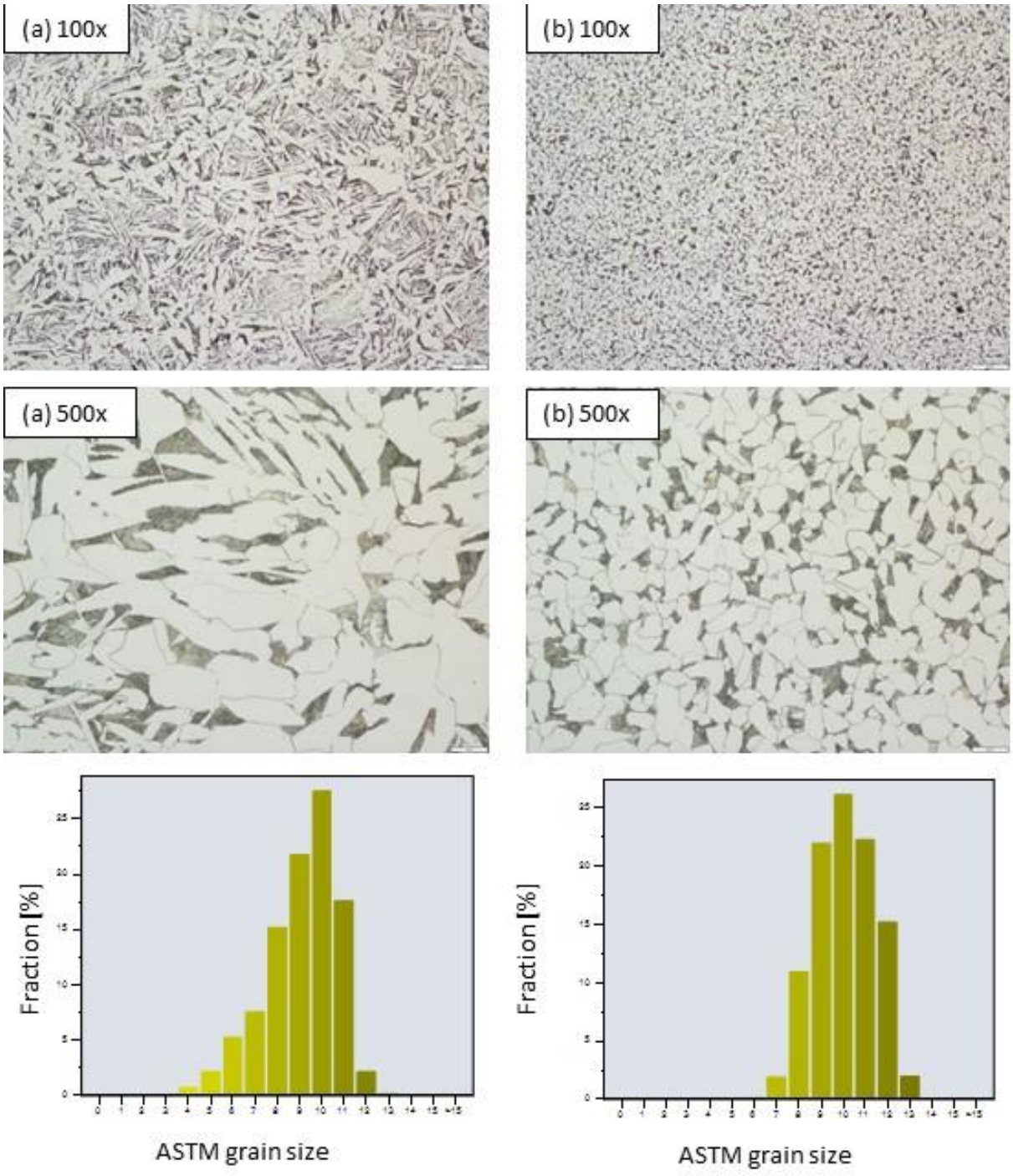

Figure 3-15: Grain size and microstructure comparison Steel Grade A:
(a) without intermediate cooling and (b) with intermediate cooling and phase transformation

3.7.2 Steel Grade B

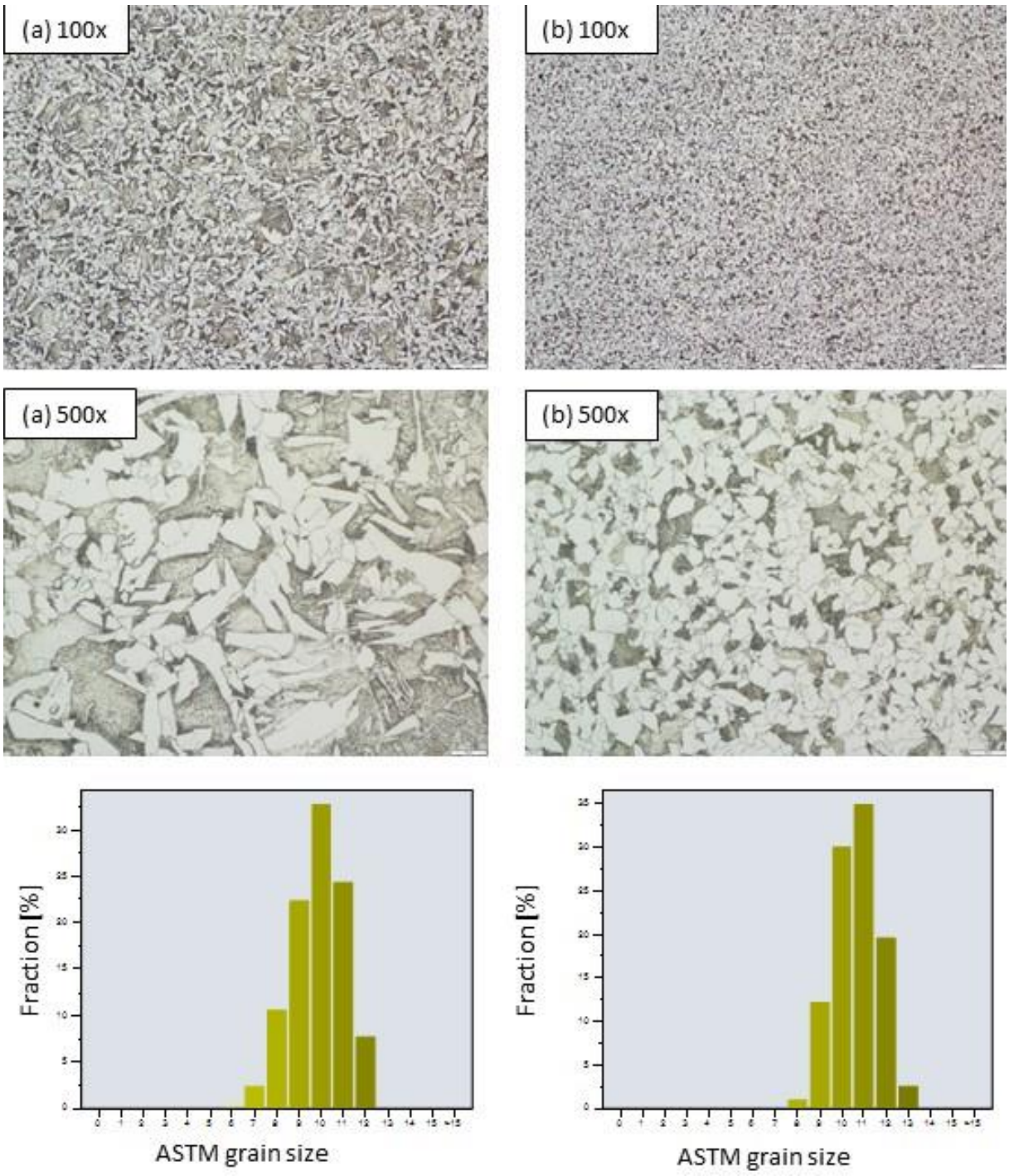

Figure 3-16: Grain size and microstructure comparison Steel Grade B:
(a) without intermediate cooling and (b) with intermediate cooling and phase transformation

3.7.3 Steel Grade C

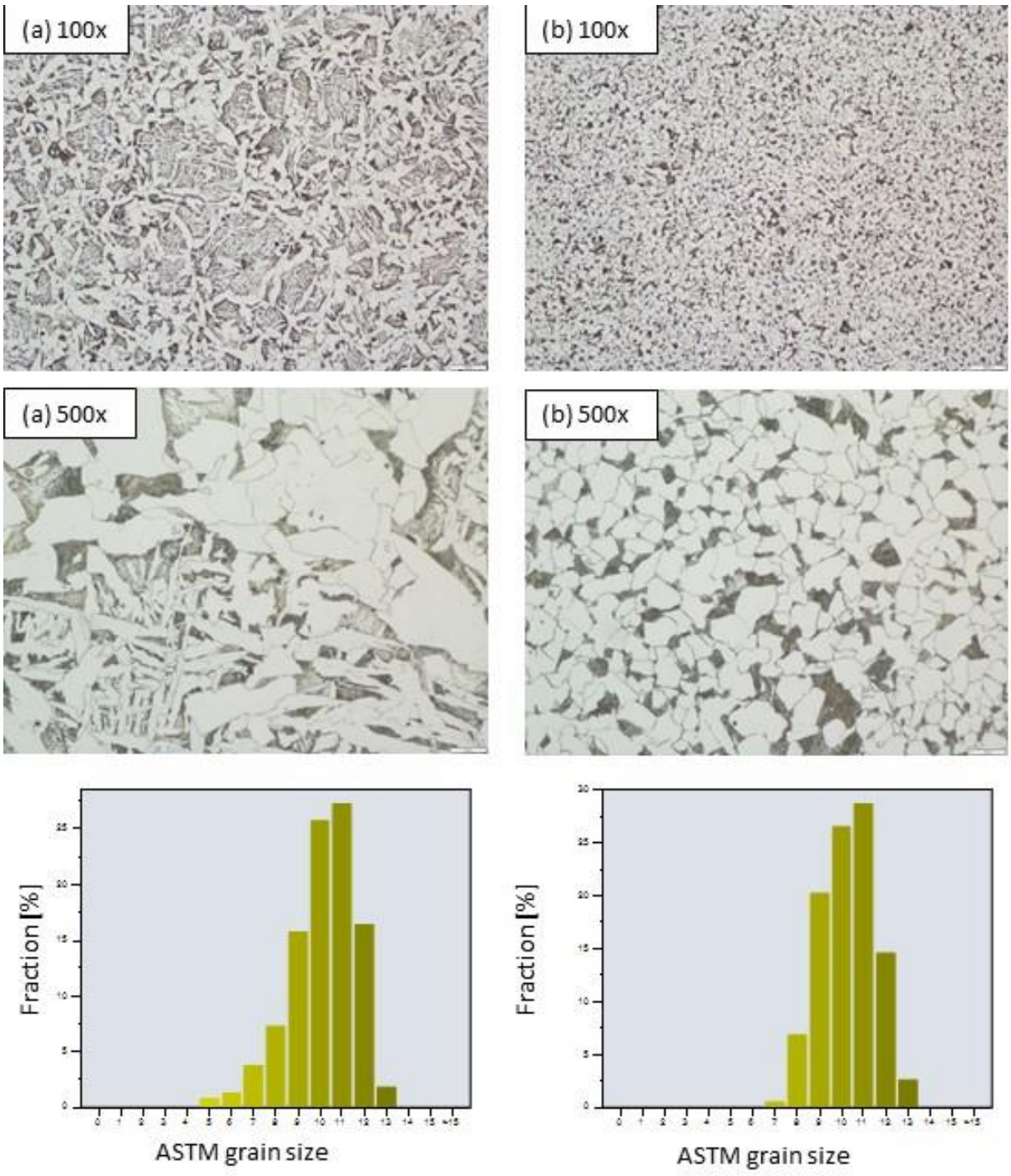

Figure 3-17: Grain size and microstructure comparison Steel Grade C:
(a) without intermediate cooling and (b) with intermediate cooling and phase transformation

3.7.4 Grain size comparison

As in the last three chapters demonstrated, the difference in the microstructure and grain sizes is extraordinary. Operational mode 2 with intermediate cooling delivers a significant finer and more homogeneous microstructure. Also a change from acicular ferrite to globular ferrite in all three cases is apparent. This conditions leads to an improved initial state for a further rapid cooling to vast higher mechanical properties by also completely using the finer microstructure compared with the use of microalloying elements in case of Steel Grade B and C.

To quantify the grain size in values, Table 3-4 summarizes the grain size of all three steel grades.

Table 3-4: Grain size analysis

	Steel grade A		Steel Grade B		Steel Grade C	
0: without intermediate cooling 1: intermediate cooling	0	1	0	1	0	1
Average grain size ISO 643	8.05	9.50	9.40	10.33	9.19	9.80
Equivalent circular diameter [µm]	24.90	15.06	15.59	11.30	16.77	13.57

3.8 Stretch reducing mill

The effect of the operational mode without any further deformation gets alleviated by the use of the stretch reducing mill. Nevertheless, a further forming process with recrystallization lets the operational mode 1 approach an improvement in the microstructure and grain size, but as in the literature mentioned also the finer austenite grains from operational mode 2 recrystallize and provides further better results by a grain refinement due to before occurred phase transformation and reverse transformation. Once more show the next chapters the three different steel grades compared with the operational mode, (a) is the conventional rolled sample, (b) the intermediate cooled one, but now all three different grade stretch reduced to the final dimension of 146 x 12 mm.

3.8.1 Steel grade A

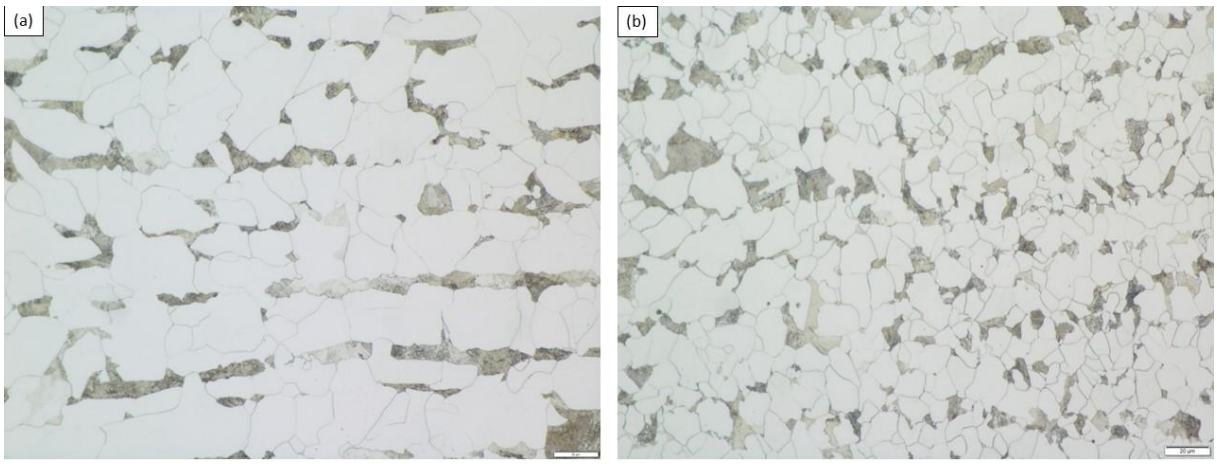

Figure 3-18: Microstructure after stretch reducing mill Steel Grade A:
(a) without intermediate cooling and (b) with intermediate cooling and phase transformation

3.8.2 Steel Grade B

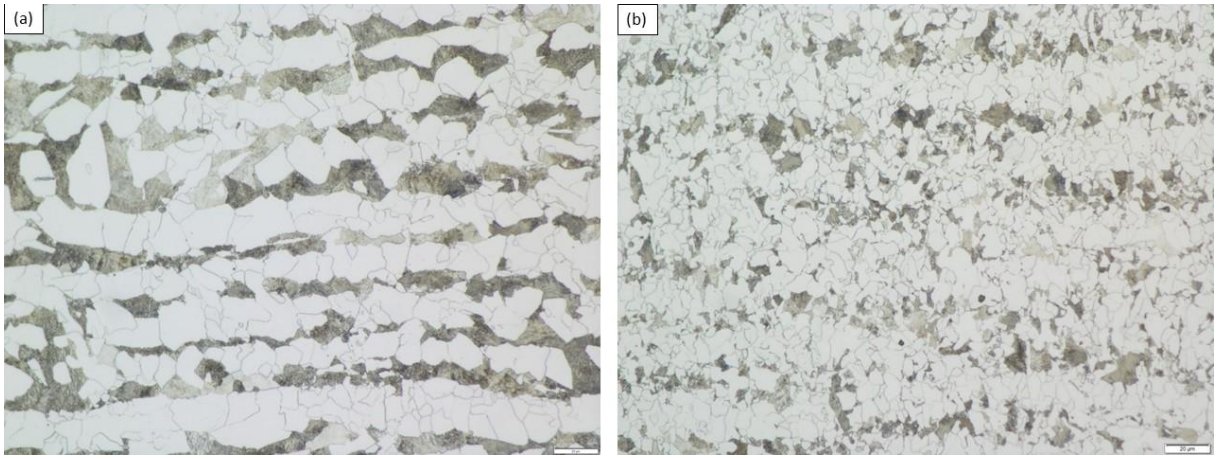

Figure 3-19: Microstructure after stretch reducing mill Steel Grade B:
(a) without intermediate cooling and (b) with intermediate cooling and phase transformation

3.8.3 Steel Grade C

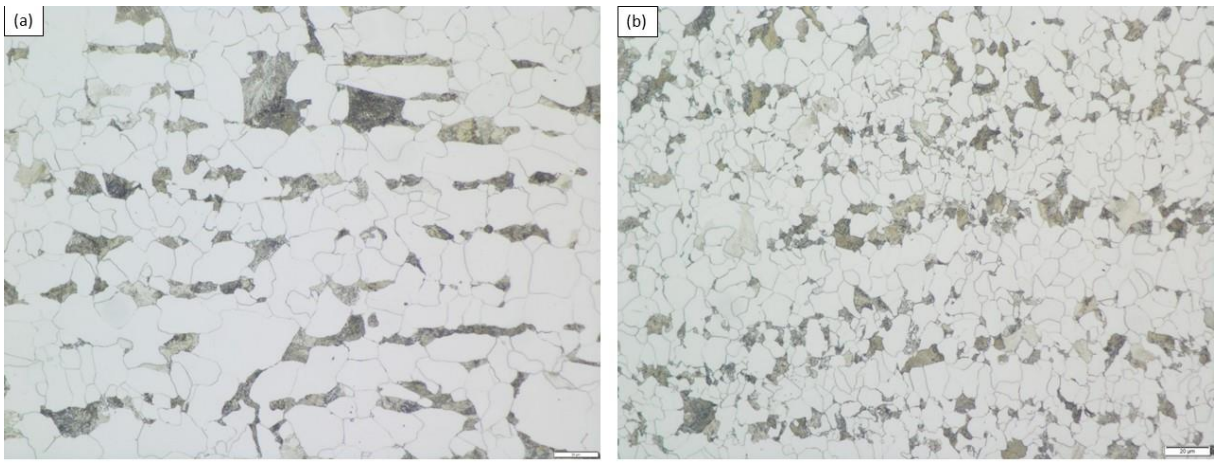

Figure 3-20: Microstructure after stretch reducing mill Steel Grade C:
(a) without intermediate cooling and (b) with intermediate cooling and phase transformation

3.8.4 Grain size comparison

Again the grain sizes between the two operational modes are compered and listed in Table 3-5. The intermediate cooled samples still show the finer and more homogeneous microstructure.

Table 3-5: Grain size analysis after stretch reducing mill

	Steel grade A		Steel Grade B		Steel Grade C	
0: without intermediate cooling 1: intermediate cooling	0	1	0	1	0	1
Average grain size ISO 643	9.67	10.96	10.73	11.98	10.27	11.45
Equivalent circular diameter [µm]	14.27	9.07	9.82	6.38	11.55	7.66

4 Results

In the chapter results the mechanical-technological properties of the before described different operational modes are analyzed. For all samples have been a complete investigation of the stress strain diagram and a notch impact energy curve determined. The results in the diagrams are always an average from at least 6 samples. All tests have been carried out according EN ISO 6892-1 (tensile test) and DIN EN ISO 148-1 (charpy V-notch test).

For the dimension 146 x 12 mm all three steel grades are investigated for mode 1 and 2 in this chapter. Further the air-cooled samples from the accelerated cooling trial in dimension 104 x 15.84 mm is analyzed for Steel Grade B for mode 1 and 2. Further for this samples the different reheating furnace temperatures were used for the report.

4.1 Mechanical properties

4.1.1 Steel Grade A

The results of the mechanical properties for Steel Grade A are shown in Figure 4-1 and the average values for the tensile test are listed in Table 4-1. As from the microstructure apparent are the mechanical-technological properties as expected increased for the intermediate cooled samples. Although Steel Grade A has no microalloying additions, the effect from the phase transformation is huge on the final properties. Also the shift in the transition temperature to lower temperatures for the intermediate cooled operational mode in Figure 4-1 verifies the positive aspect of the intermediate cooling and the included phase transformation to generate a finer grain for optimized properties. In values, the fracture elongation gets increased by 2 % and the yield strength raises from 295 MPa to 318 MPa. Both curves from the figure affirms the strengthening mechanism of grain refinement, with both a higher strength and an increased toughness.

Table 4-1: Tensile test results Steel Grade A, 146 x12 mm

Steel Grade A 146 x 12 mm	Operational Mode 1: Without intermediate cooling	Operational Mode 2: Intermediate cooling
Yield Strength YS [MPa]	295	318
Ultimate tensile Strength UTS [MPa]	452	455
Fracture elongation [%]	30.6	32.6

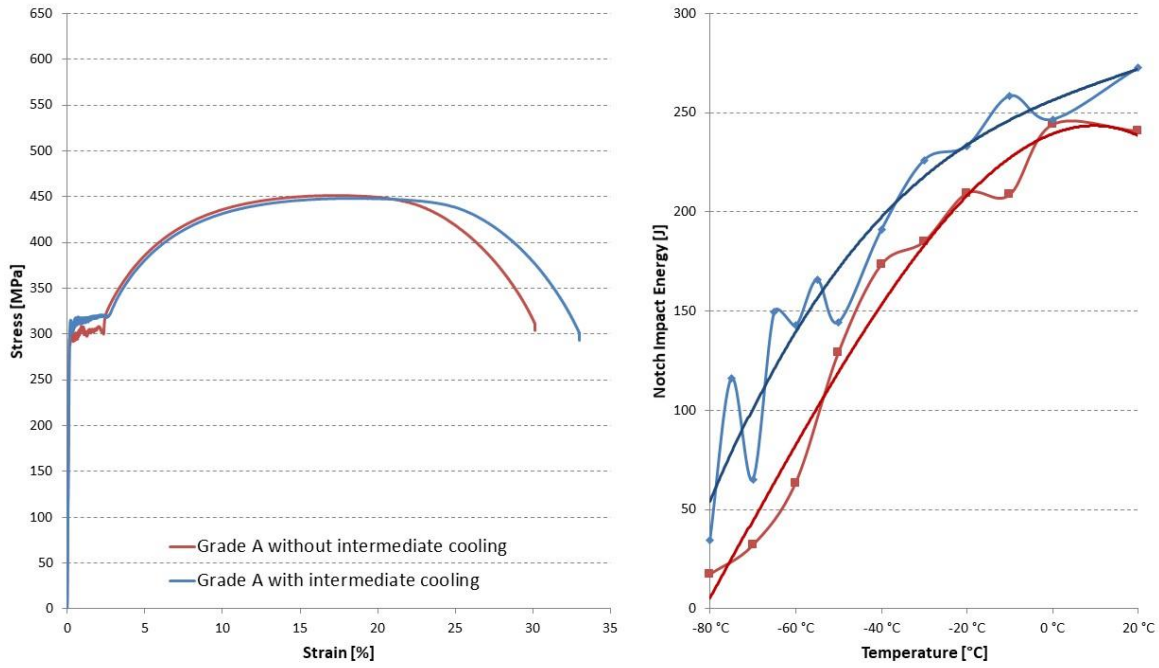

Figure 4-1: Mechanical properties Steel Grade A

4.1.2 Steel Grade B

For Steel Grade B in the dimension 146 x 12 mm applies the same phenomena as for Steel Grade A in terms of the grain refinement and increased properties. Furthermore, the positive influence of Vanadium addition as microalloying element boosts the mechanical-technological properties in combination with the intermediate cooling to a new standard. Figure 4-2 and Table 4-2 show the tremendous difference between the operational mode on a V-alloyed steel grade. The intermediate cooling uses the effect of the precipitation building element completely and builds the perfect initial state for a further rapid cooling after the final deformation at the stretch

reducing mill. Due to the fact that the tested tubes were only air-cooled for better comparability, the effect in the strengthening isn't entirely exploit. The grain refining effect on the other hand with increased toughness is clearly visible in the shift of the transition temperature in the impact energy curve.

Table 4-2: Tensile test results Steel Grade B, 146 x 12 mm

Steel Grade B 146 x 12 mm	Operational Mode 1: Without intermediate cooling	Operational Mode 2: Intermediate cooling
Yield Strength YS [MPa]	440	436
Ultimate tensile Strength UTS [MPa]	597	574
Fracture elongation [%]	21.1	28.3

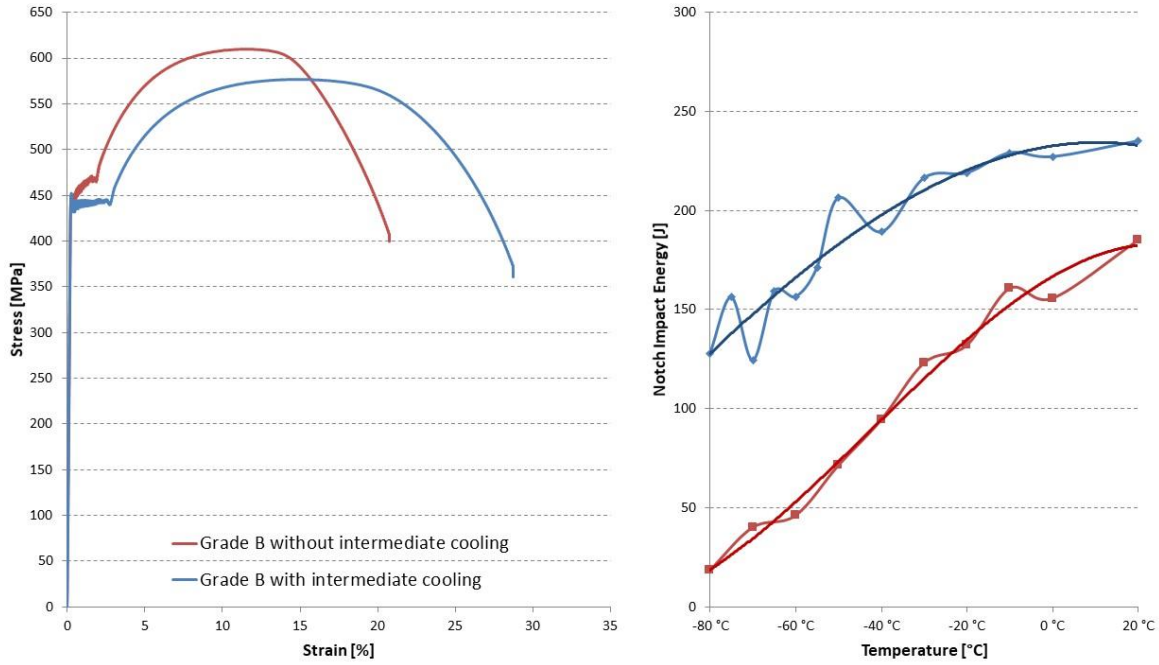

Figure 4-2: Mechanical properties Steel Grade B

Because of the biggest effect on the final product by use of intermediate cooling on Steel Grade B due to the highest amount of alloying elements, the influence of the reheating furnace was further tested with different temperatures on tubes with a dimension of 104 x 15.84 mm. The results of this trial are summarized in Table 4-3 and plotted in Figure 4-3. As expected serves the reheating furnace combined with the temperature only as austenitization unit after the

phase transformation on the intermediate cooling. A higher austenitizing temperature generates coarser austenite grains and further a decrease in the mechanical technological properties. A minimum reheating furnace temperature delivers the highest toughness. But generally show all samples with phase transformation better results than without one.

Table 4-3: Tensile test results Steel Grade B, 104 x 15.84 mm

Steel Grade B 104 x 15.84 mm	Operational Mode 1: Without intermediate cooling	Operational Mode 2: Intermediate cooling	Intermediate cooling and lowest reheating temperature	Intermediate cooling and maximum reheating temperature
Yield Strength YS [MPa]	477	417	416	435
Ultimate tensile Strength UTS [MPa]	632	569	557	582
Fracture elongation [%]	24.5	29.7	29.7	26.2

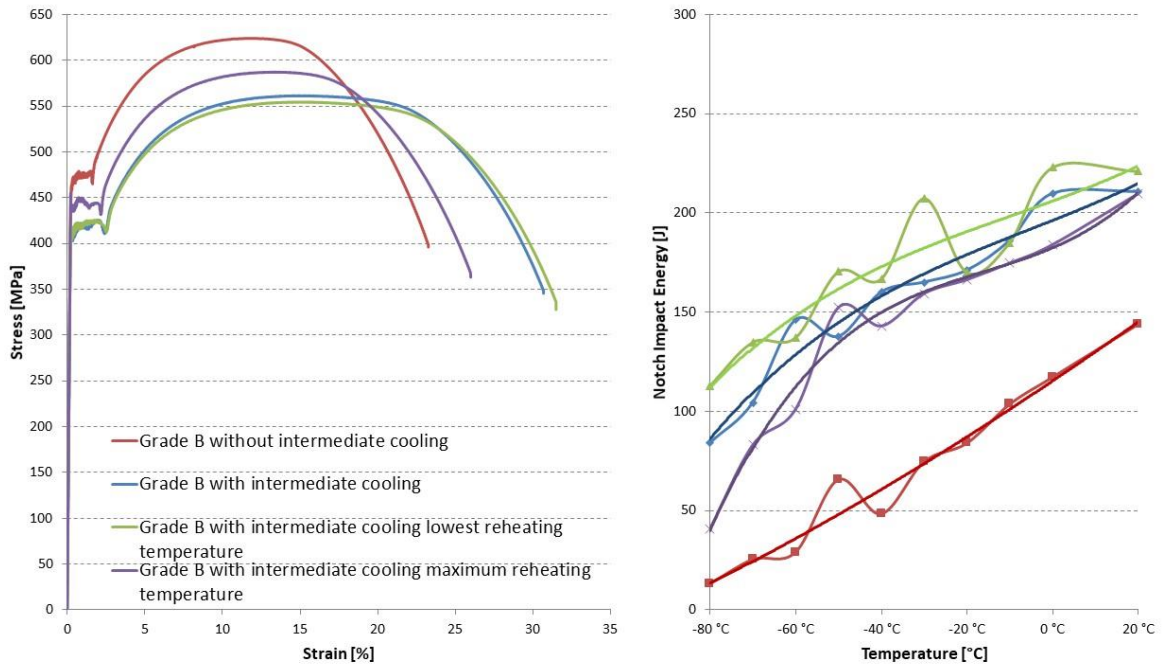

Figure 4-3: Mechanical properties Steel Grade B with different reheating furnace temperatures

4.1.3 Steel Grade C

In case of Steel Grade C, the Nb-microalloyed grade, the results remain similar to both before. The intermediate cooling increases the strength and toughness due to the grain refining effect. The values are given in Table 4-4. Noticeable in Figure 4-4 is the considerable increase of the yield strength of about 50 MPa in combination with an higher fracture elongation. The microallying effect for Nb-alloyed steel grades aren't as attractive than for V-alloyed grades, due to the fact that Niobium precipitations build before the intermediate cooling in the push bench.

Table 4-4: Tensile test results Steel Grade C, 146 x12 mm

Steel Grade C 146 x 12 mm	Operational Mode 1: Without intermediate cooling	Operational Mode 2: Intermediate cooling
Yield Strength YS [MPa]	324	373
Ultimate tensile Strength UTS [MPa]	473	501
Fracture elongation [%]	29.4	30.7

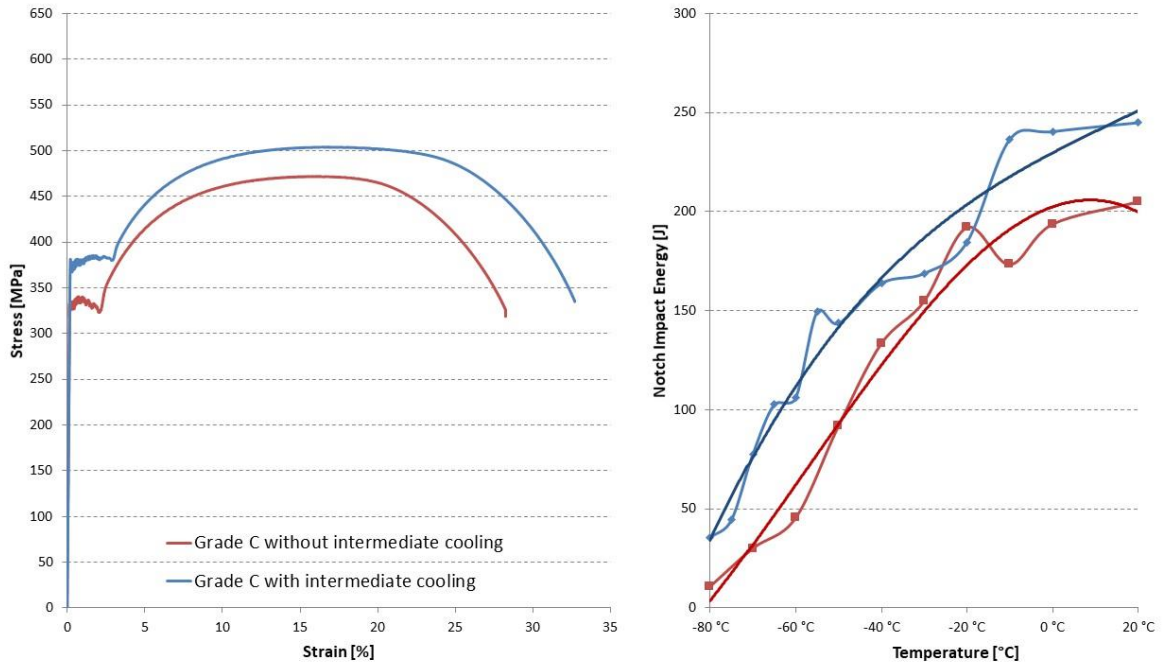

Figure 4-4: Mechanical properties Steel Grade C

4.2 Summary of Results

The positive influence of the intermediate cooling on grain refinement is the main information after all trials and evaluations, independent from the steel grade by thick walled seamless steel tubes. For all three tested grades were the transition temperature improved and shifted to lower temperatures by use of intermediate cooling and a phase transformation. Also the microstructure of all transformed samples was more homogeneous and optimized for a further rapid cooling, especially for Steel Grade B with Vanadium as microalloying element. For Steel Grade C, the Niobium grade, grain refinement leads to an increase in the yield strength and a better toughness according the strengthening mechanism of precipitation and grain size.

Also the aspect of the reheating furnace temperature concludes to the importance of the austenite grain size through the whole process. Therefore, the aim for optimized mechanical-technological properties is a fine austenite grain after every deformation process for all steel grades.

5 Conclusion

To conclude from all results and experiments, the optimization of the process route to increase the mechanical – technological properties is to run all products which aren't further heat treated with intermediate cooling to guarantee grain refinement due to the phase transformation. Especially for thick walled tubes it is important to fine the austenite grain size, because of the coarse grains after the push bench process. In case of the tested dimensions, the phase transformation and reverse transformation in the reheating furnace reduces the austenite grain size from 120 µm (without intermediate cooling) to about 40 µm, depending on the reheating temperature. This effect applies to all steel grades with also different alloying concepts, important is only the total phase transformation from austenite to ferrite/pearlite during intermediate cooling. The CCT diagrams for each steel grade defines for all cases the described phase transformation end. Consequently, the grain size plays a major role on the CCT diagram and the fulfilled phase transformation. Conversion inhibiting elements like Mn further increase the time needed for a complete phase transformation. For the thick walled tubes with 120 µm grain size of the tube blank, an air cooled sample must be cooled down on about 570 °C (Steel Grade A) to 530 °C (Steel Grade B).

General the intermediate cooling also homogenizes on the one hand the temperature gradient from one end to the other and on the other hand enhances the microstructure because of the new built austenitic structure of the reverse transformation by refining.

The intermediate cooling generates further advantages for the stretch reducing mill and especially for a rapid cooling after the finishing forming process. Particularly, V-alloyed steel grades can deploy the full impact in strengthening mechanisms with both, grain refinement and precipitation hardening.

A water quenching device as intermediate cooling can be excluded for V-alloyed steel grades, the gradient in the microstructure and in the precipitation distribution leads to an abnormal grain growth in the reheating furnace in the temperature range of 900 °C to 950 °C.

To transfer the results of all products and dimension, another test trial shall be deployed on also thin wallet tubes. Highlight may be the austenite grain size after the push bench, which may be finer due to the higher recrystallization fraction of the higher strain and strain rate depending on the used push bench set. As perspective also a reduced temperature for the last deformation steps in the push bench could lead to a grain refinement as simulations let predict.

As new target from this gained results from the thesis should be, to generate an austenite grain size after the push bench of under 40 µm to accelerate production and make the phase transformation unnecessary.

An additional outlook shell be given to the precipitations. From the results and the microstructure figures only conclusions of the effect can be made, but for a detailed analysis REM or X-Ray diffraction measurements must be done. Also a simulation and calculation in MatCalc can further explain precipitation phenomena during the tube rolling process and generate further results for an optimized process understanding.

Literature

[1] Hashmi, M.S.J., Aspects of tube and pipe manufacturing processes: Meter to nanometer diameter, Journal of Materials Processing Technology, Volume 179, Issues 1–3, (2006), 5-10.

[2] Staat, K. and Moltner, H, inventor, Seamless tube Production, U.S. Patent 4,798,071 A, June 25, 1986.

[3] Brensing, K.H. and Sommer, B., Steel tube and pipe manufacturing processes, http://www.mrw.de/downloads/stahlrohre_engl.pdf, [13.03.2018]

[4] Pater, Z. and Kazanecki, J., Thermo-mechanical analysis of piercing plug loads in the skew rolling process of thick-walled tube shell, Metallurgy and Foundry Engineering, 32, (2006), 31-40.

[5] Pschera, R., Klarner, J. and Sommitsch, C., Finite Elemente Analyse der Reibungsbedingungen beim Schrägwalzen mit Diescherscheiben, Proceedings Seminar Rohrherstellung und – verarbeitung (2007), 59-69.

[6] Baines, K., Lead as a model material to simulate mandrel rolling of hot steel tube, Journal of Materials Processing Technology 118 (2001), 422-428.

[7] Dobrucki, W. and Sobkowiak, P., Laboratory investigation of the continuous seamless-tube rolling process (mandrel mill process) using models, Journal of Mechanical Working Technology 19 (1989), 285-294.

[8] Bayoumi, L.S., Analysis of flow and stresses in a tube stretch-reducing hot rolling schedule, International Journalof Mechanical Sciences 45 (2003), 553-565.

[9] Narayanasamy, R., Parthasarathi, N.L. and Sathiya Narayanan, C., Effect of microstructure on void nucleation and coalescence during forming of three different HSLA steel sheets under different stress conditions, Materials & Design 30 (2009), 1310-1324.

[10] Calcagnotto, M., Adachi, Y., Ponge, D. and Raabe, D., Deformation and fracture mechanisms in fine- and ultrafine-grained ferrite/martensite dual-phase steels and the effect of aging, Acta Materiala 59 (2011), 658-670.

[11] Song, R., Ponge, D., Raabe, D., Speer, J.G. and Matlock, D.K., Overview of processing, microstructure and mechanical properties of ultrafine grained bcc steels, Material Science and Engineering: A 441 (2006), 1-17.

[12] Klarner, J., Buchmayr, B. and Rainer, W., Toughtubes, extrem feinkörnige nahtlose Stahlrohre, BHM 156 (2011), 168-174.

[13] Farahat, A.I.Z. and El-Badry, S.A., Effect of high temperature deformation and different cooling rates on microstructure and mechanical properties, Materials Science and Engineering: A 525 (2009), 48-54.

[14] Winter, G., Macro- and Microscopic Properties of Gradient Ultra High Strength Thermo-Mechanically Rolled Seamless Steel Tubes, Dissertation Chair of Metal Forming, University of Leoben, (2015), 2-4.

[15] Tamura, I., Ouchi, C., Tanaka, T. and Sekine, H., Thermomechanical Processing of High Strength Low Alloy Steels, Butterworth & Co. Ltd, London, 1988.

[16] Zhao, J. and Jiang, Z., Thermomechanical processing of advanced high strength steels, Progress in Materials Science 94 (2018), 174-242

[17] Llewellyn, D.T., Nitrogen in Steels, Ironmaking & Steelmaking 20 (1993), 35-41.

[18] Brimacombe, J.K. and Boyd, J.D., Steel Product-Process Integration, Proceeding of International Symposium of Canadian Institute of Mining & Metallurgy, 1989.

[19] Paules, J.R., Development in HSLA steel products, Applying Materials Science and Engineering - Metals 43 (1991), 41-44.

[20] Teoh, L.L., Thermo-mechanical processing and microstructure of microalloyed steel bar and wire products, Journal of Materials Processing Technology 48 (1995), 475-481.

[21] Fukuda, M., Hashimoto, T. and Kunishige, K., Proceedings of the Conference Microalloying 75, Washington, DC, 1975.

[22] Paules, J.R. 31st Mech. Working & Steel Processing Proc. 17 (1989) 131.

[23] Ohshiro, T., Ruddle, G.E. and Crawley, A.F., Accelerated Cooling of Rolled Steel, Pergamon (1987), 283.

[24] Mekkawy, M.F., El-Fawakhry, K.A., Mishreky, M.L. and Eissa, M.M., Effect of interrupted accelerated cooling on mechanical properties and structure of vanadium and titanium microalloyed steel bars, Materials Science and Technology 7 (1991), 28-36.

[25] Mekkawy, M.F., El-Fawakhry, K.A., Mishreky, M.L. and Eissa, M.M., Direct quenching of low manganese steels microalloyed with vanadium or titanium, Iron and Steelmaker 10 (1990), 75-88.

[26] Mishra, S.K., Das, S. and Ranganathan, S., Precipitation in high strength low alloy (HSLA) steel: a TEM study, Materials Science and Engineering: A 323 (2002), 285-292.

[27] Porter, D.A. and Easterling, K.E., Phase Transformations in Metals and Alloys, CRC Press, Taylor & Francis Group, Finland (2004).

[28] Lagneborg, R., Siwecki, T., Zajac, S. and Hutchinson, B., The Role Of Vanadium In Microalloyed Steels, Swedish Institute for Metals Research, Sweden (1999).

[29] Zajac, S. and Jansson, B., Thermodynamics of the Fe-Nb-C-N System and the Solubility of Niobium Carbonitrides in Austenite, Metall. Trans. 29B (1998), 163-176.

[30] Yoshinaga, N., Ushioda, K., Akamatsu, S. and Akisue, O., Precipitation Behaviour of Sulfides in Ti-added Ultra Low-carbon Steels in Austenite. ISIJ Int. 34 (1994), 24-32.

[31] Wilson, F.G. and Gladman, T., Aluminium nitride in steel, Int. Materials Rev. 33 (1988), 221-287.

[32] Brown, E.L. and DeArdo, A.J., Aluminium nitride precipitation in C-Mn-Si and microalloyed steels, Proc. Conf. Thermomechanical Processing of Microalloyed Austenite (1982), 319-341.

[33] Roberts, R., Recent innovations in alloy design and processing of microalloyed steels. Contribution to the 1983 Int. Conf. on Technology and Applications of High Strength Low Alloy (HSLA) Steels, Philadelphia (1983), 67-84.

[34] Zajac, S., Siwecki, T., Hutchinson, W.B. and Attlegård, M., Recrystallization controlled rolling and accelerated cooling for high strength and toughness in V-Ti-N steels, Metall. Trans. A 22A (1991), 2681-2694.

[35] Lehtinen, B. and Hansson, P., Characterisation of microalloy precipitates in HSLA steels subjected to different weld thermal cycles, Swedish Institute for Metals Research, Internal Report IM-2532, (1989).

[36] Hillert, M.; On the theory of normal and abnormal grain growth, Acta Metallurgica 13 (1965), 227-238.

[37] Irvine, K.J., Pickering, F.B. and Gladman, T., Grain coarsening of austenite, Journal of the Iron and Steel Institution 205 (1967), 161.

[38] Gladman, T. and Pickering, F.B., The grain size distribution and the detection of abnormal grain growth of austenite, Journal of the Iron and Steel Institution 205 (1967), 653.

[39] Gladman, T., The theory and inhibition of abnormal grain growth in steels, JOM 9 (1992), 21-24.

[40] Humphreys, F.J. and Hatherly, M., Recrystallization and Related Annealing Phenomena, Pergamon, Oxford, (1995).

[41] Gladman, T., On the theory of the effect of precipitate particles on grain growth in metals, Proceedings of the Royal Society 294A (1966), 298.

[42] Gao, N. and Baker, T.N., Austenite Grain Growth Behaviour of Microalloyed Al-V-N and Al-V-Ti-N steels, ISIJ International 38 (1998), 744-751.

[43] Cuddy, L.J., The Effect of Microalloy Concentration on the Recrystallization of Austenite during Hot Deformation, Proc. Conf. Thermomechanical Processing of Microalloyed Austenite, Pittsburgh (1981), 129-140.

[44] Jonas, J.J. and Weiss, I., Effect of precipitation on recrystallization in microalloyed steels, Metals Science 13 (1979), 238–245.

[45] Akben, M.G., Chandra, T., Plassiard, P. and Jonas, J.J., Dynamic precipitation and solute hardening in a V microalloyed steel and two Nb steels containing high levels of Mn, Acta Metallurgica 29 (1981), 111-121.

[46] Luton, M.J., Interaction Between Deformation, Recrystallization and Precipitation in Niobium Steels, Metal. Trans. 11A (1980), 411-420.

[47] Jones, J.D. and Rothwell, A.B., Controlled Rolling of Low-Carbon Niobium-Treated Mild Steels, ISI Publication 108 (1968), 78-82.

[48] Davenport, A.T., Brossard, L.C. and Miner, R.E., Precipitation in Microalloyed High Strength Low Alloy Steels, JOM Metals 27 (1975), 21–27.

[49] Davenport, A.T., Hot Deformation of Austenite, TMS-AIME (1977),517-536.

[50] De Ardo, A.J., Modern Thermomechanical Processing of Microalloyed Steel: A Physical Metallurgy Perspective, Iron & Steel Soc. (1995), 15–33.

[51] Palmiere, E.J., Precipitation Phenomena in Microalloyed Steels, Proc. Iron & Steel Soc. (1995), 307–820.

[52] Grajcar, A. and Kuziak, R., Softening kinetics in Nb-microalloyed TRIP steels with increased Mn content, Advanced Materials Research 314-316 (2011), 119-122.

[53] Ozgowicz, W., Opiela, M., Grajcar, A., Kalinowska-Ozgowicz, E. and Krukiewicz, W., Metallurgical products of microalloy constructional steels, Journal of Achievements in Materials and Manufacturing Engineering 44/1 (2011), 7-34.

[54] Gladman, T., The Physical Metallurgy of Microalloyed Steels, The Institute of Materials, London, (1997).

[55] Adamczyk, J., Development of the microalloyed constructional steels, Journal of Achievements in Materials and Manufacturing Engineering 14/1-2 (2006), 9-20.

[56] Opiela, M. and Ozgowicz, W., Effects of Nb, Ti and V on recrystallization kinetics of austenite in microalloyed steels, Journal of Achievements in Materials and Manufacturing Engineering 55/2 (2012), 759-771.

[57] Andrade, H.L., Akben, M.G. and Jonas, J.J., Effect of molybdenium, niobium, and vanadium on static recovery and recrystallization and on solute strengthening in microalloyed steels, Metallurgical Transactions 14A (1983), 1967-1977.

[58] Medina, S.F., Gòmez, M. and Gòmez, P.P., Effect of V and Nb on static recrystallization of austenite and precipitate size in microalloyed steels, Journal of Materials Science and Technology 45 (2010), 5553-5557.

[59] Grajcar, A., Structural and mechanical behavior of TRIP-type microalloyed steel in hot-working conditions, Journal of Achievements in Materials and Manufacturing Engineering 30/1 (2008), 27-34.

[60] Kozasu, I., Onchi, C., Sampei, T. and Okita, T., Hot Rolling as a High-Temperature Thermo-Mechanical Process, Conference of Microalloying (1975), 120-135.

[61] Siwecki, T., Hutchinson, B. and Zajac, S., Recrystallisation controlled rolling of HSLA steels, Iron and Steel Society Inc. (1995), 197-212.

[62] Lagneborg, R., Roberts, W., Sandberg, A. and Siwecki, T., Influence of processing route and nitrogen content on microstructure development and precipitation hardening in V microalloyed HSLA-steels, Conference on Thermomechanical Processing of Microalloyed Austenite (1981), 163–194.

[63] Siwecki, T. and Zajac, S., Recrystallization Controlled Rolling and Accelerated Cooling of Ti-V-(Nb)-N Microalloyed Steels, The 32nd Mechanical Working and Steel Processing Conference (1990), 441–451.

[64] Gong, S., The influence of vanadium on the austenite–ferrite transformation in microalloyed steels, Swedish Institute for Metals Research, Internal Report IM-1488, (1980).

[65] Khalid, F.A. and Edmonds, D.V., Interphase Precipitation in Microalloyed Engineering Steels and Model Alloy, Materials Science and Technology 9 (1993), 384-396.

[66] Hillert, M., Phase Equilibria Phase Diagrams and Phase Transformations, Cambridge University Press, (1998).

[67] Zajac, S., Lagneborg, R. and. Siwecki, T., The role of nitrogen in microalloyed steels, Contribution to the International Conference of Microalloying (1995), 321-340.

[68] Zajac, S., Siwecki, T. and Korchynsky, M., Importance of nitrogen for precipitation phenomena in V-microalloyed steels, Internatianal Symposium on Low Carbon Steels for the 90's (1993), 139-150.

[69] Davenport, A.T. and Honeycombe, R.W.K., Precipitation of carbides at austenite/ferrite boundaries in alloy steels, Proceedings of the Royal Society London 322 (1971), 191-205.

[70] Honeycombe, R.W.K., Transformation from austenite in alloy steels, Metall.Trans.A, 7A (1976), 915-936.

[71] Roberts, W., Hot deformation studies on a V-microalloyed steel, Swedish Institute for Metals Research, Internal Report IM-1333, (1978).

[72] Zajac, S., Siwecki, T., Hutchinson, W.B. and Lagneborg, R., Strengthening mechanisms in Vanadium Microalloyed Steels Intended for Long Products, ISIJ International 38, (1998), 1130-1139.

[73] Roberts, W. and Korchynsky, M., Proceedings of International Conference on HSLA steels – Technology and Applications, (1984), 67.

[74] Klarner, J., Thermomechanische Behandlung beim Walzen von nahtlosen Stahlrohren, Dissertation Chair of Metal Forming, University of Leoben, (2009).

[75] Buchmayr, B., Werkstoff- und Produktionstechnik mit Mathcad, Springer Verlag, Heidelberg, (2002).